Some Studies Of The Brittle To Quasi-Brittle Transition In Fiber Bundle Models

Thesis submitted for the Degree of

Doctor of Philosophy (Science)

in

Physics (Theoretical)

by

CHANDREYEE ROY

Department of Physics

University of Calcutta

2019

List of publications

The following papers have been discussed in this thesis:

1. ***Scaling forms for relaxation times of the fiber bundle models***,

   Chandreyee Roy, Sumanta Kundu and S. S. Manna,

   Phys. Rev. E 87, 062137,(2013).

2. ***Fiber bundle model with highly disordered breaking thresholds***,

   Chandreyee Roy, Sumanta Kundu and S. S. Manna,

   Phys. Rev. E 91, 032103,(2015).

3. ***Brittle-to-quasibrittle transition in bundles of nonlinear elastic fibers***,

   Chandreyee Roy and S. S. Manna,

   Phys. Rev. E 94, 032126 (2016).

4. ***Brittle-to-quasibrittle transition in a compound fiber bundle***,

   Chandreyee Roy and S. S. Manna,

   Submitted to journal.

Other Publication:

1. ***Network topology of the desert rose***,

   Sigmund Mongstad Hope, Sumanta Kundu, Chandreyee Roy, S. S. Manna and Alex Hansen,

   Front. Phys., 3:72 (2015).

Acknowledgement

I would like to express my sincere gratitude to my supervisor, Prof. Subhrangshu Sekhar Manna, for his continuous support of my Ph.D. study and related research. His patience, motivation and immense knowledge along with his guidance during the time of research helped me to finish writing my thesis. Besides my supervisor, I would like to thank the rest of my thesis committee: Prof. Manoranjan Kumar and Prof. Manu Mathur for their insightful comments and encouragement during all my evaluation talks. The questions asked by them helped me widen my research from various perspectives. I would also like to thank Prof. Alex Hansen and Dr. Srutarshi Pradhan for giving me an opportunity to work at NTNU, Norway and SINTEF, Norway. It was an enriching experience and motivated me to keep working in this field.

I want to thank my group member Sumanta Kundu for his unwavering support and stimulating discussions while we were working together. I would also like to thank the seniors in my group: Dr. Biplab Bhattacherjee and Dr. Abhijit Chakraborty who were always ready to help me at a moments notice. I would like to thank all the friends from the Statistical Physics group of our centre: Shauri, Rajkumar, Subrata da, Sayani di, Subhadeep, Dhiraj, Anirban, Arghya da, Rakesh and Sudipto for all the academic and non-academic help and support I received throughout these last five and half years.

I would also to thank all the friends that I have made here in S. N. Bose Centre: Deblina, Ayan, Ruchi, Ransell, Ritam, Dhani, Ravi, Shaili, Neeraj, Poonam and Ankan for helping me create beautiful and fun filled memories that I will cherish forever in my life. I want to thank my friends and family: Atrayee, Sneha, Nirajita, Sulagna, Aratrika, Pompa and Manta di who were not only my support but also cheered me up with phone calls when I felt down on numerous occasions.

Finally, I would like to extend my heartfelt thanks to my parents who have been the strongest pillars of support in my life. They have stuck by me through thick and thin and it is their encouragement and motivation that keeps me going whenever things go bad. They have been the epitome of patience and a source of constant mental support in many situations and I am eternally grateful for that.

Chandreyee Roy

Synopsis

A fiber bundle model (FBM) is a theoretical model used in material science to study the breakdown properties of materials. This model has been seen to be very useful in practical applications such as in studying fractures, earthquakes, traffic systems etc. It consists of a set of massless elastic fibers placed parallel to each other and clamped from both ends. At the lower end a force is applied to elongate the bundle. Every fiber has a distinct breaking threshold drawn from a random distribution. This is the only source of disorder in the system. Ideally, a fiber elongates following the Hooke's Law and breaks when the load per fiber acting on it reaches its breaking threshold. When a fiber breaks, the load carried by it is redistributed to the rest of the intact fibers in the bundle. Due to this redistribution the intact fibers experience an enhanced stress. This may cause more fibers to break and the released load again gets redistributed. This process goes on till the bundle reaches a stable state. A stable state is defined as a state when all intact fibers have their breaking thresholds below the external load per fiber or when the entire bundle has failed. In the present thesis, we have considered the Equal Load Sharing (ELS) version of the fiber bundle where the load released by a broken fiber is distributed equally to all the intact ones. Depending on the extent of disorderedness in the system the fiber bundle can either be brittle or quasi-brittle. If the weakest fiber failure causes

complete breakdown of the bundle, then the bundle is defined as brittle; otherwise it is defined as quasi-brittle. We study the transition of the bundle between these states by tuning a parameter that controls the amount of disorderedness in the bundle.

1. Relaxation time of an ELS FBM

When an external load per fiber σ is applied to a bundle then all the fibers having their breaking thresholds below it break. The load released by the broken fibers is redistributed among the intact fibers. This is defined as one relaxation time step. The remaining intact fibers will experience an enhanced stress causing more fibers to break and eventually redistribute it among the intact fibers. This process repeats itself in a series of successive time steps T till a stable state is reached. Thus, the relaxation time is not real time but a real positive integer that gives us the number of times the redistribution of load occurs in the bundle for the same externally applied load till a stable state has been reached. In the precritical regime the average relaxation time against σ is seen to increase and reach a finite but large peak at $\sigma \approx 1/4$ with the height increasing with bundle size. In the postcritical regime, the relaxation time decreases with increase in σ. In the vicinity of the critical load σ_c, the relaxation time plotted against the deviation $|\sigma_c - \sigma|$ follows a power-law form both in the precritical and post critical regime.

2. Highly Disordered ELS FBM

Next, we have analyzed the breakdown properties of the model where the breaking thresholds of the fibers are power law distributed within the limits $10^{-\beta}$ to 10^{β} with β as a parameter. We have shown that the critical load of the bundle $\sigma_c(\beta) = 10^{\beta}/(2\beta\, e\, ln10)$ for $\beta > \beta_u = 1/(2\ ln10)$. Below β_u the bundle is brittle which implies that if a load is applied to break even the weakest fiber in the bundle, it fails completely. This is a direct consequence of the extent of disorder in the material which comes from the randomness of the breaking thresholds. When β is very small all the fibers have their

breaking thresholds near unity and even the smallest fiber failure causes the breakdown of an entire bundle. As β is increased the width of the disorder increases and the bundle becomes quasi-brittle. The distribution of the avalanche sizes follows a power law and the exponent undergoes a crossover from $3/2$ to $5/2$ for lower and higher values of β respectively. We have also shown that the critical load approaches its asymptotic value following $\sigma_c(\beta, N) = \sigma_c(\beta)(N) + AN^{1/\nu(\beta)}$ where the finite size correction exponent $\nu(\beta)$ is a beta dependent quantity. It is first observed to increase sharply with β, reaches a maximum, then decreases, and finally converges to a value $\approx 3/2$ which is true for a FBM having breaking thresholds drawn from uniform distribution between $[0, 1]$.

3. Brittle to quasi-brittle transition in a FBM with non-linear fibers

Next, we have studied a FBM where the individual fibers are assumed to follow a non-linear stress-strain curve. We have mainly considered the following four different forms of non-linearity: $s = \mathcal{G}(x) = e^{\alpha x}, 1 + x^{\alpha}, x^{\alpha}$, and $xe^{\alpha x}$ where α is a tunable parameter. Analytical studies, supported by extensive numerical calculations of this model, exhibit a brittle to quasi-brittle phase transition at a critical value of α_c only in the first two cases. For the case $\mathcal{G}(x) = e^{\alpha x}$, this transition is characterized by a weak power law modulated logarithmic (brittle) and logarithmic (quasi-brittle) dependence of the maximal relaxation time on the two sides of the critical point. A study of the average avalanche size indicates a peak at the critical point α_c. Moreover, the critical load $\sigma_c(\alpha)$ for the global failure of the bundle depends explicitly on α in all cases.

4. Brittle to quasi-brittle transition in a compound FBM

Finally, we have studied the transition in a compound FBM consisting of two different kinds of fibrous materials, having distinct difference in their breaking strengths. We have considered a random fiber FBM with a bimodal distribution of the breaking strengths of the individual fibers. The bimodal distribution is assumed to be consisting of two symmetrically placed rectangular probability distributions of strengths p and $1-p$, each of width d, and separated by a gap $2s$. Different properties of the transition have been studied varying these three parameters. Our study exhibits a brittle to quasi-brittle transition at the critical width $d_c(s,p) = p(1/2-s)/(1+p)$ confirmed by our numerical results.

Contents

CHAPTER 1

Introduction

Even though present day science and engineering have allowed us to construct remarkable structures like the huge skyscrapers and long suspension bridges, we have many examples of the finest quality and most impressive architectural constructions around the world that were built thousands of years ago, but are still standing successfully at this age. In fact, the ancient architects not only designed these famous structures very cleverly, but also selected and used the materials of construction in such a way so as to avoid the future fractures and failures i.e., to make them long lasting. The Leaning Tower of Pisa, the Colosseum in Rome, the Great Wall of China are few examples of such structures which exist till now in the present day. There are also certain bridges, like the Pons Fabricius built in 62 B.C in Rome, that are still used for their intended purposes. These examples indicate that the knowledge of erosion, fracture and breakdown of materials have been prevalent ever since people started doing constructions. It was known that materials are prone to failure when they are subjected to stress. Fracture and breakdown of materials can cause damage of property and loss of lives. Quite naturally, even today houses and buildings are constructed with the aim that they will be able to withstand different weather conditions. For example, since Japan is prone to a lot of earthquakes, the buildings there are constructed in a way such that they are resilient to earthquakes.

The study of the mechanics of fracture in materials has been considered to be very important. Historically, the modern day research related to this branch of science

Figure 1.1: Around 90 out of 2700 ships manufactured by a U.S. Liberty Ship Building Program during World War II underwent serious fractures with some of them resulting in breaking completely into two halves. This picture is taken from the website [1].

started mainly due to the destruction of the Liberty cargo ships which were sent from the United States of America to Britain during World War II to support them in the battle against Germany [2, 3]. Out of around 2700 ships, nearly 90 ships were either completely destroyed or sustained serious fractures. It was widely believed that the damages occurred due to the low quality of welding, poor quality of steel used and huge stress accumulations at the deck square hatch corners. Cracks generated due to stress concentration kept on growing larger and consequently became unstable since there were no rivets to hinder their growth and this resulted in the ships breaking into halves (Fig. 1.1). This incident led the material scientists to start extensive research in the field of fracture mechanics, mostly from the engineering point of view, with emphasis on how to build and design durable structures that are able to withstand crack growths when they are kept under stress.

It was revealed later that there is a need to understand fracture in materials from the physics point of view as well. This is because no material medium is perfectly pure. In fact truly any real material has a large number of randomly distributed micro-size defects (or impurities). Therefore, any sample of real material is actually a good example of a

disordered system. Fractures or crack propagation in materials usually nucleate around the disorders present in them and eventually affect their breakdown properties.

More lately, disordered systems were being studied in Statistical Physics in the topic of Percolation Phenomena and the electrical conductivity of impure materials using Quantum mechanics under the localization phenomena. It had been realized that in general, materials undergo breakdown processes both under externally applied mechanical stress as well as under the application of high voltages. In both cases, the presence of disorder plays an important role in the determination of the breakdown point as well as behaviour of the materials in the close vicinity of the breakdown point. Different samples of the same material, having same dimensions, have different strengths that fluctuate around an average value and this demands a statistical treatment. It has been well established that fracture always nucleates from the weak sections of the material. A simple experiment pertaining to mechanical breakdown can be illustrated by pulling a rectangular piece of paper at its two ends with a single hole in it till it tears apart completely. The largest tear in it always originates from the position of the hole in the paper since that is the weakest part. The propagation of a crack in the case of a distribution of holes has been studied experimentally and analytically in Ref. [4].

The complex phenomena of breakdown in respect to earthquakes, which is known to leave a lot of destruction and loss of lives in its wake, have also been seen to follow certain empirical laws. The Gutenberg Richter Law states that the number of earthquakes with energy E decays with E following a power law; it is proportional to $E^{-(1+B)}$ where B is a suitable exponent [5, 6]. The Omori Law states that the rate of the number of aftershocks after the mainshock also decays as a power law. These laws were estimated after considering data for a very large number of events. Thus it has become evident that there is a serious need to understand the process of fracture and breakdown using a probabilistic description within the framework of Statistical Physics. Using the tools provided in this branch of study one may be able to predict the occurrence of imminent failure.

There exist other types of breakdown of physical systems as well like the electric breakdown caused by high voltages. A most common example of this in nature is the lightning. During a thunderstorm, the thunderclouds have a build up of high concentrations of negative charge at its base which induces the ground below it to form a region of positive charge. This leads to a potential difference and a voltage is developed in the gap between the cloud and the ground. At a particular voltage strength the air between the cloud and ground becomes electrically conducting which leads to a burst of electric current flashing along the conductive pathway. These types of breakdown can be modeled to study electrical breakdown and is described in details in Sec. 1.4.

In this thesis, we will present some of our studies on the breakdown properties of materials taken in the form of a bundle of fibers. Presently, it has become apparent that the breakdown point of a bundle of fibers can be looked upon as a critical point that captures certain features of the well known phenomena of phase transition in the disciplines of condensed matter and statistical physics.

1.1 Leonardo DaVinci Experiment

The experiment by Leonardo DaVinci [7, 8] is referred as the first experiment for determining the strength of materials. This experiment measures the tensile strength of wires of different lengths. An empty bucket was attached to a wire of a specific length and diameter at one end and the other end was clamped to a fixed support (Fig. 1.2). A container filled with sand was suspended next to the wire with a hole in it such that the sand inside fell into the empty bucket at a certain rate. The wire broke when it could not support the weight of the bucket anymore and dropped in a hole that was customized according to the bucket's shape and was placed right under it to maintain the stability of the bucket after falling down. This experiment was repeated using various lengths of wires and it was concluded that longer wires are indeed weaker than shorter ones. This result was explained later by the argument that the material properties of a wire is not

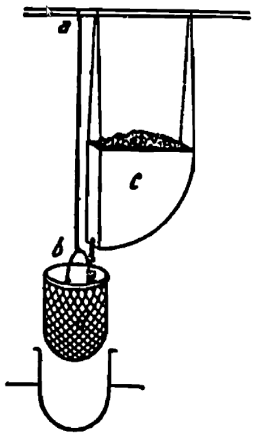

Figure 1.2: Experimental setup for measuring the strength of wires by Leonardo DaVinci [8].

homogeneous along it's length. In general, any material is truly inhomogeneous and has defects of many different sizes. The strength (or weakness) of a material sample is determined by the size of the largest defect; larger the defect, weaker is the sample. Therefore, the probability that a sample of wire would have a larger defect increases with the length of the wire. This implies that longer wire samples are weaker than shorter wires as had been observed in the DaVinci experiment.

1.2 Griffith's Energy Balance Concept

The relation between the strength of a material and the length of a crack was first studied by Griffith quantitatively using the concepts of thermodynamics [9]. He considered a plate of thickness B subjected to a load σ at its two ends normal to the crack length (Fig. 1.3(a)). A sharp crack of length $2a$ was introduced near the center of the plate. Introduction of a crack in the system reduces the mechanical energy which is composed of the elastic strain energy and the external work done to the system. This change in the energy ΔU_M due to introduction of the crack can be calculated in terms of external stress σ, plate size B, crack length a and elastic modulus E of the material:

$$\Delta U_M(a) = -\pi\sigma^2 a^2 B/E. \tag{1.1}$$

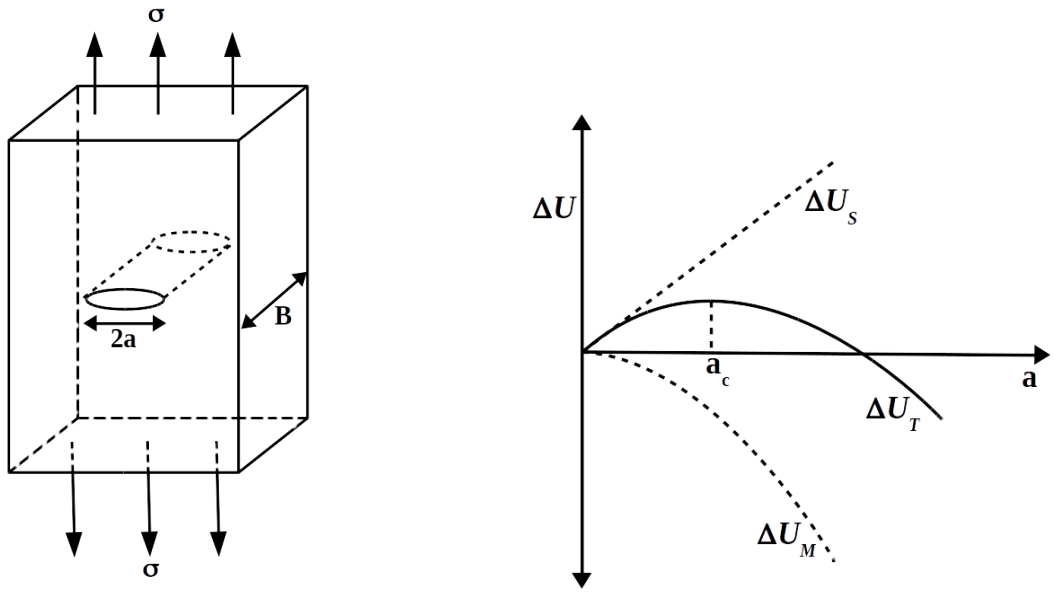

(a) (b)

Figure 1.3: Schematic diagrams of (a) a plate of width B with a crack of length $2a$ placed inside it and subjected to a uniform stress σ at both ends, and (b) the changes in mechanical energy ΔU_M, surface energy ΔU_S and the total energy ΔU_T against the crack length a. The maxima of ΔU_T occurs at the critical crack length a_c.

Introduction or propagation of a crack gives rise to two new free surfaces. Each new free surface is associated with a positive surface energy. Let γ represent the surface energy per unit area of the fracture surface. Then, the change in surface energy per unit area due to crack propagation is given by

$$\Delta U_S(a) = 4aB\gamma. \tag{1.2}$$

Thus, the total change in energy $\Delta U_T(a)$ comprises of two components given by the mechanical energy change $\Delta U_M(a)$ and the surface energy change $\Delta U_S(a)$ as

$$\Delta U_T(a) = \Delta U_M(a) + \Delta U_S(a) = -\pi\sigma^2 a^2 B/E + 4aB\gamma. \tag{1.3}$$

A schematic diagram of the plots for $\Delta U_M(a)$, $\Delta U_S(a)$ and $\Delta U_T(a)$ are shown in Fig. 1.3(b). The mechanical energy decreases because the growth of a crack releases elastic strain energy. The surface energy is an increasing function of crack length a as it is the energy required to overcome the intermolecular forces to create the surfaces of the crack. Since the mechanical energy decreases with increase in crack lengths and the surface

energy increases, the former favours elongation of the crack while the latter prevents it from happening. This is called the *Griffith energy-balance concept* which is given by $dU_T(a)/da = 0$. Therefore by applying this condition to Eq. (1.3) we get

$$\sigma_c = (2E\gamma/\pi a_c)^{1/2} \tag{1.4}$$

where σ_c is the critical value of the load applied and a_c is the critical crack length. This means that for a specific value of crack length a_c, all values of $\sigma < \sigma_c$ will not affect its length. But for $\sigma > \sigma_c$ the crack starts propagating catastrophically leading to fracture of the plate [10].

1.3 Types of fracture

In real world, we rarely come across materials that are completely perfect and are inherently disordered to some extent. This extent of disorderedness in materials plays a very important role in determining their breakdown properties. In fact, sometimes it is introduced artificially in materials to change their properties to a desired one. Depending on the level of disorderedness, the breakdown of materials under stress is mainly considered to be of two types namely, brittle and ductile.

Brittle fractures in materials occur abruptly without any kind of plastic deformation. It behaves elastically till it can endure a maximum load after which it fails catastrophically as shown in Fig. 1.4(a). This kind of fracture can be found in glass and some ceramic materials. Since these types of fractures occur very swiftly, they are not accompanied by any warning signals before complete failure of the system.

On the other hand, ductile materials exhibit considerable plastic deformation (called necking) before their catastrophic failure [11]. This type of fracture is mostly observed in metals under tensile stress and typically, the fracture proceeds through different stages as shown in Fig. 1.4(b). At the maximum load, voids begin to form in the necking region that coalesce gradually leading to the formation of larger cracks and finally break apart forming a "cup and cone" structure.

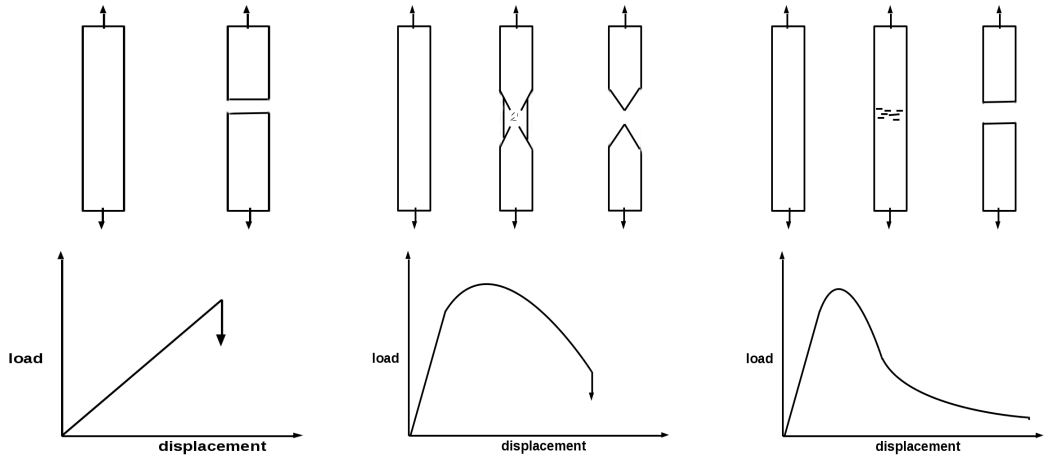

(a) (b) (c)

Figure 1.4: Different types of fracture (a) brittle, (b) ductile and (c) quasibrittle. This picture is taken from Ref. [11].

There exists another intermediate category of fracture called the quasi-brittle type fracture which can be found in many polycrystalline ceramics and cementitious materials. This type of fracture is associated with some measurable deformation before complete breakdown. The non-linear part of the load-displacement curve after the maximum load is called the softening branch as shown in the Fig. 1.4(c). It is characterized by the growth of existing defects in the material along with new defects being formed under constant loading. The crack front in this type of fracture is encompassed by a large fracture-process zone where progressive distributed cracking takes place.

Since the last two types of breakdowns are long drawn-out processes, it allows us to measure some precursors that help us in understanding whether the propagating crack is a stable or an unstable one leading to complete breakdown. Some studies have shown that these precursors can also be used to predict complete failure of the material [12]. Many natural disasters like land slide, mine collapse, earthquake end up causing immense loss of lives in its wake. Thus, research in this field to understand the underlying failure processes is extremely important to minimize these losses. This can lead us to correct detection of such warnings of imminent danger during a failure. Due to these concerns, scientific efforts have been made in this area to examine the microscopic mechanism and rupture process of disordered materials.

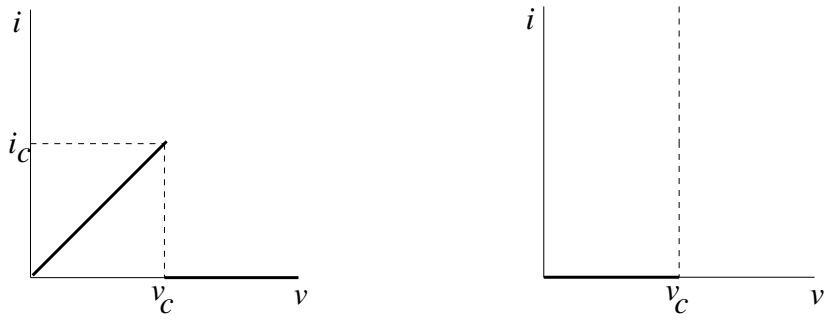

Figure 1.5: Current - Voltage ($i - v$) characteristic curves for (a) Fuse model [13] and (b) Dielectric breakdown model.

1.4 Electrical Breakdown

While the FBM is an example of mechanical breakdown that is the main topic of this thesis and has been explained in great details in Sec. 1.5, there can be other types of breakdown as well. One such breakdown is called the Electrical breakdown that can be seen to occur in devices like electrical fuses etc. Another type of breakdown called the dielectric breakdown is seen to occur in capacitors and more naturally in lightning as mentioned before. These types of breakdowns are examples of disordered systems and have been discussed in the following three subsections from the Statistical point of view using theoretical models.

1.4.1 Fuse Network

An electrical component is said to be a 'fuse' if it acts like a linear resistor if the applied voltage v across it is smaller than a threshold value v_c but it burns out and converts irreversibly to an insulator for $v > v_c$. A schematic diagram for the I-V characteristics for such a fuse has been shown in Fig. 1.5(a). A simple model of such a random electrical network had been studied by [13]. This network consists of random mixtures of resistors and fuses. How such a system undergoes a transition from a globally conducting phase to an insulating phase when the externally applied voltage is increases systematically has been studied in this model.

On a square lattice of size $L \times L$, each bond is occupied by a fuse with probability p, or by an insulator with probability $(1 - p)$. A cylindrical geometry has been used for the system i.e., it is periodic along the horizontal direction but open along the vertical direction across which the external voltage is applied. In the conducting state each bond has unit resistance, whereas v_c is also assumed to be unity for each bond as well. Starting from a high value of p one first ensures that the system is in a globally conducting state, i.e., there exists a spanning path of fuse bonds connecting the top and bottom boundaries. The conducting backbone of the network is identified, which is the subset of fuse bonds that conduct current. On this backbone the electrical potential at each node is estimated. There exists a hottest bond across which the voltage drop is maximum. The value V of the externally applied is then increased to V_{in} so that the voltage drop across the hottest bond reaches v_c and becomes sufficient to break it. Immediately there would be redistribution of voltages in the system but the system may still be conducting. Again the hottest bond in the system is identified and the external voltage is further increased to a value V'_{in} which is then broken again. This alternate process of increasing the external voltage and breaking the hottest bond is continued till the system ceases to have a globally conducting path of fuse bonds for an external voltage V_{fin}. Values of both V_{in} and V_{fin} are estimated scaled by the system size L. Numerical results in Ref. [13] observed a power law divergence of V_{fin} against the deviation from the percolation threshold $V_{fin} \approx (p - p_c)^{-z}$ with $z = 0.48 \pm 0.08$.

This model is further generalized by making the breaking voltages (currents) of different fuse bonds to be different [14]. Here all bonds of the lattice are fuse bonds and the breaking voltage v_i^c of a fuse bond i is assigned a random value drawing from a uniform distribution $p(v_c)$ defined over the range $1 - w/2 < v_c < 1 + w/2$ where the width parameter of the distribution can be tuned in the range $0 \leq w \leq 2$.

Let us first consider the limiting situation of $w \to 0$ i.e., when the distribution $p(v_c)$ is very sharp. Here, even the weakest fuse has a large breaking threshold $1 - w/2$ and for its failure the externally applied load needs to be very high. Consequently when this

bond is broken, a voltage redistribution takes place resulting in a situation where the voltage drops against a number of fuse bonds exceed their breaking thresholds. This is because in the limit of $w \to 0$, the breaking thresholds are very narrowly separated. Consequently breaking of these bonds results further breaking of fuse bonds and this cascading failure of fuse bonds eventually lead to the failure of the entire system. Such a system is called a 'brittle' system. A system is called brittle in which the failure of the weakest bond nucleates a crack that propagates across the entire system. On the other hand, a system is called ductile (quasi-brittle) in which there is a large range over which the individual bond breakings are driven by increases in the external potential. Kahng et al [14] by probabilistic argument established the existence of a transition between the brittle and ductile phases at a critical value of the system size dependent width parameter $w_c(L)$ which approaches 2 as $L \to 2$.

1.4.2 A Highly Disordered Fuse Model

Here the two dimensional system is considered in the form of an oriented square lattice. As before, each bond represents a fuse with unit resistance which can sustain a current i upto a maximum value of i_c. Therefore, i for $i > i_c$, the the fuse burns and the bond becomes an insulator with infinite resistance. The individual values for the breaking currents in the range $10^{-\beta} < i_c < 10^{\beta}$ have been drawn from a power law distribution $P(i_c) \sim i_c^{-1}$ (see Fig. 1.6). This is done by drawing random numbers R from the uniform distribution over the range $-1 < R < 1$ and defining $i_c = 10^{\beta R}$. It is assumed that the externally applied load is raised slowly from zero so that only one fuse bond burns at a time. The fuse bond having the maximal value $max(i/i_c)$ determines the next candidate to be burnt. After the failure of every fuse, the values of the potential at all sites are determined again [15].

One starts from a regular lattice of size $L \times L$, where all bonds are fuse bonds with different values of critical currents i_c. Initially all bonds carry currents. Then current carrying bonds are selected one by one determined by $max(i/i_c)$ and are burnt. The

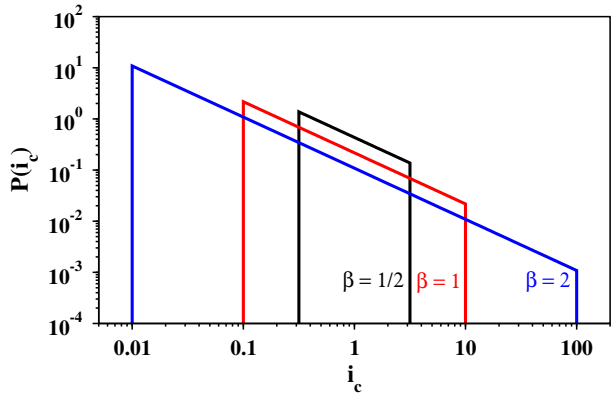

Figure 1.6: Plot of the normalized power law distribution functions $P(i_c)$ for the fuse bond breaking currents against the breaking current i_c have been shown using a double logarithmic scale. The functional form is: $P(i_c) \sim i_c^{-1}$ and this function is defined between $i_c = 10^{-\beta}$ to 10^{β}. The values of β = 1/2 (black), 1 (red) and 2 (blue) have been used.

burnt bonds are necessarily on the current carrying backbone of the cluster of fuse bonds spanning between top and bottom boundaries. There are no currents in all bonds of a dangling branch and therefore these bonds are never burnt. Consequently, the intact fuse bonds always form a single cluster until the entire system breaks and it ceases to carry any current. At this point a connected cluster of burnt bonds appear spanning the system in the horizontal direction.

Pictorially, every burnt bond is represented by the corresponding bond in the dual lattice, and colored red. Here, we present three different pictures which are the snapshots of burnt-intact bond configurations taken right after the global connectivity is lost. In the first case the strength of the disorder is chosen to be weak, and the value of β is tuned to be 0.01. Here the range of random values of i_c is very narrow. When a fuse bond is burnt, the nearby intact fuse bonds experience the maximal changes in their individual currents and as the distance increases the effect of burning also gradually fades away. This effect results, that for a narrow distribution of breaking currents, it is very likely that the next fuse bond to be burnt is selected from the local neighborhood. This is very much observed in Fig. 1.7 for $\beta = 0.01$ where a sequence of bonds are burnt one after another making only a linear path without branches, spanning the system in

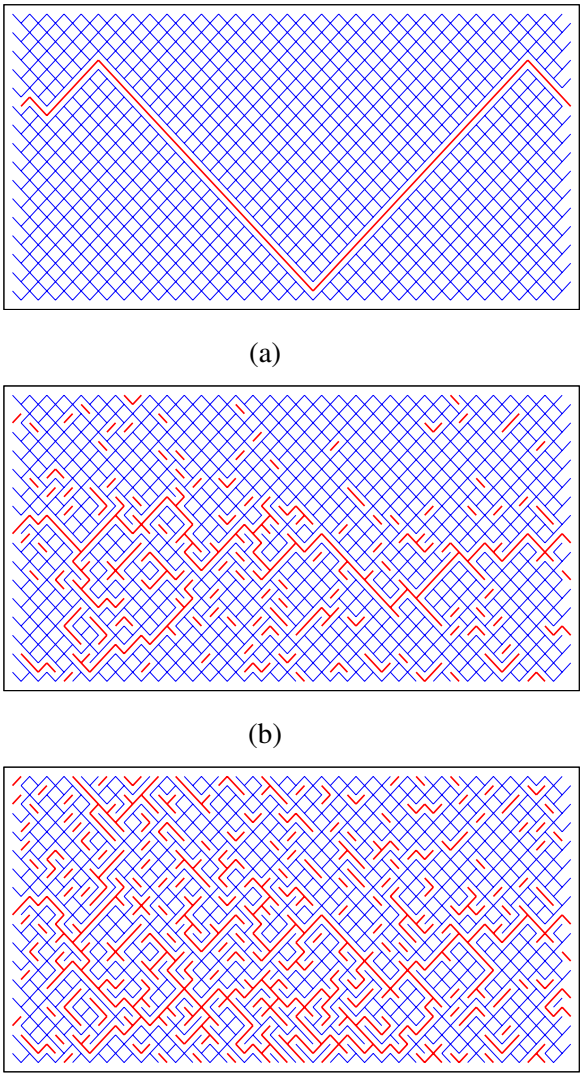

Figure 1.7: Snapshots of fracture patterns with β = (a) 0.01, (b) 1.0 and (c) 2.0 right after global connectivity of the current is lost in a highly disordered fuse model. The blue colour represents an intact bond and the red colour indicates a burnt bond [15].

the horizontal direction. For the intermediate disorder with $\beta = 1$, the burnt bonds are distributed all over the system. The fractured surface is more rough. Finally in the case of high disorder with $\beta = 2$ the backbone is very rough.

1.4.3 Dielectric Breakdown

In the dielectric breakdown problem, the situation is the opposite. It starts with a random mixture of conducting and insulating materials [16]. Again on a $L \times L$ square lattice, each

bond is labeled as a conductor with probability p and a dielectric with probability $(1-p)$. A dielectric bond can withstand a potential difference v across it upto a certain maximum value v_c and thereafter it burns out and becomes conducting (see Fig. 1.5(b)). It is assumed that all dielectric bonds are identical and are characterized by the same value of the breakdown voltage v_c. An external voltage difference V_B is applied between the top and the bottom boundaries and its value is tuned and gradually increased. Different lattice sites that are not connected to any conducting bonds are at different potentials in general. On the other hand, all lattice sites which belong to a cluster of a conducting bonds are at the same potential and its value differs from one cluster to the other. Depending on the random configuration of conducting bonds there exists one dielectric bond in the lattice which has the largest potential difference across it. The applied voltage V_B is gradually increased to a value so that the maximal potential difference across that particular bond reaches v_c. This bond burns immediately and become conducting. This results a redistribution of electric potentials at the lattice sites in general, including the sites of the conducting clusters. It may happen that due to redistribution, the potential differences across some more dielectric bonds now exceed v_c, therefore they would also fail. This way a cascade of dielectric bond failures take place, that stops when no more dielectric bond has potential difference larger than v_c. At this point, V_B is raised again so that the next avalanche of bond failures is triggered. This procedure is continued till a large cluster of conducting bonds appears that spans the system from the top to the bottom. The specific value of V_B at which the entire system becomes conducting is referred as the *Breakdown Voltage* and the current flows from the top to the bottom boundary through a spanning cluster of conducting bonds.

The precise value of the average breakdown voltage $V_B(p, L)$ depends on both the density p of conducting bonds as well as the system size L. It has been observed the average breakdown voltage vanishes as $V_B(p, L)/L \sim (p_c - p)^{t'}$ where p_c is the bond percolation threshold of the lattice and t' is referred as the breakdown exponent. It was estimated that for the square lattice $t' \approx 1.1$ [17].

1.5 The Fiber Bundle Model

The Fiber Bundle Model (FBM) describes the breakdown phenomena of materials in the form of a bunch of fibers in the disciplines of Material Science and Statistical Physics [6, 18–20]. The fiber bundle model was first studied by F. T. Pierce [21] in the year 1926 to study the strength of cotton fibers and yarns. Theories of statistics were used to study different properties of this model by H. E. Daniels [22]. About 20 years ago, this model again attracted the renewed attention of the community of statistical physics. A large number of papers have been published on different aspects as well as variants of this simple model that indeed exhibited very rich behaviour. There are different variations of the FBM that are also simple in nature. While some of them are analytically tractable, others require to be studied numerically. In fact, there are very extensive computer simulation studies in the literature of analytically non-tractable variants of the FBM to estimate their critical breakdown stresses and the associated exponents. In related topics, numerical studies have also been proven to be very useful to understand the failure mechanisms of real systems like fiber-reinforced composites [23–28], and also earthquakes [5, 20, 29–31] as well as traffic systems [32, 33] etc.

A fiber bundle consists of a collection of massless elastic fibers that are placed parallel to one another and are clamped at the two ends. For example, one can imagine that the upper end of all the fibers are attached to a clamp which is rigidly fixed with the ceiling. On the other hand the lower ends of the fibers are attached to a rigid horizontal bar. The entire bundle of fibers is subjected to an external stress. For example, a weight is suspended from the bar to provide the tunable stress. When a single fiber is subjected to a tensile stress, it experiences a longitudinal strain governed by the Hooke's Law. Under this linear regime of stress-strain characteristic, the fiber gets continuously strained on increasing stress but for only upto a certain maximum value of the stress. Beyond this value it is not able to withstand any additional stress and at this point it breaks. The minimum value of the external stress required to break the fiber is called the breaking stress of the fiber.

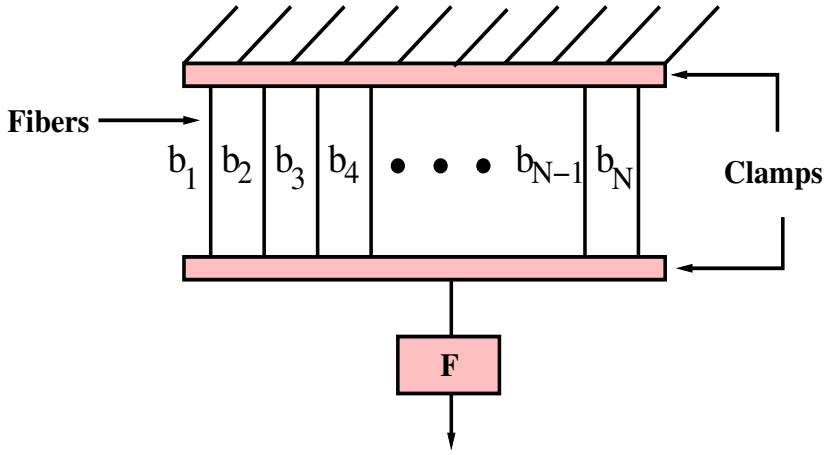

Figure 1.8: A schematic diagram of the fiber bundle model (FBM).

In FBM it is assumed that the precise values of the breaking stresses of individual fibers are distinctly different. In other words, every fiber has a unique breaking threshold that is different from the breaking thresholds of all other fibers. This implies that different fibers can withstand different amounts of stress before they break off. To mimic the disorder in real materials, the actual value of the breaking stress of each fiber is assigned randomly, drawing from a fixed probability distribution and its value remains constant through out the entire loading process.

The interaction among the fibers occur by a load redistribution process. The entire breaking dynamics is conservative, implying that in any arbitrary intermediate stage the total stress acting on the remaining intact fibers is equal to the external load applied on the system. When a fiber fails, the load carried by it is redistributed to the rest of the intact fibers in the bundle. It is assumed that if the clamps supporting the fibers are truly rigid, then the load will be redistributed equally to all the remaining intact fibers. On the other hand if the clamps are not rigid and can be deformed, then the intact fibers closest to the broken ones will receive more load compared to those at far away distances. After load redistribution, the intact fibers experience an enhanced stress acting on them. This enhancement of load may lead to the failure of additional fibers which can again eventually cause another set of fiber failures and this process continues like an avalanche [18, 19]. The FBM is also used in material science for considering

the failure of a system of pillars that are compressed longitudinally instead of being stretched [34, 35]. A schematic diagram of the FBM is shown in Fig. 1.8.

There are various versions of the FBM depending on the redistribution process of the released load. A very popular version is called the Equal Load Sharing (ELS) model where the clamps are considered to be infinitely rigid. Here, the load released by a broken fiber is equally redistributed to all remaining intact fibers in the bundle. Accordingly, fibers at large as well as small distances from the broken fiber receive equal shares of the released load. Clearly, this is a mean field model and in most cases its critical behaviour is analytically solvable [12, 22, 36–39].

In contrast, there exists another popular version of the FBM, called the Local Load Sharing (LLS) model where the clamps are not considered to be rigid [40–52]. In this case, the released load is distributed only to those intact fibers that are positioned in the vicinity of the broken fiber. A number of different prescriptions of load redistribution have been studied in the literature. The most common and widely discussed one among them is the case when the broken fiber transfers its load only to the nearest surviving neighbours [41, 47]. Another form of redistribution of load is where the amount of load received by a fiber decays as a power law when its distance from the broken fiber increases [49, 50]. This implies that the fibers far away from the broken fiber receive a very small fraction of the released load.

1.6 The Critical Stress

It is assumed that σ is the load per fiber which is applied to the bundle initially. The critical load of the fiber bundle, denoted by σ_c, is the minimal value of the external load per fiber such that a phase transition takes place between a phase $(\sigma < \sigma_c)$ of local failures to a phase $(\sigma > \sigma_c)$ of global failure where the entire system breaks down. It is now well known that the fiber bundle system exhibits various characteristics of the equilibrium critical phenomena at and around this point [18, 19].

Let us first describe the fiber bundle model consisting of N fibers under the Equal Load Sharing rule. The set $\{b_i\}$ of breaking thresholds of the fibers are drawn from a uniform threshold distribution $p(b)$ between $[0, 1]$. It's cumulative probability is given by

$$P(x) = \begin{cases} x, & \text{if} \quad 0 \leq x \leq 1 \\ 0, & \text{if} \quad x > 1. \end{cases} \tag{1.5}$$

Let an amount of external load $F = N\sigma$ be applied to the bundle at the initial stage when all N fibers are intact. This implies that each fiber is subjected to a load σ and consequently all fibers having breaking thresholds below σ would break simultaneously. On an average the number of such broken fibers is $NP(\sigma)$. Each of these fibers releases an amount of stress σ. Therefore, a total of $\sigma NP(\sigma)$ amount of stress is released which is equally distributed among remaining $N(1 - P(\sigma))$ intact fibers since load is considered to be a conserved quantity in this model. Let the new stress per fiber experienced by the intact fibers be denoted by x_t after the t-th step. Since the total load remains constant, the external applied load after the first step of redistribution is given by $F = Nx_1(1-P(\sigma))$. Using the same argument, at any instant of time during the loading process the total load is given by the stress per fiber in successive time steps $x_1, x_2, x_3, ...$ as,

$$F = Nx_1[1 - P(\sigma)] = Nx_2[1 - P(x_1)] = Nx_3[1 - P(x_2)]... \tag{1.6}$$

When a stable state is reached, the amount of stress received by each intact fiber is no longer sufficient to break even the weakest fiber of the remaining bundle. Therefore, on average, $(x_{t+1} - x_t) < 1/N$. At this stage one writes the applied load $F(x)$ as a function of the stress x per intact fiber at the stable state [12, 19].

$$F(x) = Nx[1 - P(x)]. \tag{1.7}$$

In Eq. (1.7), the quantity within the brackets is a monotonically decreasing function since the fraction of intact fibers would decrease with an increase in the value of x and x is a monotonically increasing function. Therefore the function $F(x)$, being the product

of an increasing and decreasing function, has a maximum and let that maximum occur at $x = x_c$. The criterion for the maximum $dF/dx = 0$ yields the following condition:

$$1 - P(x_c) - x_c p(x_c) = 0. \tag{1.8}$$

For a bundle with a uniform distribution of breaking thresholds $p(x) = 1$, one obtains $x_c = 1/2$ and $F_c = N/4$. The total critical applied load F_c corresponds to the critical initial load per fiber [19] for large N

$$\sigma_c = F_c/N = 1/4. \tag{1.9}$$

1.7 Avalanche dynamics

There are two different ways of loading the bundle with an external stress. In one way, the external load is increased in such a manner so that only one fiber breaks at a time. In the second way of loading the bundle, the applied stress per fiber is increased at a constant rate. In this process at every loading step multiple fibers can break simultaneously. The limiting case of this loading process is the first one which is called the quasi-static loading.

In both the processes when the extent of disorder is moderately high, the complete failure of the bundle never occurs in only one shot. Instead, it exhibits a series of bursts like activities, called "avalanches". In general, when a group of fibers break simultaneously, the net load released by them is redistributed among the remaining intact fibers depending on the different load redistribution rules. This enhances the loads of the intact fibers which may exceed their breaking threshold causing them to break. This iterative process continues till a stable state is reached. In a stable state either all the fibers are completely broken or the bundle is partly broken when the load per fiber is smaller than the breaking thresholds of all the intact fibers. The entire activity in the form of a sequence of steps, each step being associated with a number of fiber failures, is defined as an avalanche which stops when a stable state is reached. The total number of

fibers broken in the avalanche is called the size of the avalanche, which is a measure of the strength of the avalanche. Then the external load is increased again to start the next avalanche to break another set of fibers among the intact ones. This process continues till the complete failure of the bundle takes place.

One typically calculates the avalanche size distribution of this breakdown process which is estimated by the normalized frequency histogram of the avalanche sizes. It is seen to decay as a power law with an exponent of $5/2$ for the ELS case [41, 53]. It has been seen that this exponent value changes to $3/2$ when the avalanche size distribution is measured near breakdown of the bundle [54]. The change in the exponent values is a signature for complete breakdown and can be treated as a precursor of the failure. On the contrary, the avalanche size distribution in the LLS version of the FBM has no such power law [41].

1.8 Studies on transition from a brittle to a quasi-brittle phase in FBM

Systems like the FBMs display non-trivial breakdown properties and are used in the literature to understand its critical behaviour [6, 36, 55–57]. Here, the source of disorder is introduced in the form of breaking threshold values that are drawn from some pre-fixed random probability distribution. If the bundle has very little disorder in it then the fracture usually tends to be of brittle type. In the following discussions, the process of breakdown is modeled in the following way. An external load is applied to the bundle in such a way that only the weakest fiber among them breaks. If this causes a devastating avalanche of broken fibers leading to complete failure of the bundle, then it is described in the literature as a brittle bundle. On the other hand, if the avalanche stops before reaching complete failure with some fibers still intact in the stable state then it is described as a quasi-brittle bundle which is caused due to disorder in the system. This implies that for such a bundle more than one avalanche is required for complete failure. By altering the

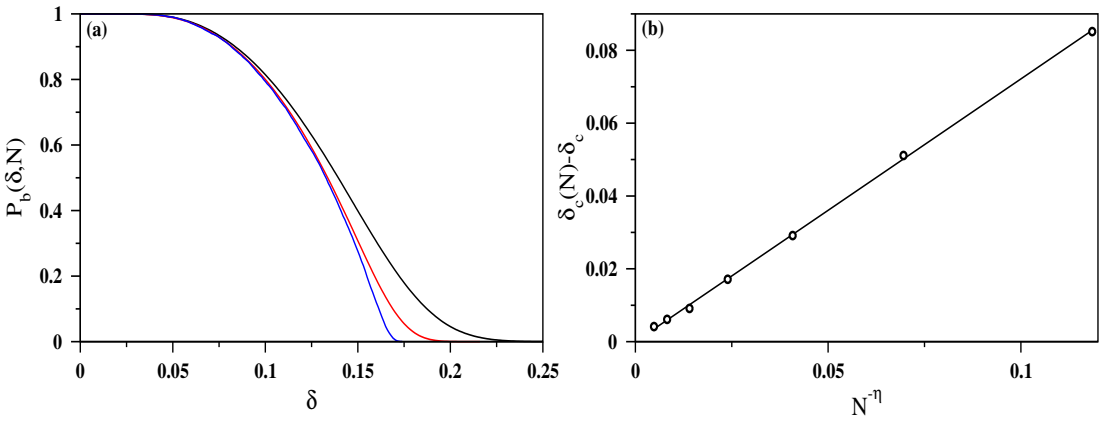

Figure 1.9: (a) Plot of the probability of brittle bundles $P_b(\delta, N)$ against tuning parameter δ for $N = 2^8$(black), 2^{10}(red) and 2^{16}(blue) with N increasing from right to left. (b) Plot of $\delta_c(N) - \delta_c$ against $N^{-\eta}$ with $\eta = 0.385$ and $\delta_c = 0.165$ [58].

extent of disorderedness in the system we can study the transition between these two types of fractures that have been discussed extensively in the following chapters.

The transition from a brittle to quasi-brittle state of a fiber bundle has been studied previously in certain models of the FBM in the literature. In a study done by Roy and Ray [58], they consider a FBM following the ELS rule of load redistribution where each fiber is assigned a random value of breaking threshold drawn from a uniform probability distribution within limits $\{1/2-\delta, 1/2+\delta\}$ with δ as a tuning parameter that determines the width of the uniform distribution. Thus, small values of δ means that the breaking threshold values of individual fibers are similar to each other implying less disorder in the system. On the other hand, a large value of δ leads to a wide variety of values for the breaking thresholds leading to greater disorder in the system. It is observed that for small values of δ the fiber bundle is mostly brittle and for large values of δ, the system is mostly quasi-brittle. Thus, by tuning the value δ one can obtain a transition between the brittle and the quasi-brittle phases of the bundle.

The critical width $\delta = \delta_c$ is found to be 1/6 from analytical calculations. Therefore, for $\delta < \delta_c$, the bundle is brittle, otherwise it is quasi-brittle. To estimate it numerically, the probability $P_b(\delta, N)$ is calculated that a randomly selected sample out of a large number of independent bundles is brittle. This quantity is ≈ 1 for very small values of δ and decreases continuously for increasing values of δ (Fig. 1.9(a)). This indicates that

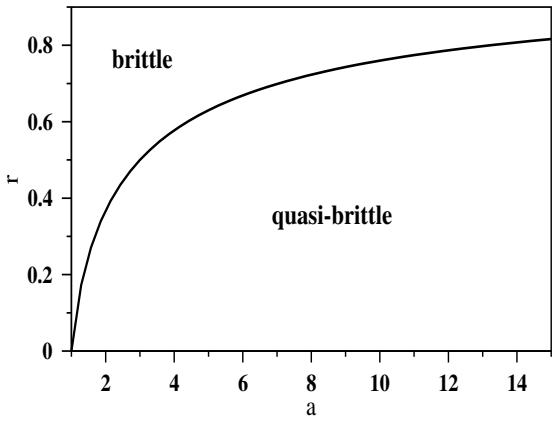

Figure 1.10: Plot of the phase diagram for the fiber bundle with power-law distributed values of Young's modulus E and constant breaking thresholds where r is the ratio E_{min}/E_{max} and a is the power-law exponent. The curve $r(a)$ denotes the transition points in the system [59].

the bundles are mostly brittle for a narrow distribution of breaking thresholds and mostly quasi-brittle for a wider distribution. The decrease in $P_b(\delta, N)$ becomes sharper with increase in bundle size N. The minimum value of δ at which $P_b(\delta, N) = 0$ is denoted by $\delta_c(N)$. The variation of $\delta_c(N)$ against N is plotted in Fig. 1.9(b) assuming that it follows the relation: $\delta_c(N) - \delta_c = AL^{-\eta}$; where A is a constant and $\eta = 0.33 \pm 0.02$. This process of finding the critical width has been explained in more details in Chapter 4 and Chapter 5.

In another study done by Karpas and Kun [59], a FBM is considered where the source of disorderedness in the model comes from the individual fibers having random values of Young's modulus E while keeping the breaking thresholds constant. A power law distribution is considered for the random values of Young's modulus $p(E) \sim E^{-a}$ within limits E_{min} and E_{max}. Their ratio $r = E_{min}/E_{max}$ is fixed and the exponent a is tuned to study the transition from a brittle to a quasi-brittle phase. In this way, they constructed a phase diagram in the $r - a$ plane where the critical curve given by $r_c(a) = (a-1)^{1/(2-a)}$ separates the brittle phase from the quasi-brittle phase as shown in Fig. 1.10.

1.9 Plan of the thesis

In the previous sections we briefly reviewed the literature of the FBM and discussed some variations of the model. In this thesis we have considered only the equal load sharing rule of the FBM. In Chapter 2, the relaxation time of the FBM has been discussed in more details. In Chapter 3, we examine a variant of the model where the breaking thresholds of the individual fibers are drawn from a power law distribution. In Chapter 4, we study a fiber bundle model with non-Hookean fibers and analyze its transition from a brittle to a quasi-brittle phase in details. Finally, in Chapter 5, we have studied the transition properties of a compound fiber bundle with bimodal distribution of the breaking thresholds.

CHAPTER 2

Scaling forms for relaxation times of the fiber bundle model

2.1 Introduction

When a physical system in a stable state is disturbed by any external force, it always tries to come back to its original state or to reach another stable state following its own prescribed dynamics. This relaxation behavior of the system due to external agitation, that involves moving between states, is characterized by a time period called the relaxation time. The damage in a FBM due to application of an external load is an irreversible change of stable states. It occurs in bursts of activity which is a recursive process of breaking fibers followed immediately by redistribution of the load released by the broken fibers. Since the stress applied to the bundle is a conserved quantity, this iterative process goes on till the bundle relaxes to a stable state [12, 19]. Here, a stable state can either be a state where the entire bundle has failed or a state where the bundle still has fibers intact in it. It should be noted that the relaxation time T [1] in the case of the FBMs is not real time. It is identified as a pseudo-time which is the total number of redistribution steps required to arrive at a stable state.

[1] The work reported in this chapter is based the publication "Scaling forms of relaxation times of the fiber bundle model", **Chandreyee Roy**, Sumanta Kundu and S. S. Manna, Phys. Rev. E, **87**, 062137 (2013).

It is important to understand that there are two different time scales involved in the process of loading a fiber bundle. One is associated to the number of times load is applied externally to the system that initiates an avalanche of breaking fibers and the other is associated to the number of load redistribution steps within an avalanche, after load has been applied externally to the system. In this chapter, the behavior of the relaxation time is studied by adding load in finite amounts to the intact bundle that may cause more than one fibers to fail at the same instant. In some realistic cases, fracturing in materials like ceramic rocks is always associated with the phenomenon "aging" that can happen due to thermally activated environmentally assisted stress corrosion [60]. Variations of the FBM that includes its fibers breaking due to a time dependent accumulated damage have been considered in Ref. [61–63]. However, in our study this mechanism has not been used and a fiber is assumed to break immediately when the load per fiber acting on it becomes greater than its threshold value. It has also been assumed that the load released by a broken fiber gets distributed instantaneously to the the rest of the intact fibers. In comparison there are some versions of the FBM where this process of load redistribution takes place at a finite speed [64, 65].

In this chapter, using extensive numerical methods we analyze the average relaxation time very near the critical point of the system at which the bundle fails completely. It is identified as the critical load per fiber σ_c as defined in Sec. 1.6 and at this point the system undergoes a change from a state of local failure to a state of global failure. Thus, σ_c acts similarly to the critical point of a phase transition and the behavior of the bundle around this point is associated with all characteristics of critical phenomena. In the case of fiber bundle following ELS dynamics, there are no spatial correlations since fibers at distances far away from the breaking fiber can also be affected by the load redistribution.

This chapter is organized in the following way. In Sec. 2.2 we describe the model in detail and the algorithm used to estimate the relaxation time. In Sec. 2.3 we show that away from the critical point the relaxation times obey the usual finite-size scaling theory. Interestingly, we find that the amplitude of variation has no logarithmic dependence

in the precritical regime as predicted in the mean-field theory of fiber bundles [12, 19]. Finally, we summarize our results in Sec. 2.4.

2.2 Model and Algorithm

We consider a completely intact bundle comprising of N fibers. Each of the individual fibers are assigned breaking thresholds $\{b_i\}$ drawn from a uniform distribution between $\{0, 1\}$. An external load per fiber σ is applied to the bundle. This causes the bundle to relax in a series of T successive time steps, following its own dynamics described in Sec. 1.7. When a fiber breaks, the released stress gets instantaneously distributed among all the intact fibers, which may cause more fibers to break in one relaxation step. The total number of relaxation time steps $T(\sigma, N)$ is measured for the corresponding initial applied load per fiber σ. This measurement is repeated for different σ values varying from 0 to 1/2 at intervals of $\Delta\sigma = 0.001$ using the same configuration of breaking thresholds $\{b_i\}$. The entire calculation is then reciprocated for a large sample of fiber bundles with uncorrelated sets of breaking thresholds $\{b_i\}$ and for different bundle sizes N.

It is observed that the average relaxation time $\langle T(\sigma, N)\rangle$ increases sharply as σ increases and has a finite but large peak at $\sigma_c \approx 1/4$. This is called the precritical regime and in this regime it is seen that after the system has reached a stable state, there still exist some intact fibers that have their breaking thresholds above the external load per fiber acting on them. The height of the peak near the critical point increases with increasing N as shown in Fig. 2.1. In the postcritical regime, $\langle T(\sigma, N)\rangle$ is seen to decrease gradually with further increase of σ beyond σ_c. In this regime a bundle breaks off completely when $\sigma > \sigma_c$ is applied to it. These numerical results on the relaxation dynamics are supported by mean-field calculations. In this analysis [12] it has been assumed that for a uniform distribution of breaking thresholds, the critical load per fiber is $\sigma_c = 1/4$ for all bundle

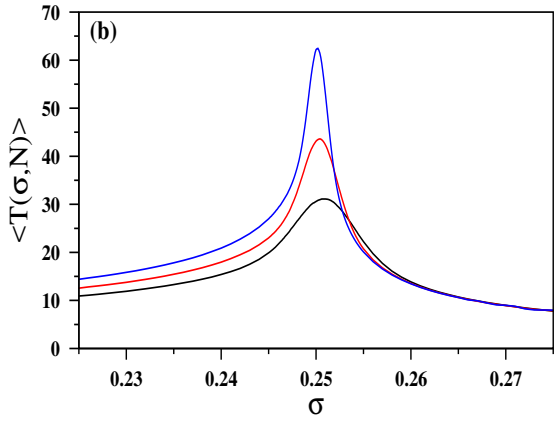

Figure 2.1: Plot of $\langle T(\sigma, N)\rangle$ against σ for bundle sizes N = 10000 (black), 30000 (red) and 100000 (blue); $\sigma_c \approx 0.25$.

sizes N. In the postcritical regime of $\sigma > \sigma_c$

$$T(\sigma, N) \approx \frac{\pi}{2}(\sigma - \sigma_c)^{-1/2} \tag{2.1}$$

and in the precritical regime of $\sigma < \sigma_c$

$$T(\sigma, N) \approx \frac{\ln(N)}{4}(\sigma_c - \sigma)^{-1/2}. \tag{2.2}$$

It is important to note that for fiber bundles with uniformly distributed breaking thresholds the average critical applied load per fiber σ_c = 1/4 is valid only for infinitely large bundles i.e., for $N \to \infty$. For bundles of finite sizes the critical load depends on N and therefore, we need to calculate $\sigma_c(N)$ for different values of N. The critical applied load $\sigma_c^{\alpha}(N)$ for a particular fiber bundle α using a given set of breaking thresholds $\{b_i\}$ is defined as the maximum value of the applied load σ per fiber for which the system remains in the precritical state. This means that if the applied load is increased by the least possible amount to break only a single additional fiber among the intact ones, then the system crosses over to the postcritical state. On an average, this requires enhancing the applied load by $1/N$.

The value of $\sigma_c^{\alpha}(N)$ for the α_{th} configuration of breaking thresholds can be numerically estimated in two different ways. The first is the bisection method where the simulation is started with an arbitrary pair of initial guesses for the values of σ_{pre}^{α} and σ_{post}^{α} corresponding to the precritical and postcritical states respectively. In the precritical

state the relaxation dynamics stops without breaking the entire bundle whereas in the postcritical state all fibers in the entire bundle break. The mean of the two stress values, $\sigma = (\sigma^{\alpha}_{pre} + \sigma^{\alpha}_{post})/2$, is applied to the bundle and then allowed to relax to a stable state. If the final stable state is precritical, then σ^{α}_{pre} is raised to σ; otherwise σ^{α}_{post} is reduced to σ. This procedure is iterated till $\sigma^{min}_{post} - \sigma^{max}_{pre} \leq 1/N$ and at this stage we define $\sigma^{\alpha}_{c}(N) = (\sigma^{\alpha}_{pre} + \sigma^{\alpha}_{post})/2$. This procedure is then repeated for a large samples of un-correlated bundles α and their critical loads are averaged over them to obtain $\sigma_c(N) = \langle \sigma^{\alpha}_{c}(N) \rangle$ for a fixed bundle of size N. Finally, the entire calculation has been repeated for different N values.

The critical initial load per fiber $\sigma^{\alpha}_{c}(N)$ can also be calculated in a more straightforward method. The breaking thresholds are arranged in ascending order i.e. $b^{\alpha}_{(1)} < b^{\alpha}_{(2)} < b^{\alpha}_{(3)} < ... < b^{\alpha}_{(N)}$ for a particular bundle configuration α. The bundle will support the initially applied load per fiber σ if the conditions $\sigma < b^{\alpha}_{(1)}$ or $\sigma N/(N-1) < b^{\alpha}_{(2)}$ or $\sigma N/(N-2) < b^{\alpha}_{(3)}$ or . . . $\sigma N < b^{\alpha}_{(N)}$ are satisfied. If all these inequalities fail to satisfy then the bundle will no longer support the load and it will break apart. Now if σ is such that it is sufficient to break n fibers, then at this stage the bundle will support the load if $\sigma N/(N-n) < b^{\alpha}_{(n+1)}$, i.e.,

$$\sigma < [(N-n)/N] b^{\alpha}_{(n+1)}. \tag{2.3}$$

The term inside the parenthesis of the above equation decreases with n and b^{α}_{n+1} is an increasing function of n since the breaking thresholds are pre-arranged in increasing order. Thus, the function at the right-hand side of Eq. (2.3) will have a maximum value at some n and if the external load σ is raised to this maximum value, then the bundle will break immediately. So the maximum of $[(N-n)/N] b^{\alpha}_{(n+1)}$ determines the critical load per fiber for the bundle α. Therefore [66–68],

$$\sigma^{\alpha}_{c}(N) = \max\Big\{ b^{\alpha}_{(1)}, \frac{N-1}{N} b^{\alpha}_{(2)}, \frac{N-2}{N} b^{\alpha}_{(3)}, ..., \frac{1}{N} b^{\alpha}_{(N)} \Big\}. \tag{2.4}$$

In both these methods the major share of the CPU is used up to sort the breaking thresholds in an increasing sequence. The well-known QUICKSORT method takes CPU

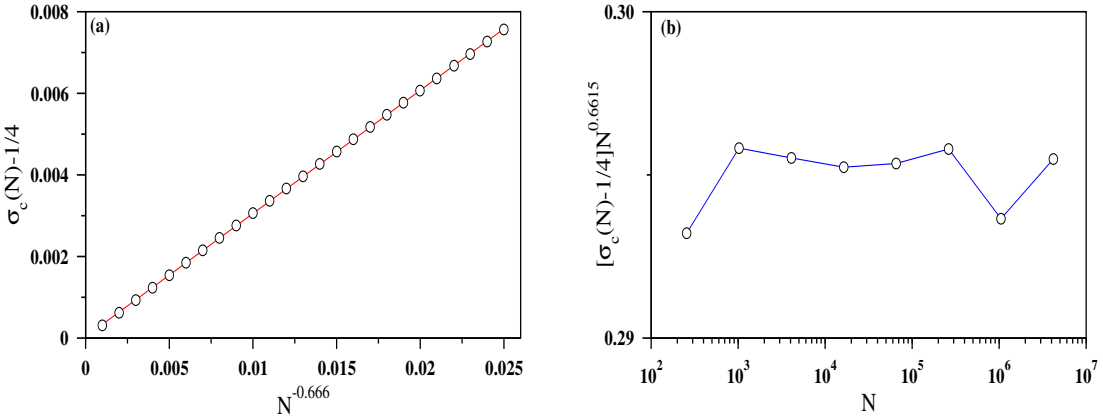

Figure 2.2: (a) Plot of $\sigma_c(N) - 1/4$ with $N^{-0.666}$ for system sizes up to $N = 31623$ which fits nicely to a straight line that passes very close to the origin. (b) Data for larger values of N upto 2^{22} are plotted as $[\sigma_c(N) - 1/4]N^{0.6615}$ against $ln(N)$, which exhibits approximately constant variation.

of the order of $N\ ln(N)$ [69]. On comparing the two different methods we see that the bisection method takes little more time, e.g., for a single bundle of $N = 2^{24}$ the bisection method takes ≈ 1.15 times the time required in the second method.

2.3 Results

2.3.1 The critical stress

The $\sigma_c^\alpha(N)$ for a particular bundle α is calculated for a bundle of size N. This is first averaged over a large number of samples to get $\langle\sigma_c^\alpha(N)\rangle = \sigma_c(N)$. Then we calculate these average values for increasing sizes of N and assume that they converge to a specific value $\sigma_c = \sigma_c(\infty)$ as $N \to \infty$ according to the following form:

$$\sigma_c(N) - \sigma_c = AN^{-1/\nu} \tag{2.5}$$

where ν is a critical exponent. The $\sigma_c(N)$ values have been plotted in Fig. 2.2(a). We show a plot of $\sigma_c(N) - \sigma_c(\infty)$ against $N^{-1/\nu}$ using $\sigma_c(\infty) = 0.25$ with $1/\nu = 0.666$ such that the plots fit to an excellent straight line. The least square fitted straight line misses the origin very closely and has the form $\sigma_c(N) - 1/4 = 3.33 \times 10^{-5} + 0.302N^{-1/\nu}$. In Fig. 2.2(b) the data for larger values of N is plotted as $[\sigma_c(N) - 1/4]N^{0.661}$ against

N on a lin - log scale. The intermediate part appears approximately constant implying again that $1/\nu \approx 0.662$. Thus, we conclude that $\nu = 1.50(2)$ and $\sigma_c(\infty) = 0.2500(1)$. We conjecture that the finite size correction exponent $\nu = 3/2$ and $\sigma_c(\infty) = 1/4$ exactly [70]. These results are well known in the literature from analytical studies in Ref. [67, 68]. It has been estimated that [67]

$$\sigma_c(N) = \sigma_C + 0.996 N^{-2/3} \beta_c, \tag{2.6}$$

where

$$\beta_c = \left[\frac{P'(x_c)^2 x_c^4}{2P'(x_c) + x_c P''(x_c)} \right]^{1/3}, \tag{2.7}$$

where $P'(x) = dP/dx = p(x)$. In our case with the uniformly distributed breaking thresholds in the range $\{0, 1\}$; $P(x) = x$ which gives $\sigma_c = 1/4$, $x_c = 1/2$, $P'(x) = 1$, and $P''(x) = 0$ for all $0 < x < 1$, which makes $\beta_c = (1/2)^{5/3} \approx 0.3150$. This gives

$$\sigma_c(N) - \sigma_c = 0.996 N^{-2/3} \beta_c = 0.3137 N^{-2/3}. \tag{2.8}$$

Accordingly, apart from the exponent $\nu = 3/2$, one can also check the value of the amplitude A, which is estimated numerically as 0.302 compared to its analytically obtained value of 0.3137. The correspondence between the two values is quite good and this is a confirmation of the rigorous result of Ref. [67].

The distribution of the values of the critical loads per fiber $\sigma_c^\alpha(N)$ for a large uncorrelated samples of fiber bundles of specific size N is known to follow a Gaussian distribution around its mean value $\sigma_c(N) = \langle \sigma_c^\alpha(N) \rangle$. Let its cumulative distribution be denoted by $\mathcal{H}_N(\sigma_c^\alpha)$. As the bundle size increases to very large values, this cumulative distribution approaches its Gaussian approximation $\Phi_N(\sigma_c^\alpha)$ which is also the cumulative distribution of the Gaussian form:

$$A \exp\big\{ -(\sigma_c^\alpha - \sigma_c)^2/(2s^2) \big\}, \tag{2.9}$$

where $\sigma_c = x_c[1 - P(x_c)] = 1/4$, $s = \gamma_c N^{-1/2}$, and $\gamma_c = x_c P(x_c)[1 - P(x_c)]^{1/2}$. Using these results, it has been shown that [67]

$$\chi(N) = \max |\mathcal{H}_N(\sigma_c^\alpha) - \phi_N(\sigma_c^\alpha)| < K N^{-1/6}. \tag{2.10}$$

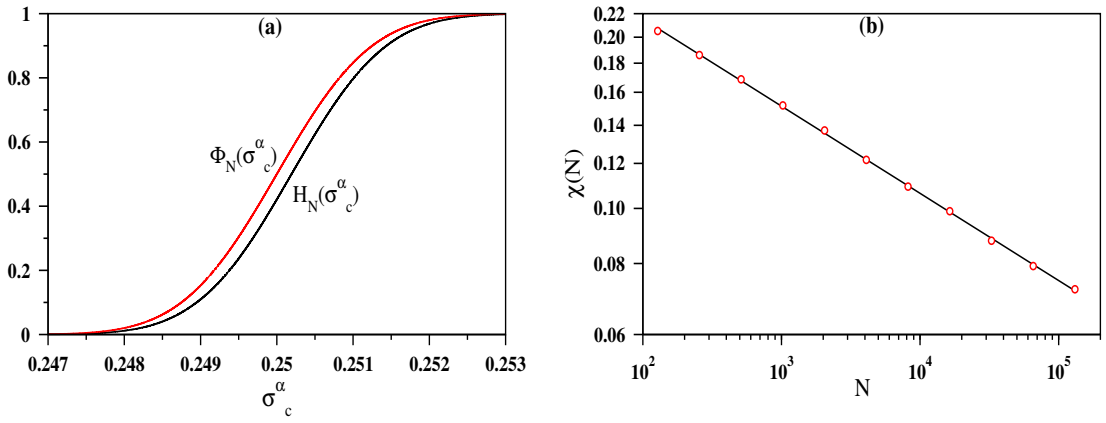

Figure 2.3: (a) Plot of the cumulative probability distribution of $\mathcal{H}_N(\sigma_c^\alpha)$ for $N = 2^{16}$ and for a sample size of 10^6 bundles with red . The cumulative distribution of the Gaussian approximation $\phi_N(\sigma_c^\alpha)$ also is plotted using black. (b) The maximal difference $\chi(N)$ between two cumulative distributions is plotted against N using the log-log scale. The slope is found to be 0.155(5).

This relation is also verified numerically in Fig. 2.3(a). For the bundle size $N = 2^{16}$, the cumulative distribution $\mathcal{H}_N(\sigma_c^\alpha)$ obtained from simulation and the $\phi_N(\sigma_c^\alpha)$ obtained from the Gaussian approximation are plotted. In simulation, we study a sample size of 10^6 bundles for each bundle of size N. The critical loads σ_c^αs obtained are arranged in the increasing order which implies that the number of such thresholds below a certain σ_c^α is simply the $\mathcal{H}_N(\sigma_c^\alpha)$. For each of these σ_c^α values the cumulative Gaussian function $\phi_N(\sigma_c^\alpha)$ is calculated. The absolute value of the difference between these two distributions is estimated for each σ_c^α and their maximal value $\chi(N)$ is obtained. In Fig. 2.3(b) the function $\chi(N)$ is plotted with N on a log-log scale for 11 different bundle sizes. A power-law variation of $\chi(N)$ is observed as follows:

$$\chi(N) \sim N^{-\kappa} \tag{2.11}$$

with $\kappa = 0.155(5)$ [Fig. 2.3(b)].

2.3.2 Relaxation time at the critical point

After calculating the system-size-dependence of the critical loads $\sigma_c(N)$ we studied how the average relaxation time $\langle T(\sigma)\rangle$ diverges as the critical load is approached. For every bundle α we first calculated its critical load σ_c^α using either of the two methods

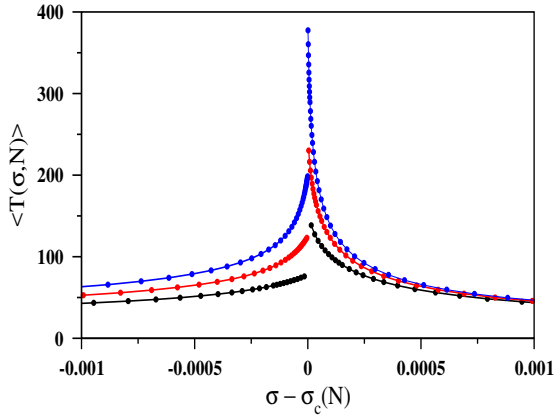

Figure 2.4: Plot of $\langle T(\sigma, N)\rangle$ with the deviation from the critical point $\sigma - \sigma_c(N)$ per fiber for $N = 2^{16}$ (black), 2^{18} (red) and 2^{20} (blue). Here, for each bundle α first its critical point σ_c^α is determined. Then for the same bundle the relaxation times are measured for prefixed deviation from σ_c^α and then averaged over.

described in Sec. 2.2. Then, for the same bundle we calculated the relaxation times for certain pre-fixed deviations $|\Delta\sigma| = |\sigma_c^\alpha - \sigma|$ from the critical stress and averaged them over different uncorrelated bundles. Fig. 2.4 shows how $\langle T(\sigma, N)\rangle$ approaches the critical relaxation time as $\sigma \to \sigma_c(N)$ i.e., $|\Delta\sigma| \to 0$. We observe that there exists a distinctive jump in the relaxation time at the critical point when $|\Delta\sigma| \to 0$ as opposed to a continuous curve observed in Ref. [12]. We denote the limiting relaxation times at the critical point in the precritical and postcritical states as $\langle T^{pre}(\sigma_c(N), N)\rangle$ and $\langle T^{post}(\sigma_c(N), N)\rangle$ respectively. Then we calculated the average relaxation time T when the applied load per fiber takes the critical load value. For every bundle α, there are two different values of T corresponding to the two states at the critical point. More specifically T^{pre} denotes the relaxation time corresponding to maximal σ_{pre}^α, i.e., the largest value of T in the precritical state. Similarly T^{post} is the largest value of T in the postcritical state corresponding to the minimal value of σ_{post}^α. It is observed that T^{post} is much larger than T^{pre}. On averaging over a large sample size $\langle T^{post}\rangle / \langle T^{pre}\rangle$ approaches to 2 as $N \to \infty$ [71].

In Fig. 2.5(a) the values of $\langle T^{pre}(\sigma_c(N), N)\rangle$ and $\langle T^{post}(\sigma_c(N), N)\rangle$ against N are plotted on a $\log - \log$ scale for a wide range of values of N extending from 2^8 to 2^{24} where at each step the system size is increased by a factor of 4. Both the curves are

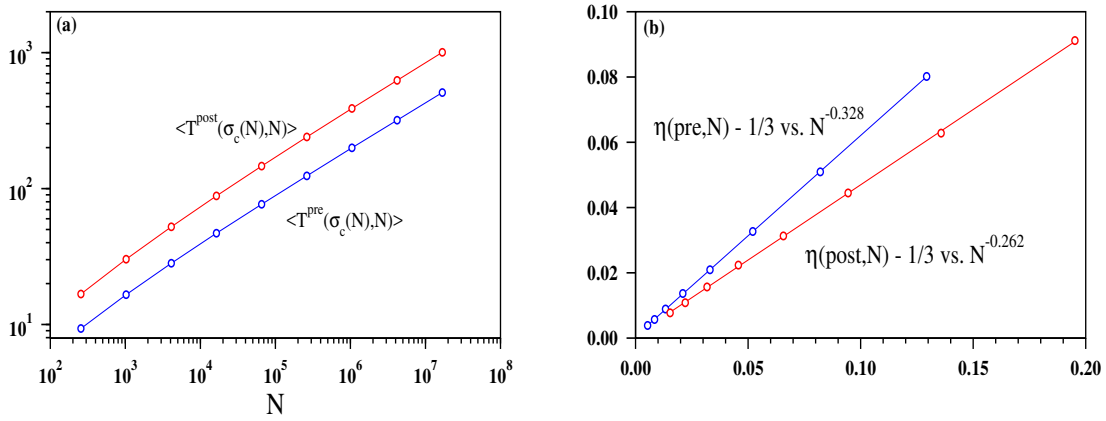

Figure 2.5: (a) Plots of the average maximal relaxation time $\langle T^{post}(\sigma_c(N), N)\rangle$ in the postcritical regime (red) and the average maximal relaxation time $\langle T^{pre}(\sigma_c(N), N)\rangle$ in the precritical regime (blue) against the system size N using $\log - \log$ scale. Both plots exhibit certain amount of curvature for small N. (b) Slopes $\eta(N)$ between successive points in (a) are estimated and $\eta(N) - 1/3$ are extrapolated against $N^{-0.328}$ and $N^{-0.262}$ for precritical and postcritical regime respectively. The solid lines are obtained by least square fits that pass very close to the origin for both the plots.

seen to be nearly straight and parallel for large N but have slight curvatures for small N values. Till $N = 2^{22}$ the averaging has been done for 10^6 independent configurations of the fiber bundle and for $N = 2^{24}$ a total of 409000 independent configurations have been used. Therefore, the data points are accurate enough to be analyzed more precisely. The slope between two successive points in Fig. 2.5(a) is denoted as $\eta(N)$ and we observe that these slopes gradually approach 1/3 for larger system sizes in both the precritical and postcritical regimes. This estimation was carried out by using suitable extrapolation methods minimizing the errors. Fig. 2.5(b) shows the extrapolated $\eta(pre, N) - 1/3$ against $N^{-0.328}$ and $\eta(post, N) - 1/3$ against $N^{-0.262}$ for the precritical and postcritical regimes respectively. The individual plots fit excellently to straight lines and their intercepts with the vertical axes are 0.00061 and 0.00085 respectively. Thus, we conclude that when the system is loaded with the precise value of the critical stress the relaxation time grows as a power of the system size as:

$$\langle T(\sigma_c(N), N)\rangle \sim N^{\eta}, \tag{2.12}$$

with $\eta = 0.333(1)$.

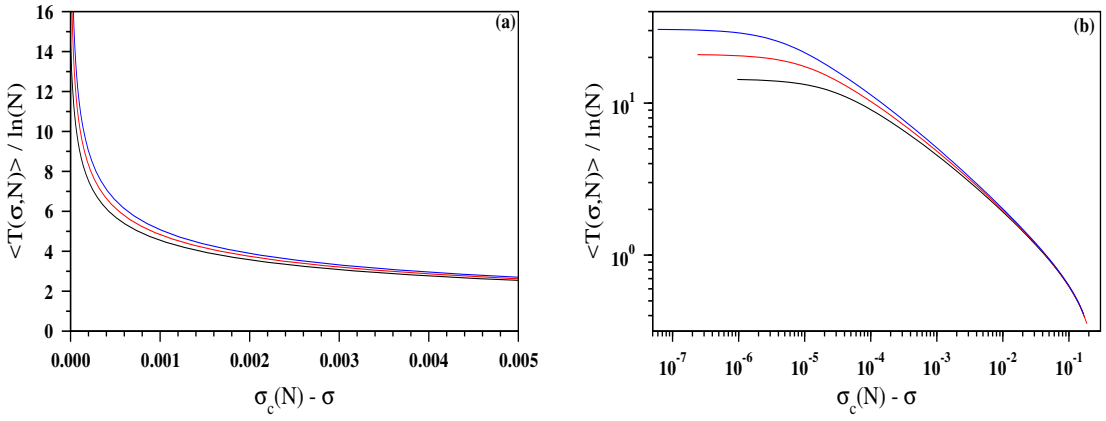

Figure 2.6: (a) Comparison with the similar plots in Ref. [12]. Plot of $\langle T(\sigma, N)\rangle/ln(N)$ against $\Delta\sigma = \sigma_c(N) - \sigma$ for the precritical regime but for much smaller window of $\Delta\sigma$ = 0.005 and for $N = 2^{20}$ (black), 2^{22} (red) and 2^{24} (blue) with N increasing from left to right. On a lin-lin scale the three plots separate out from one another as $\Delta\sigma \to 0$. (b) The data in (a) are replotted on a $\log - \log$ scale and the absence of data collapse is clearly visible in this plot, with N increasing from bottom to top.

2.3.3 Relaxation time away from the critical point

Next, we compare our data for relaxation times away from the critical point with similar data in Ref. [12] where the assumption was that $\sigma_c = 1/4$ for all bundles. The plot for $\langle T(\sigma, N)\rangle/\ln(N)$ against $\sigma_c(N) - \sigma$ for the precritical regime for three different system sizes is shown in Fig. 2.6(a) on a linear scale. The data for large sample sizes of the bundle yielded very little noise enabling us to plot for a much smaller window size i.e. $\Delta\sigma = 0.005$ compared to Ref. [12]. It is seen that as we approach the critical point i.e. $\Delta\sigma \to 0$, the three curves separate out distinctly and systematically from each other. Thus, the data collapse exhibited in Ref. [12] is perhaps not working well in this limiting situation. In Fig. 2.6(b) the same data have been plotted but using a $\log - \log$ scale and here the failure of data collapse is even more pronounced. This difference in the two plots may be because the claimed validity of data collapse exhibited in Ref. [12] is for a window size 10 times larger than ours. On approaching the critical point even closer by reducing the window size we noticed that the scaling by $ln(N)$ no longer works in the vicinity of the critical point. Instead we show that a simple power-law scaling works quite well.

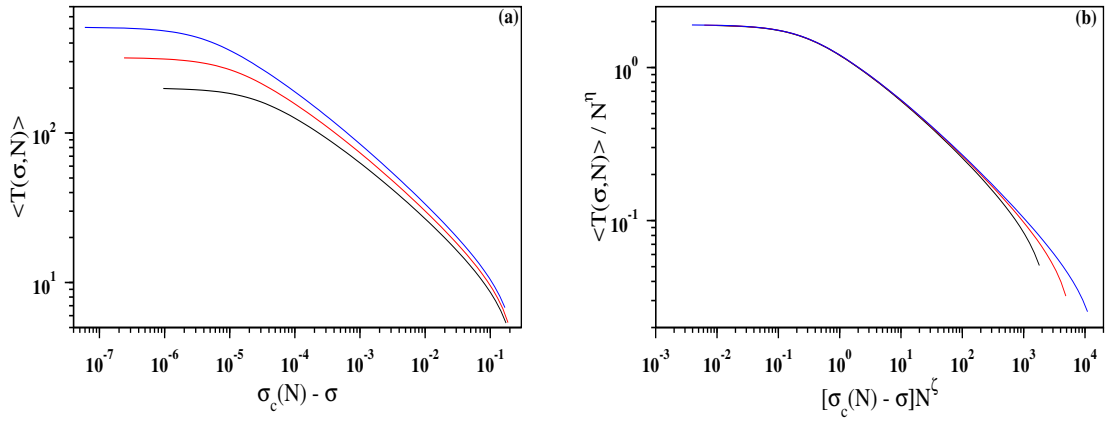

Figure 2.7: Scaling for the precritical regime. (a) Plot of $\langle T(\sigma, N)\rangle$ against $\sigma_c(N) - \sigma$ and for $N = 2^{20}$ (black), 2^{22} (red) and 2^{24} (blue) with N increasing from bottom to top. (b) The data in (a) are scaled suitably: $\langle T(\sigma, N)\rangle/N^{\eta}$ against $[\sigma_c(N) - \sigma]N^{\zeta}$ exhibits a good collapse of the data as $\Delta\sigma \to 0$ with $\eta = 0.336$ and $\zeta = 0.666$, with N increasing from left to right.

The data for $\langle T(\sigma, N)\rangle$ against $\sigma_c(N) - \sigma$ is replotted in Fig. 2.7(a) for the precritical regime in a log-log scale. The plots corresponding to three different N values are seen to be completely separated from each other. We carry out a finite size scaling of the two axes as shown in Fig. 2.7(b) by use of appropriate powers of the bundle size N. This indeed results in an excellent collapse of the data for the three different bundle sizes. This implies that the following scaling form may be used to describe the collapse:

$$\langle T(\sigma, N)\rangle/N^{\eta} \sim \mathcal{G}[\{\sigma_c(N) - \sigma\}N^{\zeta}]. \tag{2.13}$$

where $\mathcal{G}$ is an universal scaling function of the scaled variable y. The best possible tuned values of the scaling exponents obtained are $\eta = 0.336$ and $\zeta = 0.666$. The collapsed plots have two different regimes, an initial constant part for very small values of $\Delta\sigma = \sigma_c(N) - \sigma$. In this regime the scaled variable $[\langle T(\sigma, N)\rangle]/N^{\eta}$ is a constant, say $\mathcal{C}$. This means that $\langle T(\sigma, N)\rangle = \mathcal{C}N^{\eta}$ which is the retrieval of the Eq. (2.12). This constant regime of $\langle T(\sigma, N)\rangle]/N^{\eta}$ extends approximately up to $\{\sigma_c(N) - \sigma\}N^{\zeta} \approx 1$. This implies that the width of the constant regime is:

$$\sigma_c(N) - \sigma \sim N^{-\zeta}. \tag{2.14}$$

The exponent ζ can also be interpreted in the following way. For a certain bundle size

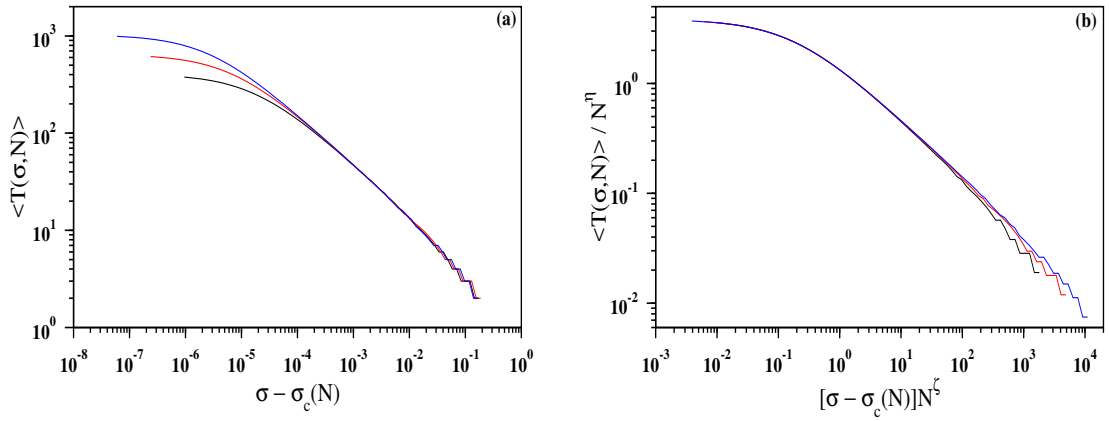

Figure 2.8: Scaling for the postcritical regime. (a) Plot of $\langle T(\sigma, N)\rangle$ against $\sigma - \sigma_c(N)$ and for $N = 2^{20}$ (black), 2^{22} (red) and 2^{24} (blue) with N increasing from bottom to top. (b) The data in (a) are scaled suitably: $\langle T(\sigma, N)\rangle/N^{\eta}$ against $[\sigma - \sigma_c(N)]N^{\zeta}$ exhibits a good collapse of the data as $\Delta\sigma \to 0$ with $\eta = 0.336$ and $\zeta = 0.666$, with N increasing from left to right.

N there exists a specific value of $|\Delta\sigma(eq, N)|$, where $\langle T(pre, \sigma, N)\rangle = \langle T(post, \sigma, N)\rangle$. Around this window size $\langle T(pre, \sigma, N)\rangle > \langle T(post, \sigma, N)\rangle$ for $|\Delta\sigma(N)| > |\Delta\sigma(eq, N)|$ and $\langle T(pre, \sigma, N)\rangle < \langle T(post, \sigma, N)\rangle$ for $|\Delta\sigma(N)| < |\Delta\sigma(eq, N)|$. We have verified that $|\Delta\sigma(eq, N)|$ also approaches zero as $N^{-\zeta}$ with $\zeta \approx 0.666$. The exponent ζ is recognized as the inverse of the exponent ν defined in Eq. (2.5).

Beyond this constant regime there is the power law regime. Assuming that the scaling in Fig. 2.7(b) is valid for all bundle sizes till $N \to \infty$ one would expect an N independent power law form holds in this limit:

$$\langle T(\sigma)\rangle \sim (\sigma_c - \sigma)^{-\tau}. \tag{2.15}$$

To ensure that Eq. (2.15) indeed holds good we need to assume $\mathcal{G}(y) \sim y^{-\tau}$ which implies the following scaling relation:

$$-\tau\zeta + \eta = 0 \tag{2.16}$$

and, therefore, $\tau = \eta/\zeta = 0.50(1)$.

In Fig. 2.8 we show similar plots for the postcritical regime. We show a plot of $\langle T(\sigma, N)\rangle$ against $\sigma - \sigma_c(N)$ on a log-log scale in Fig. 2.8(a). The same data is scaled suitably and plotted in Fig. 2.8(b) as $\langle T(\sigma, N)\rangle/N^{\eta}$ against $[\sigma - \sigma_c(N)]N^{\zeta}$ which again

shows a very nice data collapse. Here also the exponent values obtained are very similar to the values found in the precritical regime with $\eta = 0.336$ and $\zeta = 0.666$. The range of validity of the finite-size scaling form in Eq. (2.13) may be determined from Fig. 2.8(b). Here the data collapse is observed from the smallest value of $[\sigma_c(N) - \sigma]N^{\zeta}$ to about 100. Therefore, the range of validity is $1/N < [\sigma_c(N) - \sigma] < 100N^{-\zeta}$.

We have repeated all the calculations again for fiber bundles having their breaking thresholds drawn from a more general distribution like the Weibull distribution. The cumulative distribution is given by

$$P(\sigma) = 1 - exp(-\sigma^{\rho)} \tag{2.17}$$

with the shape parameter $\rho = 5$ and the scale parameter 1. A similar use of Smith's results yield $\sigma_c = (\rho e)^{-1/\rho}, x_c = \rho^{-1/\rho}$, and $\beta_c = \rho^{(\rho+3)/(3\rho)}e^{-1/3\rho}$. Using $\rho = 5$ gives $\beta_c = 5^{-8/15}e^{-1/15} = 0.3965$. This gives

$$\sigma_c(N) - \sigma_c = 0.3949N^{-2/3}. \tag{2.18}$$

The values of $\sigma_c(N)$ are estimated numerically using five different bundle sizes between 2^{16} to 2^{24} with the sizes increased by a factor of 4 at every step. We plot these values against $N^{-2/3}$ and extrapolate it to obtain $\sigma_c(\infty) = 0.5934(10)$ for $N \to \infty$ and $A = 0.392(4)$. These results are very much consistent with the analytical results. We have also estimated the exponents ν, η, ζ and τ whose values are quite consistent with similar exponents with uniformly distributed breaking thresholds. These values of the critical exponents have been summarized in Table 2.1.

2.3.4 Relaxation time for a deterministic FBM

Next, we consider a simpler version of the FBM which is the deterministic case. Here, the breaking thresholds of the N fibers are uniformly spaced as $b_i = n/N$ where $n = 1, 2, 3, ..., N$. Since this case does not have any randomness in the breaking threshold values, no averaging is required and studying only one configuration is sufficient. The

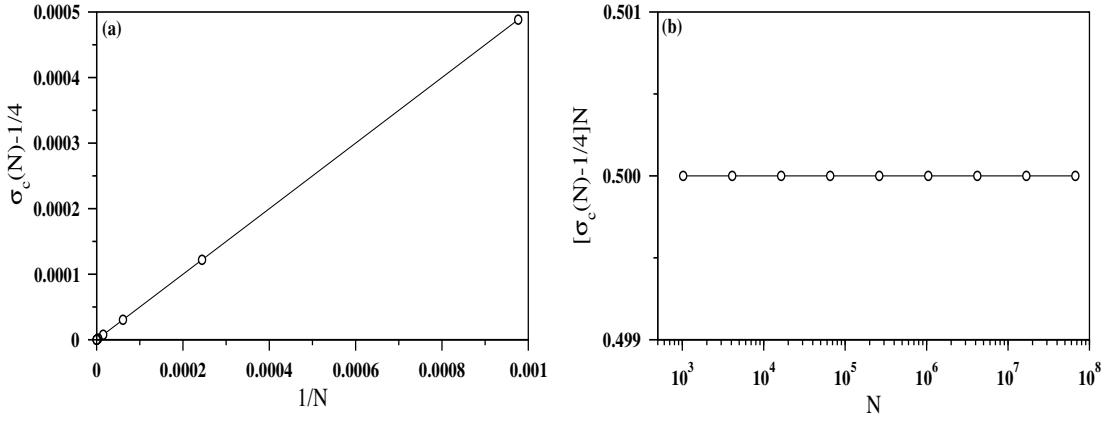

Figure 2.9: The variation of the critical load $\sigma_c(N)$ on the system size N in the deterministic case. (a) Plot of $\sigma_c(N) - 1/4$ vs. $1/N$ gives an excellent straight line that passes very close to the origin: $\sigma_c(N) - 1/4 = -1.3 \times 10^{-15} + 0.5/N$. (b) Same data as in (a) but here $[\sigma_c(N) - 1/4]N$ is plotted with N on a semi-log scale and the plot exhibits a horizontal straight line indicating that quite possibly $\sigma_c(N) = 1/4 + \frac{1}{2N}$.

breaking thresholds are already arranged in ascending order. In spite of the absence of randomness, the system shows a very systematic dependence on the size of the bundle N. In Fig. 2.9(a) we show the plot of $\sigma_c(N) - 1/4$ with $1/N$ for different values of N starting from 2^{10} to 2^{26} and we observe that all points fall on a straight line. It is seen that these points fit excellently to a straight line by a least square fit that passes very close to the origin: $\sigma_c(N) - 1/4 = -1.3 \times 10^{-15} + 0.5/N$. To see the variation even more distinctly we plot in Fig. 2.9(b) $[\sigma_c(N) - 1/4]N$ vs. $\log N$ on a lin - log scale. The fitted straight line is very much parallel to the log(N) axis and has the value 0.5000(1).

P(σ)	σ_c	ν	η	ζ	τ
Uniform	0.250(1)	1.50(1)	0.336(5)	0.666(5)	0.50(1)
$P(x) = x$	1/4	3/2	1/3	2/3	1/2
Weibull	0.593(1)	1.50(1)	0.335(5)	0.663(5)	0.50(1)
$P(x) = 1 - e^{-x^5}$	$(5e)^{-1/5}$	3/2	1/3	2/3	1/2
DFBM	0.2500(1)	1.00(1)	0.50(1)	1.00(1)	0.50(1)
	1/4	1	1/2	1	1/2

Table 2.1: Summary of the values of critical points and critical exponents for different distributions of breaking thresholds, uniform and Weibull. The results for the deterministic fiber bundle model (DFBM) are also included. For each distribution the numerical estimates are given in the first row and the conjectured values are given in the second row.

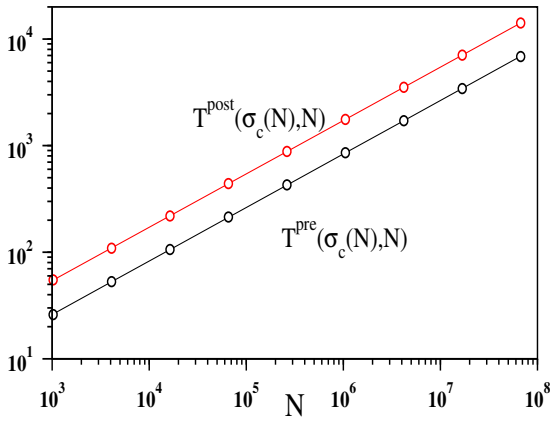

Figure 2.10: The deterministic case where breaking thresholds for individual fibers are uniformly spaced at an interval of $1/N$. The average relaxation time $T(\sigma_c(N), N)$ has been plotted with the bundle size N on a $\log - \log$ scale for $N = 2^{10}$ to 2^{26}. The slopes are 0.502 and 0.501 for the precritical and postcritical regimes respectively.

We conclude that the exact form of variation may be $\sigma_c(N) - 1/4 = \frac{1}{2N}$.

We also calculate the maximal relaxation times $T^{pre}(\sigma_c(N), N)$ and $T^{post}(\sigma_c(N), N)$ at the critical loads for the deterministic FBM. Both these plots are shown in Fig. 2.10 against N using a $\log - \log$ scale for the same sizes of the fiber bundles as in Fig. 2.9. Unlike the case of the stochastic fiber bundles, here the plots fit nicely to straight lines without any systematic curvatures for small bundle sizes. From the slopes we estimate the exponents as 0.502 and 0.501 for the precritical and postcritical regimes respectively. Thus, we conclude that a common value of $\eta = \eta_{pre} = \eta_{post} = 0.500(5)$ for both exponents.

Finally, we study the finite size scaling of the relaxation times as a function of deviation from the critical load as shown in Fig. 2.10. In Fig. 2.11(a), we have plotted $T(\sigma_c(N), N)$ against $\sigma_c(N) - \sigma$ using the double logarithmic scales for bundles of sizes N = 2^{18} to 2^{26}. Even though each curve has considerable curvature, yet it is apparent that as the bundle sizes become increasingly larger they tend to assume a power-law form. A finite size scaling of these plots is shown in Fig. 2.11(b) to determine whether a data collapse for very small deviations from the critical load is possible or not as we did in the case of a stochastic fiber bundle. We do find a reasonably good collapse for the small values of the abscissa when $T(\sigma, N)/N^{1/2}$ is plotted against $(\sigma_c(N) - \sigma)N$. From

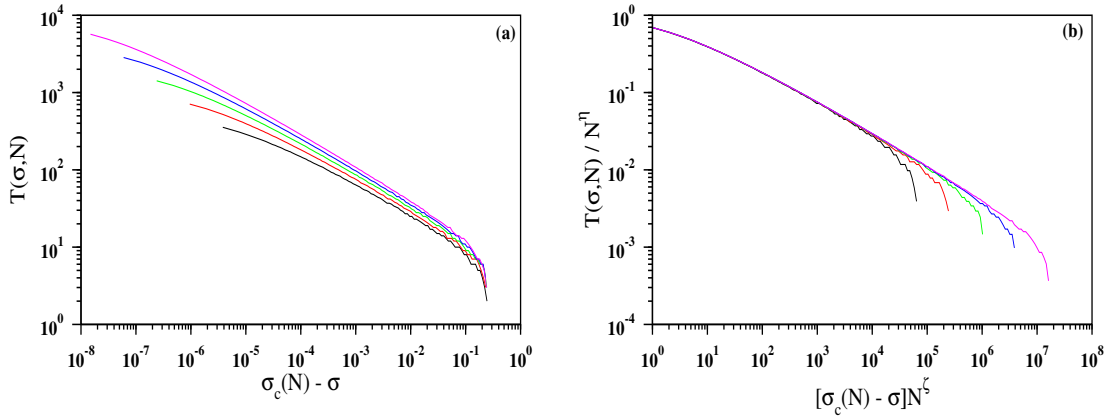

Figure 2.11: The deterministic case: (a) Plot of $T(\sigma, N)$ against $[\sigma_c(N) - \sigma]$ for N = 2^{18} to 2^{26}, the bundle size is increased by a factor of 4 at each step with N increasing from bottom to top. (b) A finite-size scaling analysis of the data in (a) using the scaling form in Eq. (2.13) with $\eta = 1/2$ and $\zeta = 1$. Here, N increases from left to right.

the scaling exponent values $\eta = 1/2$ and $\zeta = 1$ we conclude a value for the exponent $\tau = 1/2$ for the precritical regime. A similar analysis of the postcritical regime yields same exponent values for η, ζ and τ.

2.4 Summary

To summarize, we have carried out extensive numerical calculations to study the relaxation behavior of the FBM with ELS dynamics. The numerical estimates of the exponents associated with the critical points and the critical load per fiber have been accurately calculated and they match well with their analytical counterparts known in the literature. The critical load per fiber of a bundle of size N approaches its asymptotic value of 1/4 and $(5e)^{-1/5}$ for the cases when the breaking thresholds are distributed uniformly and with Weibull distribution respectively. The numerical estimate of the finite size correction exponent was obtained to be very close to its exact result $\nu = 3/2$. More importantly, the average relaxation time $\langle T(\sigma_c(N), N)\rangle$ is discontinuous at the critical point and the limiting value of the relaxation grows as $N^{\eta(N)}$. This exponent $\eta(N)$ depends on the bundle size and approaches its asymptotic value of $1/3$. Our most crucial result is that away from the critical point we do not find any $ln(N)$ dependence

of the average relaxation time $\langle T(\sigma, N)\rangle$ in the precritical regime as predicted before. Our extensive numerical calculations suggests that it obeys the usual scaling form with respect to N and the deviation from the critical point $|\Delta\sigma|$.

CHAPTER 3

Fiber bundle model with highly disordered breaking thresholds

3.1 Introduction

In nature, disorder can be found in the form of micro-cracks, grain boundaries etc. It is known that disorder plays a crucial role in regulating the strength of materials and also in the fracture process. The size and number of these cracks determine how strong a material or a structure is going to be. A lot of studies have been done to get greater insights in the role of disorder in material breakdown as it is important for technological purposes in the process of making materials that have high strength and low weight, or to build composite structures like bridges, buildings etc. Disorder is integral to natural disasters such as landslide, mine collapse, earthquakes etc that cause great losses of human lives and property. Fracture happens because of a cooperative effect of the disorder and the cumulative effect of stress concentration around the disordered regions. Homogeneous materials with very little disorder in them mostly fail through brittle type fractures [1]. A brittle fracture in nature is characterized by a very abrupt failure of the system. Since it is a very fast process, predicting the failure is difficult. However, ductile

[1]The work reported in this chapter is based on the publication "Fiber bundle model with highly disordered breaking thresholds", **Chandreyee Roy**, Sumanta Kundu and S. S. Manna, Phys. Rev. E, **91**, 032103 (2015).

or quasi-brittle type fractures is a gradual process. Since it proceeds slowly, we are able to study some precursors for the process which helps us in not only understanding the breakdown statistically, but also provides a way to be able to predict a catastrophic failure in the system .

The FBM is able capture the concept of disorder appropriately [72,73]. This model is characterized by a number of fibrous elements in the system that have different threshold capacities. This is the source of disorder in the system and by tuning the extent of the disorder in it, various properties of material breakdown can be understood. This extent of disorder present in a fiber bundle determines whether the failure on application of external stress will be brittle or quasi-brittle. When the failure of the weakest element causes a catastrophic failure leading to complete breakdown of the system, then we define it as a brittle fracture. On the other hand, when the external load has to be applied several times to cause complete failure then it is defined as a quasi-brittle fracture. In this chapter we study a version of the FBM following ELS dynamics. We introduce a high disorder in the system by using a power law distribution to assign values for the threshold capacities of the individual elements. This type of distribution can be useful to study systems like traffic jams in roads, where the distribution of the width of the roads are highly disordered and act as its capacity to accommodate cars that are analogous to breaking thresholds of the individual elements of the FBM.

This chapter is organized in the following way. In Sec. 3.2 we discuss how the high disorder has been incorporated in the model. Further, we discuss the effects of this high disorder on the critical load of the fiber bundle at which it fails completely and the fraction of fibers broken right before the catastrophic failure of the bundle. In Sec. 3.3 we study the avalanche-size statistics of the system having high disorder and finally we summarize our results in Sec. 3.4.

3.2 Highly disordered fiber bundles

In this version of the fiber bundle we consider an extreme case of heterogeneous disorder where the breaking thresholds of the individual fibers are power law distributed. This is similar to the fuse model discussed previously in Sec. 1.4.2 where every bond of a square lattice was considered to be a fuse with unit resistance that could withstand current upto a certain threshold value i_c [15]. As in other models of the fiber bundle, the source of disorder comes from the random distribution of breaking thresholds. The power law distribution used ensures the high disorder in the system in a way such that large number of fibers have small values of threshold and few fibers have very large values of threshold. Therefore, the breaking threshold b_i for the i_{th} fiber is drawn from a probability distribution $p(b) \sim b^{-\gamma}$ with $\gamma = 1$. Initially, we draw a set of N uniformly distributed random numbers q_i within the range $-1 < q_i < 1$. Then, the breaking threshold $b_i^{-10^{\beta q_i}}$ for the i_{th} fiber is assigned. As a result, the probability distribution takes the form $p(b) \sim b^{-1}$ within the range $10^{-\beta}$ to 10^{β} where β is a cutoff parameter that can be tuned to control the extent of disorder in the system [15].

3.2.1 The critical Stress

We used the same formulation as described in Sec. 1.6 to calculate the critical load per fiber σ_c as a function of the cutoff parameter β for power-law distributed breaking thresholds $\{b_i\}$. We first evaluate the constant of proportionality by normalizing the probability distribution. This gives us the following form of the probability density

$$p(b) = b^{-1}/(2\beta \ln 10) \tag{3.1}$$

within the limits $10^{-\beta}$ to 10^{β}. Consequently the cumulative distribution has the form

$$P(b) = \int_{10^{-\beta}}^{b} p(z)dz = \ln b/(2\beta \ln 10) + 1/2. \tag{3.2}$$

By substituting this in the force Eq. (1.7), the expression of $F(x)$ is obtained as

$$F(x) = Nx[1/2 - \ln x/(2\beta \ln 10)]. \tag{3.3}$$

where x represents the load per fiber at the stable state as described in Sec. 1.6. Clearly the function $F(x)$ has a maximum at $x = x_c$, for which $dF(x)/dx = 0$. This yields $x_c = 10^{\beta}/e$ and thus, the total critical applied load is obtained to be $F_c \equiv F(x_c) = N10^{\beta}/(2\beta e \ln 10)$. Thus, the critical initial applied load per fiber is given by $\sigma_c(\beta) = F_c/N$ which results in

$$\sigma_c(\beta) = 10^{\beta}/(2\beta e \ln 10). \tag{3.4}$$

If b^* is denoted as the lowest value of the breaking thresholds then the condition $b^* = x_c$ implies that the weakest fiber failure causes complete breakdown of the bundle since x_c signifies the stress per fiber for which complete failure of the bundle occurs (see Sec. 1.6). This fixes the upper bound of β denoted as $\beta_u = 1/(2\ln 10)$ uptil which the weakest fiber failure leads to the complete breakdown of the bundle. Thus the complete expression for $\sigma_c(\beta)$:

$$\sigma_c(\beta) = \begin{cases} 10^{\beta}/(2e \ln 10^{\beta}) & \text{for } \beta \geq \beta_u \\ 10^{-\beta} & \text{for } \beta \leq \beta_u \end{cases} \tag{3.5}$$

The above expression for the average critical applied load per fiber $\sigma_c(\beta)$ for a given value of cutoff parameter β is valid only for infinitely large bundles, i.e., $N \to \infty$.

As discussed before, a bundle is defined to be brittle if the weakest fiber failure leads to complete breakdown of the bundle; otherwise it is defined as quasi-brittle. By tuning the value of β we can tune the width of the distribution of breaking thresholds and the critical load per fiber $\sigma_c(\beta)$ varies accordingly. When the value of $\beta = 0$, then all the fibers have breaking thresholds equal to unity and so the $\sigma_c(0) = 1$. When β is very small then the minimum breaking threshold has a value very close to unity. In these cases, the fiber bundle tends to behave like a brittle bundle. This implies that the load released after the failure of the weakest fiber is sufficient enough to break all other fibers. As a result the critical load is equal to the value of the minimum breaking threshold which is $10^{-\beta}$. This situation continues till β reaches β_u, and therefore $\sigma_c(\beta)$ decreases as the strength of the weakest fiber, i.e., $10^{-\beta}$. When β increases further, gradually the

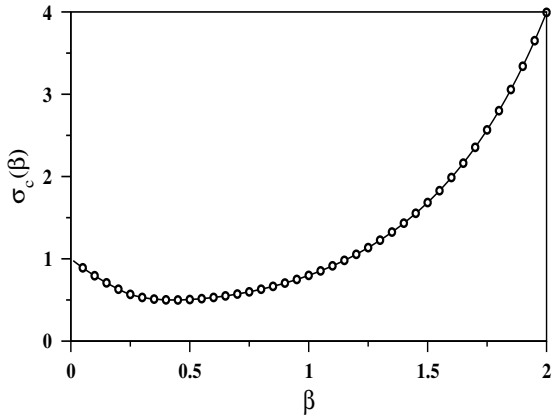

Figure 3.1: Plot of the critical load per fiber $\sigma_c(\beta)$ for a particular β calculated analytically (solid line) matches excellently with its numerical estimates (open circles).

fibers with higher breaking thresholds appear and they take over the control. Here the weakest fiber failure is not enough anymore to break all the fibers in the system and the bundle is referred to as a quasi-brittle bundle. Consequently, $\sigma_c(\beta)$ must increase with increase in β for large β with a minimum at $\beta = \beta_m$. The exact position of the minimum of $\sigma_c(\beta)$ can be calculated by using the condition $d\sigma_c(\beta)/d\beta = 0$ in Eq. (3.5) which results in $\beta_m = 1/(\ln 10)$. This is exactly twice the value of β_u.

To obtain the critical load $\sigma_c(\beta)$ numerically, we follow the procedure described in Sec. 2.2. For a given value of β we first calculate the critical load per fiber $\sigma_c^\alpha(\beta, N)$ for a particular configuration of bundle α having N fibers with a given set of breaking thresholds $\{b_i\}$. This calculation is then repeated over a large number of uncorrelated bundles α and the values of their critical loads are averaged over to obtain $\sigma_c(\beta, N) = \langle \sigma_c^\alpha(\beta, N) \rangle$. This procedure is again repeated for different values of N. The values of $\sigma_c^\alpha(\beta, N)$ are obtained following the algorithm described in Sec. 2.2 where the breaking thresholds are first ordered in an increasing sequence. Then $\sigma_c^\alpha(\beta, N)$ is calculated using Eq. (2.4).

We assume that the average value of the critical load per fiber $\sigma_c(\beta, N)$ for a given value of β and for the bundle size N reaches its asymptotic value $\sigma_c(\beta)$ according to the following form:

$$\sigma_c(\beta, N) - \sigma_c(\beta) = AN^{-1/\nu(\beta)} \tag{3.6}$$

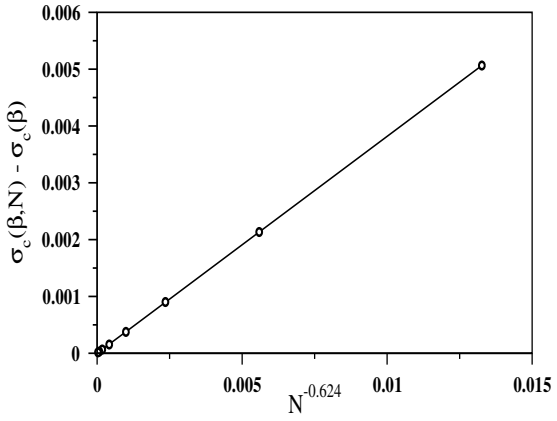

Figure 3.2: Variation of the critical load $\sigma_c(\beta, N)$ with the system size N for $\beta = 0.225$ has been shown. Plot of $\sigma_c(\beta, N) - \sigma_c(\beta)$ vs. $N^{-0.624}$ with $\sigma_c(\beta) = 0.596$ shows a nice straight line that passes very close to the origin.

where $\nu(\beta)$ is a critical exponent for the cut-off parameter β. We plotted the variation of $\sigma_c(\beta, N)$ against $N^{-1/\nu(\beta)}$ for $N = 2^{18}$ to 2^{24}, N being increased by a factor of 4 at each stage. We tune the value of $\nu(\beta)$ for a particular β so that at a specific value of $\nu(\beta)$ we get a best fitted straight line by the least square fit method. Using this best value of $\nu(\beta)$ and on extrapolation to $N \to \infty$ we get $\sigma_c(\beta)$. In Fig. 3.1 we exhibit an excellent matching of the analytical data with the numerical values of $\sigma_c(\beta)$ for the range $0 < \beta \leq 2$.

Next, we investigate the dependence of the finite-size correction exponent $\nu(\beta)$ on the cutoff parameter β. In the case of a uniform threshold distribution we discussed in Sec. 2.2 that the plot of $\sigma_c(N) - \sigma_c$ as a function of $N^{-1/\nu}$ gives an excellent straight line with $\sigma_c = 1/4$ and $\nu = 3/2$ [67,68,74]. Similarly, in our case of a highly disordered distribution, we plot $\sigma_c(\beta, N) - \sigma_c(\beta)$ against $N^{-1/\nu(\beta)}$ for different values of β. For example, we show in Fig. 3.2 a particular case for $\beta = 0.225$ where the best possible value of $\nu(\beta)$ is found to be 1.603. In this way the critical exponent $\nu(\beta)$ is calculated for different β and its variation is shown in Fig. 3.3(a) using $N = 2^{10}$ to 2^{16}, 2^{14} to 2^{20} and 2^{18} to 2^{24}. The value of $\nu(\beta)$ first increases, attains a maximum value (≈ 1.63), then decreases and then saturates to 1.5 for higher values of β. The same data in Fig. 3.3(a) can be collapsed on top of each other when plotted against $(\beta - \beta_u)N^{0.33}$ as shown in Fig. 3.3(b). Thus we conclude that the nature of the critical exponent $\nu(\beta)$ remains same

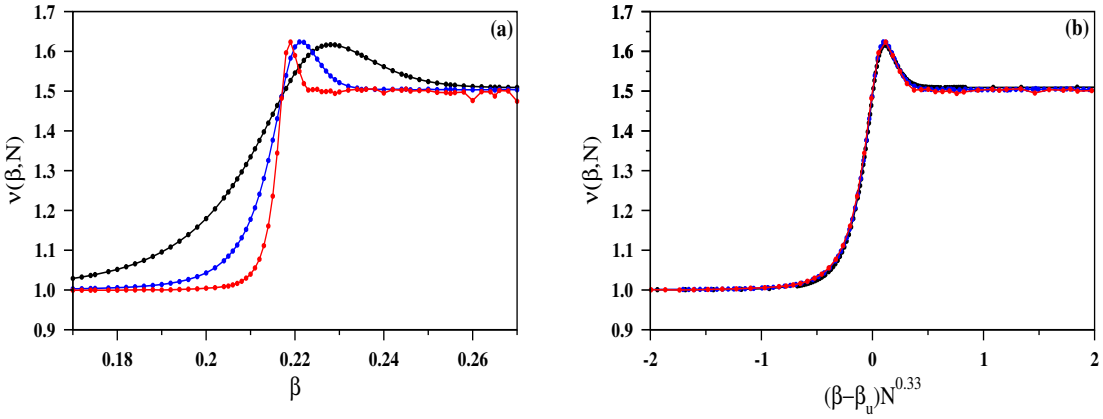

Figure 3.3: (a) Plot of $\nu(\beta, N)$ vs β for systems of different sizes. The value of $\nu(\beta, N)$ is calculated using the four bundle sizes from $N = 2^{10}$ to 2^{16} (black), 2^{14} to 2^{20} (blue) and 2^{18} to 2^{24} (red); N is increased from left to right. (b) A collapse of the data of the same three system sizes in (a) works excellently for a suitably scaled β axis.

for large system sizes.

3.2.2 Fraction of broken fibers

We calculate the fraction of broken fibers denoted by $f_b(\beta)$ just before the complete breakdown of the bundle which is observed to be a function of the cutoff parameter β. Since the fiber bundle fails completely at x_c, so the quantity $f_b(\beta)$ is calculated as:

$$f_b(\beta) = \int_{10^{-\beta}}^{x_c} p(x)dx = 1 - 1/(2\beta \ln 10). \tag{3.7}$$

The fraction of broken fibers $f_b(\beta)$ is always a real and positive quantity. Thus, the condition $1 - 1/(2\beta \ln 10) > 0$ again reproduces the result that for $\beta < 1/(2 \ln 10)$ the bundle will be brittle, i.e., weakest fiber failure will lead to complete failure of the bundle.

To find $f_b(\beta)$ for a given value of β numerically, we use the same method used to calculate $\sigma_c(\beta)$. We increase the external load quasistatically until the bundle fails. The fraction of broken fibers $f_b(\beta, N)$ just before complete breakdown of the bundle is calculated for a particular β of bundle size N and averaged over a large number of uncorrelated samples. This procure is repeated for six values of $N = 2^{16}, 2^{18}, ..., 2^{26}$ and assumed that it converges to $f_b(\beta)$ for $N \to \infty$. The extrapolated values of $f_b(\beta)$ are

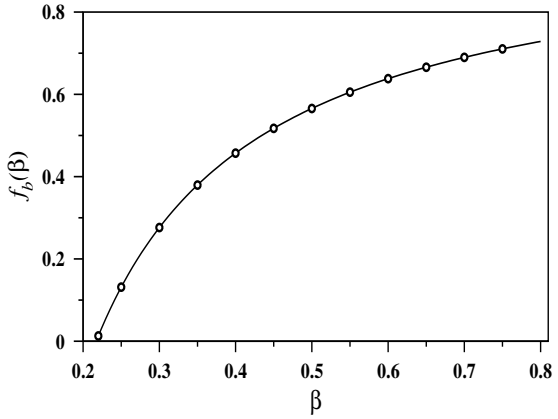

Figure 3.4: The fraction of broken fibers $f_b(\beta)$ for a particular value of β right before complete breakdown of the bundle is plotted using the analytical expression given in Eq. (3.7) with solid line. The numerically obtained data represented by open circles matches very well with the analytical curve.

plotted against β in Fig. 3.4. The analytical expression is seen to match very well with its numerical estimates.

3.3 Avalanche size distribution

A stable state in a fiber bundle is a state when the breaking thresholds of the intact fibers in the bundle are greater that the stress acting through them. When an external load is applied to an intact bundle to break only the weakest fiber, then it may trigger a cascade of fiber failures which ends when the bundle reaches a new stable state. The total number of fibers that fail in this event is called the avalanche size and is denoted by Δ. Starting from a completely intact fiber bundle, this process is carried out repeatedly until a state of global failure is achieved by raising the external load quasistatically, breaking only the weakest fiber among the intact ones after every avalanche. It is well known in the literature that the probability of the avalanche sizes $D(\Delta)$ is a power-law [41, 53] for fiber bundles having uniformly distributed breaking thresholds following ELS dynamics:

$$D(\Delta) \sim \Delta^{-\xi} \tag{3.8}$$

with $\xi = 5/2$. It is has been shown before in Ref. [54, 75] that when the width of the uniform distribution is changed then the exponent ξ experiences a crossover from $3/2$ to

$5/2$. The same crossover is seen to happen in a highly disordered fiber bundle as well when the cut-off parameter β is varied. To exhibit this crossover we follow the method given by Ref. [75]. For a bundle having large number of fibers, the number of avalanches of size Δ is given by [53]

$$\frac{D(\Delta)}{N} = \frac{\Delta^{\Delta-1}e^{-\Delta}}{\Delta!}\int_0^{x_c} p(x)r(x)[1-r(x)]^{\Delta-1}e^{\Delta r(x)}dx, \tag{3.9}$$

where,

$$r(x) = 1 - \frac{xp(x)}{1-P(x)}. \tag{3.10}$$

The expression for $D(\Delta)$ can be simplified to the following form [75]:

$$\frac{D(\Delta)}{N} = \frac{\Delta^{\Delta-2}e^{-\Delta}}{\Delta!}\frac{p(x_c)}{|r'(x_c)|}(1-e^{-\Delta/\Delta_c}), \tag{3.11}$$

with

$$\Delta_c = \frac{2}{r'(x_c)^2(x_c-b^*)^2}. \tag{3.12}$$

Using the Stirling approximation $\Delta! = \Delta^{\Delta}e^{-\Delta}\sqrt{2\pi\Delta}$, Eq. (3.11) can be written as

$$\frac{D(\Delta)}{N} = C\Delta^{-5/2}(1-e^{-\Delta/\Delta_c}), \tag{3.13}$$

where $C = (2\pi)^{-1/2}p(x_c)/|r'(x_c)|$ is a constant. From Eq. (3.13), a clear evidence of crossover in the exponent ξ around the avalanche size Δ_c is prominent. So we have:

$$\frac{D(\Delta)}{N} \propto \begin{cases} \Delta^{-3/2} & \text{for } \Delta \ll \Delta_c, \\ \Delta^{-5/2} & \text{for } \Delta \gg \Delta_c. \end{cases} \tag{3.14}$$

In our case, we use power law distribution $p(b) \sim b^{-1}$ in the range from $10^{-\beta}$ to 10^{β} to obtain $r'(x_c) = -e/10^{\beta}$, $x_c = 10^{\beta}/e$ and $b^* = 10^{-\beta}$. Substituting these values in Eq. (3.14) we get the crossover avalanche size:

$$\Delta_c(\beta) = \frac{2}{(1-e10^{-2\beta})^2}. \tag{3.15}$$

This crossover of the exponents has also been studied using numerical simulations. For $\beta = 1/(2\ln 10)$, Eq. (3.15) yields $\Delta_c = \infty$. This implies that for this particular

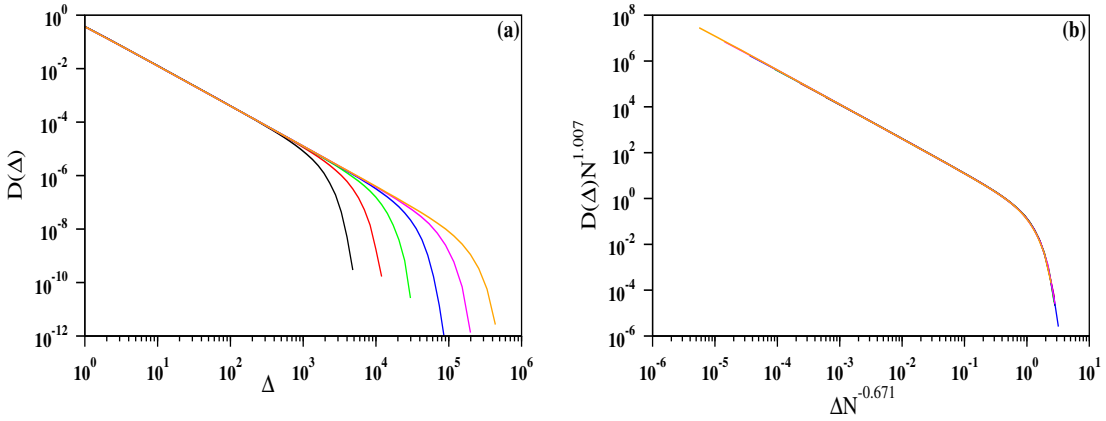

Figure 3.5: (a) Log-log plot of the binned data for avalanche size distribution $D(\Delta)$ vs. Δ for $\beta = \beta_u = 1/(2\ln 10)$ for $N = 2^{16}, 2^{18}...2^{26}$ (from left to right). (b) A finite-size scaling works well: $D(\Delta)N^{\eta}$ against $\Delta N^{-\zeta}$ exhibits a good collapse of data with $\eta = 1.007$ and $\zeta = 0.671$, implying $\xi = \eta/\zeta = 1.50(1)$. This value is consistent with the directly measured value of 1.50(2) from the slopes in the intermediate region. The crossover is not observed here since $\Delta_c = \infty$ for this particular value of β.

value of β, only the power law with exponent $\xi = 3/2$ is observed as any avalanche of finite size Δ will be less than the value of Δ_c. The numerical data for avalanche size distribution for $\beta = 1/(2\ln 10)$ has been plotted in Fig. 3.5(a) for six different values of N starting from $N = 2^{16}$ to 2^{26} where N is increased by a factor of 4 at each stage. For $N = 2^{16}$ to 2^{22} the data has been averaged over 10^6 samples and 400 000 and 100 000 samples for 2^{24} and 2^{26} respectively. In Fig. 3.5(b) we plot the same data in (a) and scale the axes with suitable powers of the bundle size N to get an excellent collapse of the data. From the scaled data we obtain the following scaling form:

$$D(\Delta)N^{\eta} \sim \mathcal{G}[\Delta/N^{\zeta}] \tag{3.16}$$

where $\mathcal{G}(y)$ is an universal scaling function of the scaled variable $y = \Delta/N^{\zeta}$. The best possible tuned values of the scaling exponents obtained are $\eta = 1.007$ and $\zeta = 0.671$. Using these scaling exponents the value of $\xi = \eta/\zeta = 1.50(1)$ is calculated, which matches well with the analytical result of 3/2 [76].

We carry out the same analysis for three different β values which are 0.22, 0.24 and 0.28. By substituting these values of β in Eq. (3.15) we have obtained $\Delta_c(\beta) = 11\,741$, 200.4 and 31.66 respectively. We can clearly observe a crossover in the exponent value ξ

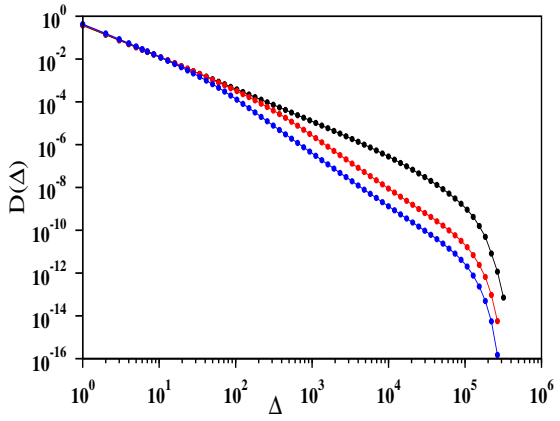

Figure 3.6: The avalanche size distribution for β = 0.22 (black), 0.24 (red) and 0.28 (blue) (from right to left) for bundles of size $N = 2^{24}$. Slopes of the curve are ≈ 1.5 and ≈ 2.5 for small and large avalanche sizes. The crossover size $\Delta_c(\beta)$ are approximately 11741, 200.4 and 31.66 respectively evaluated using Eq. (3.15).

around $\Delta = \Delta_c(\beta)$ as shown in Fig. 3.6 for $N = 2^{24}$. The slope of the curve gradually crosses over from ≈ 1.5 to ≈ 2.5 for large values of Δ. It has also been observed that as β is increased, $\Delta_c(\beta)$ gradually shifts towards the origin and therefore the regime over which $\xi = 5/2$ is valid, gets extended. These results are consistent with Ref. [54, 75] where this kind of a crossover in the exponents has been observed for the FBM with uniformly distributed breaking thresholds that ranged between a certain lower cut-off b_{1c} and unity. In this case the avalanche sizes smaller (larger) than some crossover size $\Delta(b_{1c})$ correspond to avalanche size exponents 3/2 (5/2). This implies that in our model, even for the highly heterogeneous distribution of breaking thresholds, similar crossover between the same two exponents takes place across the crossover avalanche size $\Delta_c(\beta)$.

Lastly, we calculate the total number of avalanches $\Lambda(N)$ required to break the entire bundle and it has been observed that it depends on the system sizes N as N^{χ}, where $\chi = 0.336$ and 0.985 for $\beta = 1/(2\ln 10)$ and 0.240 respectively. The log-log plot of $\Lambda(N)$ against N for these two values of β fits to excellent straight lines a shown in Fig. 3.7. We conjecture that χ may be 1/3 and 1 exactly for $\beta = \beta_u$ and $\beta > \beta_u$ respectively.

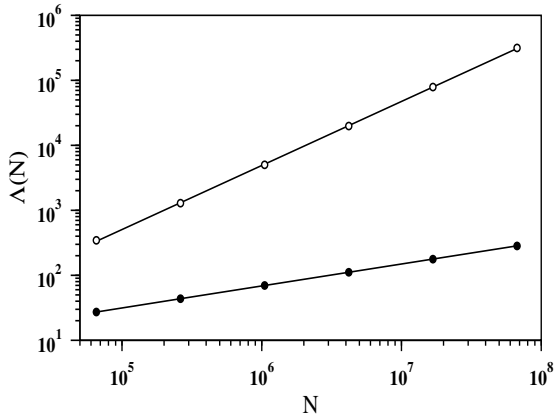

Figure 3.7: Plot of the average number of avalanches $\Lambda(N)$ required to break the bundle of size N on a log-log scale: for $\beta = 1/(2\ln 10)$, $\Lambda(N) \sim N^{0.337}$ (filled circles) and for $\beta = 0.240$, $\Lambda(N) \sim N^{0.985}$ (open circles).

3.4 Summary

We have studied various properties of the FBM following the ELS dynamics with individual fibers having breaking thresholds drawn from a power law distribution given by $p(b) \sim b^{-1}$ within the limits $10^{-\beta}$ to 10^{β} where β is considered to be a cutoff parameter. First, we calculated the critical initial load per fiber $\sigma_c(\beta)$ required for complete breakdown of the bundle which is found to be a β dependent quantity analytically as well as numerically. We found a good correspondence between the two data. The $\sigma_c(\beta)$ first decreases, reaches a minimum and then increases with increasing values of β. When β is very small, the weakest fiber failure triggers a massive avalanche that causes complete breakdown of the bundle. This implies that $\sigma_c(\beta)$ is equal to the breaking threshold value of the weakest fiber, i.e. $10^{-\beta}$. This behavior continues till $\beta = \beta_u$ and is analogous to brittle failure of materials. For values of $\beta > \beta_u$, equating the external load to the strength of the weakest fiber is no longer sufficient to break the entire bundle even though a large number of fibers having small breaking thresholds still dominate the system. This is analogous to quasi-brittle type failure of the fiber bundle. With more increase in the value of β, the number of avalanches required for the breakdown of the bundle gradually increases and the $\sigma_c(\beta)$ slowly increases from the weakest strength of $10^{-\beta}$ but for $\beta > \beta_u$, $\sigma_c(\beta)$ remains smaller than $10^{-\beta}$. Thus, there exists a minimum in $\sigma_c(\beta)$

given by $\beta_m = 2\beta_u$ after which it keeps on increasing with increase in β value. At very large values of β, there exist very few extremely strong fibers in the bundle and they cause the critical load of the system to increase since the external load has to be raised to $\sigma_c(\beta) \approx 10^{\beta}$ to break the strongest fiber. This salient feature is a direct consequence of the power law distribution used for the breaking thresholds.

We have also calculated the fraction of fibers $f_b(\beta)$ just before the last avalanche and we have observed a good correspondence of the analytical and the numerical results. More importantly, we have shown numerically that the critical load $\sigma_c(\beta, N)$ approaches its asymptotic value as $\sigma_c(\beta, N) = \sigma_c(\beta) + AN^{-1/\nu(\beta)}$. This variation of the critical exponent $\nu(\beta)$ was found to be a β dependent quantity which is first seen to increase sharply with β, reaches a maximum, then decreases and then finally saturates to a value $\approx 3/2$ which is the same as the value of the finite size exponent of a fiber bundle with uniform distribution of breaking thresholds following the ELS rule. We also did a statistical analysis of the avalanche sizes. The avalanche size distribution is seen to follow a power law with an exponent ξ that crosses over from 3/2 to 5/2 through a crossover avalanche size $\Delta_c(\beta)$.

CHAPTER 4

Brittle to quasi-brittle transition in bundles of nonlinear elastic fibers

4.1 Introduction

All studies regarding the FBM in the literature consider massless elastic fibers with a linear stress-strain curve following the Hooke's law. It is observed that even though every individual fiber is linearly elastic, the model as a whole is not due to interaction of the fibers with one another through stress redistribution processes. This ultimately leads to very interesting results as have been discussed in the previous chapters. However, in practice, the precise validity of Hooke's law is limited to a very small region of loading. The deviation from linearity is observed when the materials are subjected to larger mechanical stress. To our knowledge, no systematic study of a fiber bundle with fibers following nonlinear elastic fibers has been done, i.e., when the stress grows nonlinearly against increasing strain. Therefore, it would be important to study the behavior of loaded materials under nonlinear stress-strain response functions of the individual fibers within the framework of the FBM.

In this chapter [1] we present a version of the fiber bundle with the individual fibers hav-

[1] The work reported here is based on the publication "Brittle-to-quasi-brittle transition in bundles of nonlinear elastic fibers", **Chandreyee Roy** and S. S. Manna, Phys. Rev. E, **94**, 032126 (2016).

ing nonlinear stress-strain characteristics. We study the brittle to quasi-brittle transition in such cases and have observed that it takes place at a specific value of a continuously tunable parameter parameter α_c that characterizes the nonlinearity of the fibers. This is in contrast to the results of the existing literature of linear fiber bundles where a similar brittle to quasi-brittle transition takes place when the width of the probability distribution of the breaking thresholds of individual fibers is tuned. In this chapter we have mainly considered four different nonlinear forms of the stress-strain characteristic curve of the fibers.

The sections are arranged in the following way. In the Sec. 4.2 we have described the algorithm used for the numerical studies. In Sec. 4.3 we have calculated the critical stress of the fiber bundle. In Sec. 4.4 we describe the transition from brittle to quasi-brittle phase in three different ways and then we study this transition in terms of the relaxation time in Sec. 4.5. Avalanche size distributions are discussed in Sec. 4.6. In all the above sections we first describe at length, our numerical as well as analytical results for exponential form of nonlinearity followed by brief description of the results of other nonlinear forms. A number of additional cases also exhibit the brittle to quasi-brittle transitions and have been discussed in Sec. 4.8. Finally, we summarize in Sec. 4.9.

4.2 Algorithm

Let the general functional form of the nonlinear dependence of stress (s) on the strain (x) for an arbitrary fiber be denoted by

$$s = \mathcal{G}(x). \tag{4.1}$$

In the case of linear fibers where each of the individual fibers follow Hooke's Law, the form of $\mathcal{G}(x)$ is simply given by $\mathcal{G}(x) = x$. Unlike the linear case of FBM, here a fiber breaks if the external load acting on it is such that the strain produced in it following Eq. (4.1) exceeds a preassigned critical value of the strain. Therefore, for an arbitrary bundle λ, the individual fibers i have their breaking strain values x_i^{λ} drawn from a uniform

probability distribution $p(x)$ between $\{0, 1\}$. Consequently, its cumulative probability distribution is given by $P(x) = x$ when $0 \leq x \leq 1$ and 0 for $x > 1$.

For a particular bundle λ every fiber will have a breaking strain $\{x_i^\lambda\}$ and a corresponding set of breaking stress $\{s_i^\lambda\}$ calculated using the Eq. (4.1). Both these sets of breaking threshold values of strain and stress are arranged in increasing order for a bundle having N fibers such that $x_{(1)}^\lambda < x_{(2)}^\lambda < x_{(3)}^\lambda < ... < x_{(N)}^\lambda$ and $s_{(1)}^\lambda < s_{(2)}^\lambda < s_{(3)}^\lambda < ... < s_{(N)}^\lambda$ respectively. To an intact fiber bundle an external load is applied gradually such that every fiber gets strained gradually. Let the uniform strain x in all the fibers be increased till it reaches the minimum value of the strain $x_{(1)}^\lambda$ which is by definition the weakest fiber in the bundle. This fiber breaks immediately and releases a load equal to $\mathcal{G}(x_{(1)}^\lambda)$. The released load is then shared equally among all the remaining $N - 1$ intact fibers in the bundle. Due to this, the load on these fibers gets uniformly enhanced. Let the magnitude of this enhanced load be s. Then the corresponding value of strain, developed in all the intact fibers because of the enhanced load, can be calculated from the inverse function $x = \mathcal{G}^{-1}(s)$. As a result, this can cause more fibers to have their breaking strains exceeded by the acting strain which may lead to a cascade of broken fibers which is defined in previous chapters as an avalanche. Then we wait for the system to stabilize i.e. all the fibers in the stable state will have their breaking strains above the external strain acting on them. To trigger a new avalanche we increase uniformly the value of strain by controlling the external load so that the next minimal value of breaking strain is reached. Because of the nonlinearity of Eq. (4.1), we need to consider the evolution of both the stress and the strain for every fiber separately. Though the breaking strains are uniformly distributed, their corresponding breaking stress values are not and is determined by the function $\mathcal{G}(x)$. This is the root cause for non trivial results in this model.

The critical load per fiber $\sigma_c(\alpha)$ can be found out in the same method as described in the earlier chapters i.e. by using the set of breaking stresses $\{s_i^\lambda\}$. Here, α is the tuning parameter that characterizes the nonlinear stress strain curve. The critical load

$\sigma_c^{\lambda}(\alpha, N)$ for an arbitrary bundle λ with a particular value of α for bundle size N is calculated and then averaged over many samples to get $\sigma_c(\alpha, N) = \langle \sigma_c^{\lambda}(\alpha, N) \rangle$. This entire calculation is then repeated for different values of N assuming that the critical load per fiber converges to a value in the asymptotic limit according to the following equation:

$$\sigma_c(\alpha, N) - \sigma_c(\alpha) = AN^{-1/\nu(\alpha)} \tag{4.2}$$

where $\nu(\alpha)$ is a critical exponent that is a function of the tuning parameter α.

4.3 The critical stress

We have considered several cases of our nonlinear FBM. We first consider the exponential growth of stress as a function of strain: $s = \mathcal{G}(x) = e^{\alpha x}$. Let the externally applied load be denoted by $F(x)$, which is a function of the uniform strain x of all the intact fibers in the stable state. This total load can be written as [12, 18, 19]:

$$F(x) = Ns[1 - P(x)] = Ne^{\alpha x}[1 - x]. \tag{4.3}$$

In the above equation the external load $F(x)$ has a maximum at $x = x_c$. Thus, the condition $dF/dx = 0$ yields the following equation:

$$\alpha e^{\alpha x_c}[1 - P(x_c)] - e^{\alpha x_c} p(x_c) = 0 \tag{4.4}$$

from which we get the results $x_c = (\alpha - 1)/\alpha$ and $F_c = Ne^{\alpha - 1/\alpha}$ for a nonlinear bundle with a uniform distribution of breaking thresholds. The total critical applied load F_c corresponds to the critical initial load per fiber [18, 19]

$$\sigma_c(\alpha) = F_c/N = e^{\alpha - 1}/\alpha. \tag{4.5}$$

To check this expression, we have numerically estimated the values of the critical load per fiber $\sigma_c(\alpha, N)$ for a specific value of $\alpha = 2$ and for different bundle sizes N, using the algorithm discussed in Sec. 4.2. The variation of $\sigma_c(\alpha, N)$ is plotted against $N^{-1/\nu(\alpha)}$ with N values increasing from 253 to 31 623. The value of $\nu(\alpha)$ was tuned to

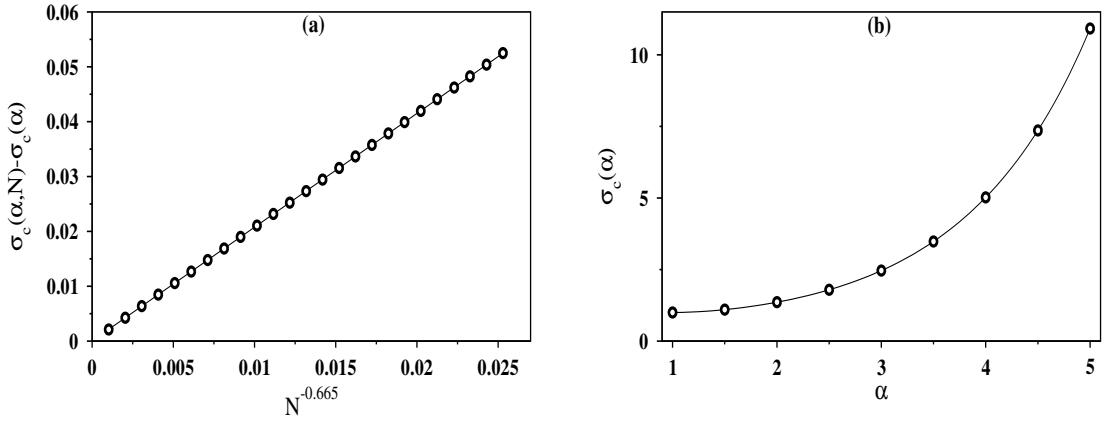

Figure 4.1: $\mathcal{G}(x) = e^{\alpha x}$: (a) Plot of the critical value of $\sigma_c(\alpha, N) - \sigma_c(\alpha)$ with respect to $N^{-0.665}$ with $\alpha = 2$ for N = 253 to 31623. The least square fit line has the form $\sigma_c(\alpha, N) - 1.3591 = 2.0733N^{-0.665}$. Therefore, $\sigma_c(\alpha)$=1.3591 which is very close to its analytical value $e/2$ in Eq. (4.5) for $\alpha = 2$. (b) Plot of the variation of $\sigma_c(\alpha)$ against α. The solid line represents the analytically obtained expression given by Eq. (4.5) and the circles represent the numerical data which matches well with the analytical values.

get a specific value for which the plots fit excellently to a straight line using the least square fit method.Using this specific value of $\nu(\alpha)$ and on extrapolation to $N \to \infty$ we obtained $\sigma_c(\alpha) = \sigma_c(\alpha, \infty)$ as shown in Fig. 4.1(a). This analysis gives $\nu(2) = 0.665$ and we have observed that the value of $\nu(\alpha)$ does not depend explicitly on the value of α and is approximately 2/3 for all values of α. Further, we have plotted the variation of $\sigma_c(\alpha)$ with respect to the tuning parameter α in the range $1 \leq \alpha \leq 5$ in Fig. 4.1(b). The analytical form obtained in Eq. (4.5) matches excellently with the numerical estimates. It is seen that for $\alpha > 1$ the bundle is always in the quasi-brittle regime and for $0 < \alpha < 1$ the bundle is in the brittle regime. This has been discussed in great detail in the next sections of this chapter. For the brittle phase, we get $\sigma_c(\alpha) \approx 1$ and the corresponding $\nu(\alpha) \approx 1$ for all values of α.

For the stress-strain characteristic $\mathcal{G}(x) = x^\alpha$, the external load

$$F(x, \alpha) = Nx^\alpha[1 - x], \tag{4.6}$$

$$x_c(\alpha) = \alpha/(\alpha + 1), \tag{4.7}$$

$$\sigma_c(\alpha) = \alpha^\alpha/(\alpha + 1)^{(\alpha+1)}. \tag{4.8}$$

It is to be noted that by putting $\alpha = 1$ in the above expressions, we get back the well

known results for the linear fiber bundle case following the ELS dynamics.

Similarly, for $\mathcal{G}(x) = xe^{\alpha x}$, the external load

$$F(x,\alpha) = Nxe^{\alpha x}[1-x], \tag{4.9}$$

$$x_c(\alpha) = (\alpha - 2 + \sqrt{4+\alpha^2})/2\alpha, \tag{4.10}$$

$$\sigma_c(\alpha) = \frac{1}{\alpha^2} e^{\frac{1}{2}(\alpha-2+\sqrt{4+\alpha^2})}(\sqrt{4+\alpha^2}-2). \tag{4.11}$$

Here also, we get back the well established results in the limit of $\alpha \to 0$ on applying L'Hospital's rule.

4.4 Brittle to quasi-brittle transition

The definitions of a brittle and a quasi-brittle bundle in the nonlinear FBM case is the same as described in previous chapters which states that a fiber bundle is defined to be 'brittle', if and only if, the failure of the weakest fiber causes the failure of the complete bundle. Thus, if the external load is tuned in such a way that only the fiber having minimal breaking strain breaks, leading to the failure of all the remaining fibers in the bundle in the form of a cascading process, then such a bundle is said to be brittle. On the other hand, if a bundle needs at least two avalanches for the global failure, then it is said to be 'quasi-brittle'. Here, we use the parameter α as a tuning parameter to observe the transition from a brittle phase to quasi-brittle phase since it characterizes the stress-strain characteristics of the individual fibers. We observed that the transitions takes place at a specific value of $\alpha = \alpha_c$.

4.4.1 Probability distribution of brittle states

To estimate the value of α_c where the brittle to quasi-brittle transition takes place we consider a few quantities that characterize this transition. The first quantity we study numerically is the probability $P(\alpha, N)$ that a randomly selected sample of the fiber bundle is found to be brittle. For a given value of α, we construct a random sample of

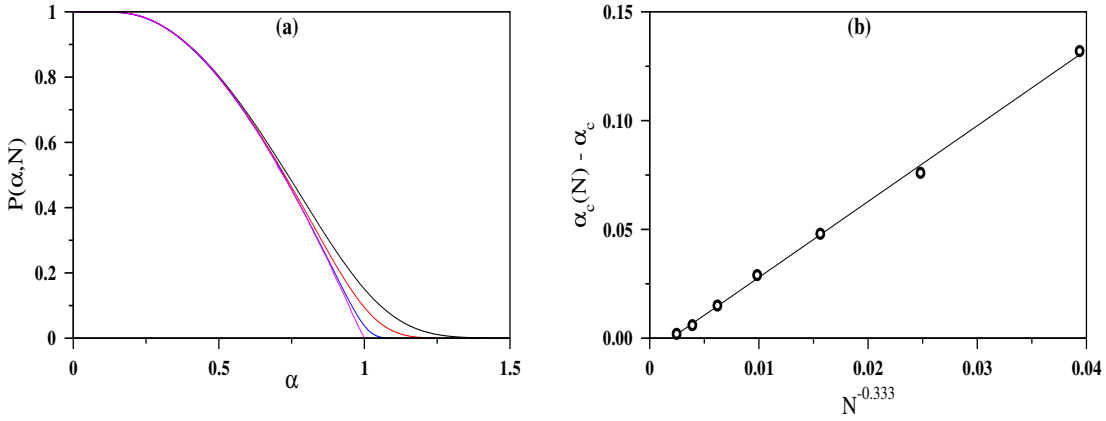

Figure 4.2: $\mathcal{G}(x) = e^{\alpha x}$: (a) Plot of the probability of brittle bundles $P(\alpha, N)$ against α for $N = 2^{08}$ (black), 2^{10} (red), 2^{14} (blue), and 2^{26} (magenta) (N increasing from right to left). (b) Plot of $\alpha_c(N) - \alpha_c$, with $\alpha_c = 1$ against $N^{-0.333}$. The least square fitted straight line misses the origin very closely.

the fiber bundle and raise the external load to break the weakest fiber with the smallest breaking strain [58]. Then we use a large number of samples and calculate the fraction of bundles that fail completely due to weakest fiber failure out of all the samples considered. We plot this fraction in Fig. 4.2(a) and it is seen to be a function of the tuning parameter α for different values of N for the case when $\mathcal{G}(x) = e^{\alpha x}$. For the bundles of arbitrary size N, when the value of α is very small, the probability is unity and it gradually decreases and ultimately vanishes with increase in the value of α. The minimum value of α where $P(\alpha, N) = 0$ is considered to be the transition point for the bundle of size N and is denoted by $\alpha_c(N)$. This is then repeated for several values of N and the variation of $\alpha_c(N)$ with respect to N is then plotted in Fig. 4.2(b). We assume that $\alpha_c(N)$ converges to its asymptotic value α_c according to

$$\alpha_c(N) = \alpha_c + BN^{-1/\kappa}. \tag{4.12}$$

Fig. 4.2(b) shows the best fitted plot of $\alpha_c(N) - \alpha_c$ against $N^{-1/\kappa}$ for $\alpha_c \approx 1.0$ and $1/\kappa$ = 0.333.

A similar plot of $P(\alpha, N)$ against α for the case $\mathcal{G}(x) = 1 + x^{\alpha}$ shows an even sharper transition from quasi-brittle ($\alpha < 1$) to brittle ($\alpha > 1$) transition. The $\alpha_c(N)$ values for different bundle sizes, when extrapolated against $N^{-0.23}$, gives nicely $\alpha_c = 1$

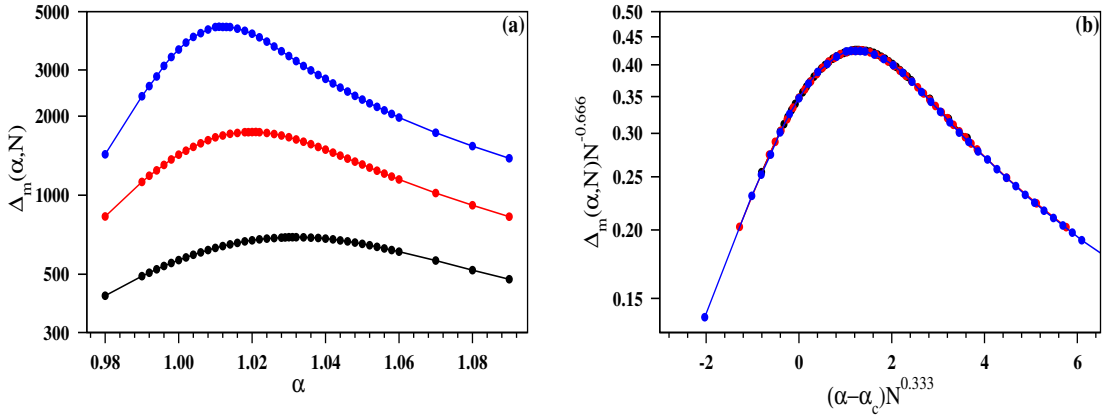

Figure 4.3: $\mathcal{G}(x) = e^{\alpha x}$: (a) Plot of the average avalanche size $\Delta_m(\alpha, N)$ against α for $N = 2^{16}$ (black), 2^{18} (red), and 2^{20} (blue) with N increasing from bottom to top. The values of α for the maximum value of $\Delta_m(\alpha, N)$ defined in Eq. (4.13) are $1.030, 1.021$ and 1.011 respectively, leading to $\alpha_c = 1$ as $N \to \infty$. (b) Finite size scaling of the average avalanche size $\Delta_m(\alpha, N)N^{-0.666}$ against $(\alpha - \alpha_c)N^{0.333}$ using the data in (a) exhibits an excellent data collapse.

again. No such transition has been observed for $\mathcal{G}(x) = x^\alpha$ and $xe^{\alpha x}$.

4.4.2 Estimation of α_c from the moment analysis of avalanche sizes

We can also estimate the transition point α_c by using the moment calculation method of the size of the avalanches. In general, the n-th moment of the avalanche sizes is denoted by $\langle \Delta^n(\alpha, N)\rangle$. The average avalanche size can be defined as the ratio of second moment to the first moment of the avalanche sizes [59],

$$\Delta_m(\alpha, N) = \langle \Delta^2(\alpha, N)\rangle / \langle \Delta(\alpha, N)\rangle. \tag{4.13}$$

This quantity is plotted as a function of α in Fig. 4.3(a) for three different system sizes $N = 2^{16}$, 2^{18} and 2^{20}. As the value of α increases the average avalanche size also increases, attains a maximum and then decreases. The maximal value of the average avalanche increases with increasing size of the system. Moreover, the position of the maximum, i.e., the value of α where the maximum value occurs is seen to drift towards $\alpha_c = 1$ as N increases.

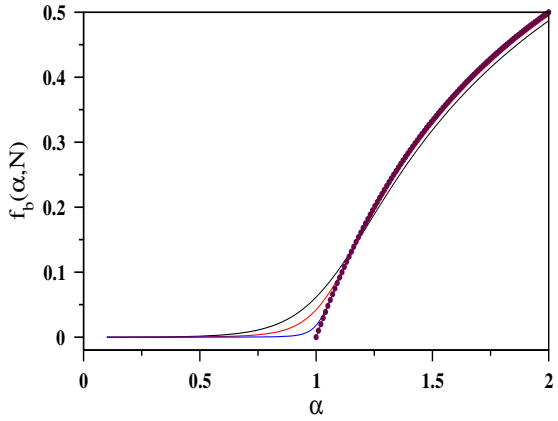

Figure 4.4: $\mathcal{G}(x) = e^{\alpha x}$: Plot of the fraction of broken fibers $f_b(\alpha, N)$ before the last avalanche against α for $N = 2^{08}$ (black), 2^{10} (red), and 2^{14} (blue) with N increasing from left to right. The plot with filled circles represents the analytical form given in Eq. (4.14).

Fig. 4.3(b) exhibits an excellent collapse of the data for the exponents of the three curves in Fig. 4.3(a). The abscissa and the ordinate are suitably scaled by the system size dependent factors $N^{0.333}$ and $N^{-0.666}$ respectively. We observe that a plot of $\Delta_m(\alpha, N)N^{-0.666}$ against $(\alpha - \alpha_c)N^{0.333}$ exhibits an excellent data collapse for $\alpha_c = 1$.

Similar moment analysis for the $\mathcal{G}(x) = 1 + x^{\alpha}$ case also gives the same result of $\alpha_c \approx 1$.

4.4.3 Fraction of fibers broken before the last avalanche

The next quantity that we study is the fraction of broken fibers just before complete breakdown of the bundle denoted by $f_b(\alpha)$. Since at $x = x_c$ the fiber bundle fails completely, so the quantity $P(x_c)$ gives the fraction of fibers that has already broken due the strain x_c. Therefore, the fraction of fibers just before the last avalanche will be given by

$$f_b(\alpha) = P(x_c) = (\alpha - 1)/\alpha. \tag{4.14}$$

The quantity $f_b(\alpha, N)$ has been plotted against α for different system sizes $N = 2^8, 2^{10}$, and 2^{14} in Fig. 4.4. As N increases, the plots can be seen to tend towards the analytical plot given by Eq. (4.14). The quantity $f_b(\alpha) = 0$ by definition when $\alpha < \alpha_c$ since the bundle is brittle and all the fibers break in one avalanche. On the other hand it will be

non-zero for $\alpha > \alpha_c$ since the bundle is in the quasi-brittle state and it requires more than one avalanche to break the whole bundle completely. The condition that $f_b(\alpha) \geq 0$ is a real and positive quantity reinforces the fact that the transition occurs at $\alpha_c = 1$.

For $\mathcal{G}(x) = x^\alpha$ case,

$$f_b(\alpha) = \alpha/(\alpha + 1) \tag{4.15}$$

and this retrieves correctly $f_b = 1/2$ for the ordinary ELS for $\alpha = 1$.

Similarly, for $\mathcal{G}(x) = xe^{\alpha x}$,

$$f_b(\alpha) = (\alpha - 2 + \sqrt{4 + \alpha^2})/2\alpha. \tag{4.16}$$

Here, the specific limiting case of $\alpha \to 0$ corresponds to $\mathcal{G}(x) = x$ and therefore, $\lim_{\alpha\to 0} f_b(\alpha) = 1/2$ is exactly the result of the ordinary ELS model with Hookean fibers.

4.4.4 Phase diagram

We can now generalize the nonlinear form by subtracting a constant term as, $\mathcal{G}(x) = e^{\alpha x} - a$, where a is a tuning parameter that varies between zero and unity. When $a = 0$ we get back the same case as described above and when $a = 1$ then the nonlinear curve $\mathcal{G}(x) = e^{\alpha x} - 1$ starts at the origin. For this case, we observe no transition from a brittle to quasi-brittle phase. However, for all value of $0 < a < 1$, we observe the brittle to quasi-brittle phase transition, and the critical point $\alpha_c(a)$ is measured for a number of values of a. To calculate it analytically, we first determine the force expression for the nonlinear stress-strain characteristic function $\mathcal{G}(x) = e^{\alpha x} - a$ which is given by:

$$F(x) = N(e^{\alpha x} - a)(1 - x). \tag{4.17}$$

If $\frac{dF(x)}{dx}\Big|_{x=0} = N(\alpha + a - 1) < 0$, then the bundle is brittle, else it is quasi-brittle [59]. This condition implies that, the relation between α_c and a is

$$\alpha_c + a = 1. \tag{4.18}$$

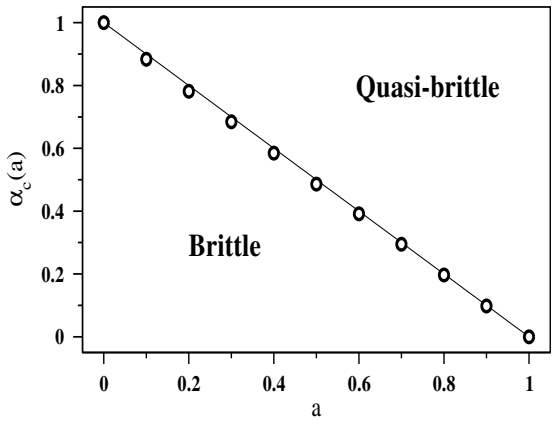

Figure 4.5: $\mathcal{G}(x) = e^{\alpha x}$: Subtracting a tunable parameter a from $\mathcal{G}(x)$ we calculate the critical value $\alpha_c(a)$ of the transition point as a function of a. For 11 different equi-spaced values of a, the values of α_c are estimated numerically and plotted. These points fit excellent with the Eq. (4.18) which describes the boundary between the brittle and the quasi-brittle regimes.

We have plotted numerical estimates of $\alpha_c(a)$ against a for 11 equi-spaced values of a in Fig. 4.5 using the same method described in the previous sections along with the analytical form given by Eq. (4.18). We observe a good correspondence between the numerical and the analytical data. The line given by Eq. (4.18) is the boundary of the brittle and the quasi-brittle phases. We have also observed transition in cases $\mathcal{G}(x) = e^{\alpha x}$ and $1 + x^{\alpha}$ which are curves that do not start from the origin and have an initial discontinuity. We have shown here that as the magnitude of the discontinuity is continuously reduced to zero, the phase transition disappears only when the discontinuity vanishes [77].

4.5 The relaxation time

Next, we study the relaxation time T as described in details in Chapter 2. When we load a bundle quasistatically, then the first avalanche is always triggered from the failure of the weakest fiber. If the bundle is in the brittle phase, then this particular avalanche is a catastrophic one and leading to complete failure of the bundle. On the other hand, if it is in the quasi-brittle phase, then this avalanche ceases to spread after the failure of few fibers. The lifetime of an avalanche is determined by the number of discrete updating

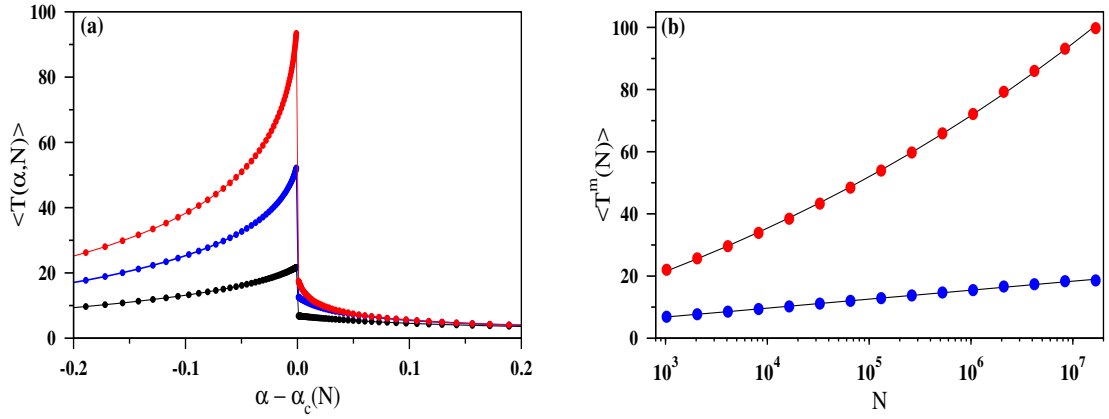

Figure 4.6: $\mathcal{G}(x) = e^{\alpha x}$: (a) Plot of the average relaxation time $\langle T(\alpha, N)\rangle$ against $\Delta\alpha = \alpha - \alpha_c^\lambda$. The brittle and the quasi-brittle phases correspond to the negative and positive values of $\Delta\alpha$. The bundle sizes are N = 2^{10}, (black) 2^{17} (blue), and 2^{24} (red) (N increases from bottom to top). (b) Variations of the maximal relaxation times $\langle T_b^m(\alpha, N)\rangle$ (upper curve) and the $\langle T_{qb}^m(\alpha, N)\rangle$ (lower curve) in the brittle and quasi-brittle regions respectively. The solid lines are the fitted functional forms given in the text.

steps. Here we study the relaxation of only the first avalanche and denote its lifetime by T. We observe that there is a vast difference in the values of T for these two regimes. We study how the relaxation time diverges as the critical value α_c is approached. For an arbitrary fiber bundle λ, we define a critical value α_c^λ which denotes the maximum value of α such that if $\alpha < \alpha_c^\lambda$ the bundle λ is brittle, otherwise it is quasi-brittle. Therefore α_c = max $\{\alpha_c^\lambda\}$ taken over all bundles in the sample of the nonlinear FBM is the same α_c as defined in Eq. (4.12).

First we calculate the precise value of critical α_c^λ for a bundle λ using the bisection method with a tolerance of 10^{-8}. This is done by choosing two initial guess values for α_{lo}^λ and α_{hi}^λ that correspond to the brittle and the quasi-brittle phases, and then halving the interval between the pair to choose an α value. This process is repeated successively till the difference $[\alpha_{hi}^\lambda - \alpha_{lo}^\lambda]$ is less than the tolerance. The relaxation time is then calculated for some prefixed intervals of $\Delta\alpha = \alpha - \alpha_c^\lambda$ for both positive and negative values. For $\Delta\alpha < 0$, it is the brittle phase, otherwise it is the quasi-brittle phase. It is observed from Fig. 4.6(a) that as we approach the critical α_c, i.e. $\Delta\alpha \to 0-$, the relaxation time $\langle T(\alpha, N)\rangle$ grows rapidly in the brittle regime and then jumps down to a

very small value when $\Delta\alpha$ is just larger than zero,and then it decreases fast as $\Delta\alpha$ takes its positive values. Clearly there is a discontinuity at $\Delta\alpha = 0$. To study it in more detail, we study the maximal relaxation times just before and after $\Delta\alpha = 0$. They are denoted by $\langle T_b^m(\alpha, N)\rangle$ and $\langle T_{qb}^m(\alpha, N)\rangle$ that correspond to maximum relaxation times in the brittle and the quasi-brittle regime. We plot these two quantities for different bundle sizes N in Fig. 4.6(b). As can be seen from the figure that both are increasing functions of the bundle size. After trying different functional forms for best fitting, we get that in the quasi-brittle regime $\langle T_{qb}^m(\alpha, N)\rangle = A_{qb} ln(B_{qb}N)$ with constants $A_{qb} = 1.25$ and $B_{qb} = 0.22$. On the other hand, in the brittle regime we found a weak power law, modulated by a logarithmic form: $\langle T_b^m(\alpha, N)\rangle = A_b N^\gamma ln(B_b N)$ with the exponent $\gamma = 0.04$ and the constants $A_b = 3.40$ and $B_b = 0.11$ [Fig. 4.6(b)].

We have observed a similar brittle to quasi-brittle transition for the nonlinear function $\mathcal{G}(x) = 1 + x^\alpha$ as well. In this case the quasi-brittle phase occurs for $\Delta\alpha < 0$ and the brittle phase is observed for $\Delta\alpha > 0$. For the other two nonlinear functions, namely, $\mathcal{G}(x) = x^\alpha$ and $\mathcal{G}(x) = xe^{\alpha x}$, no brittle to quasi-brittle transition has been observed.

4.6 Avalanche size distribution

The estimation of avalanche sizes, and in particular study of the distribution of the avalanche sizes are quite commonly done in the literature to characterize the dynamics of the FBMs. An avalanche is triggered by the loading of a bundle in a stable state in a quasistatic manner such that only one fiber is broken which is the weakest fiber among the set of intact fibers. As a result, this causes a cascade of fiber failures, and the avalanche size Δ is defined by the number of broken fibers before the bundle arrives at the next stable state. Therefore, the entire dynamical evolution of the bundle consists of a sequence of such avalanches. These avalanches are of widely different sizes, and in the case of a linear fiber bundle following ELS dynamics, their probability distribution $D(\Delta)$ against the avalanche size decays as a power law in the asymptotic limit of large

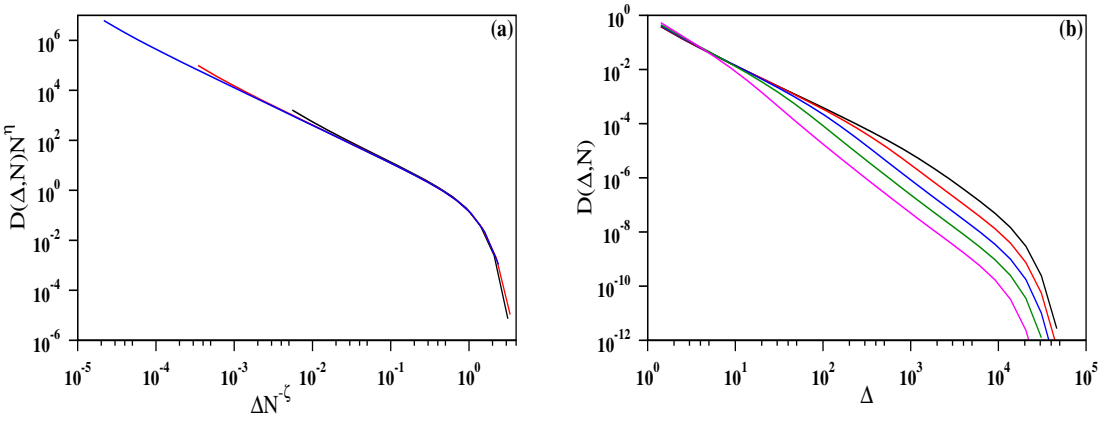

Figure 4.7: $\mathcal{G}(x) = e^{\alpha x}$: (a) A finite-size scaling of the avalanche size distribution using $D(\Delta, N)N^{\eta}$ against $\Delta.N^{-\zeta}$ for $\alpha = 1$ and $N = 2^{12}$ (black), 2^{18} (red), and 2^{24} (blue). A good collapse of data is obtained with $\eta = 1.0$ and $\zeta = 0.66$, implying $\tau = \eta/\zeta \approx 1.5$. (b) For a specific bundle size $N = 2^{20}$, the avalanche size distribution $D(\Delta, N)$ has been plotted against Δ for α = 1.05 (black), 1.1 (red), 1.2 (blue), 1.4 (green), and 2.0 (magenta) (from top to bottom). As α approaches unity, the crossover avalanche size gradually diverges.

bundle sizes: $D(\Delta) \sim \Delta^{-\tau}$, with $\tau = 5/2$ [41, 53].

In the case of our nonlinear FBM, we have estimated that exponent $\tau \approx 2.5$ in the strongly quasi-brittle regime $\alpha >> \alpha_c$. However, right at α_c, the situation is different, the exponent $\tau \approx 1.5$. Thus, there exists a crossover in the avalanche size exponent from ≈ 1.5 to ≈ 2.5 as α is continuously increased from unity. For a specific value of α in between these two limits, there exists a threshold value $\Delta_c(\alpha)$ of the avalanche size, such that for $\Delta << \Delta_c$, one gets $\tau \approx 1.5$ and for $\Delta >> \Delta_c$, one gets $\tau \approx 2.5$. This implies that even though the width of the distribution of breaking strains is kept unchanged, there exists a phase transition from brittle to quasi-brittle regime. Fig 4.7(a) shows the avalanche size distribution at $\alpha_c = 1$ where the exponent is ≈ 1.5. On the other hand, Fig. 4.7(b) shows the avalanche size distribution for five different values of $\alpha > 1$ and for a fixed bundle size $N = 2^{20}$. For each curve, a value of Δ_c can be identified as the crossover avalanche size, such that the slopes of the curve for the Δ smaller and larger than Δ_c are approximately 1.5 and 2.5 respectively [15].

For the case $\mathcal{G}(x) = 1 + x^{\alpha}$, a similar crossover from $\tau \approx 1.5$ to $\tau \approx 2.5$ has been observed. However, no such crossover has been seen in the other two cases.

4.7 Dependence on the width of the disorder distribution

Next, we studied how the behavior of the nonlinear fiber bundle is affected when the width of the distribution of the breaking strains of individual fibers is varied. Here, the breaking strains $\{x_i\}$ were distributed within the range $\{0, 1\}$. We now make the distribution $p(x)$ tunable, and assume that $p(x)$ is again a normalized uniform distribution within the limits $(\frac{1}{2} - \delta)$ to $(\frac{1}{2} + \delta)$ where the δ is a continuously tunable parameter that changes the width of the distribution. Therefore, the normalized probability distribution is given by $p(x) = 1/2\delta$ and the cumulative probability $P(x) = (x - 1/2 + \delta)/2\delta$ for $(1/2 - \delta) \leq x \leq (1/2 + \delta)$. Again, using $\mathcal{G}(x) = e^{\alpha x}$ and following Eq. (4.3), the functional form of the external load is found to be

$$F(x, \alpha, \delta) = \frac{Ne^{\alpha x}}{2\delta}(\delta + \frac{1}{2} - x). \tag{4.19}$$

In the same way as mentioned before, maximizing $F(x)$ at the critical strain x_c yields

$$x_c(\alpha, \delta) = \delta + 1/2 - 1/\alpha. \tag{4.20}$$

We have discussed before that in a brittle bundle, the weakest fiber failure leads to complete failure of the bundle. When the value of δ is small then the value of the minimum breaking strain x_m is large and consequently the stress released by that fiber is also large. This released stress is thus high enough to trigger a devastating avalanche that breaks the remaining intact fibers in successive load redistribution steps. On the other hand when δ is a large value then x_m is small and so the load released after the breaking of this fiber is small and the avalanche created by the failure of this weakest fiber quickly gets arrested. Since a bundle is quasi-brittle, if the number of avalanches required for the global failure is at least two, therefore, tuning the value of $\delta > \delta_c$ the bundle shifts from the brittle to the quasi-brittle phase. Therefore, in the limit of $N \to \infty$, the critical value of δ_c can be calculated by equating the critical strain x_c to the lowest possible breaking threshold in the bundle which is the lower limit of the uniform distribution.

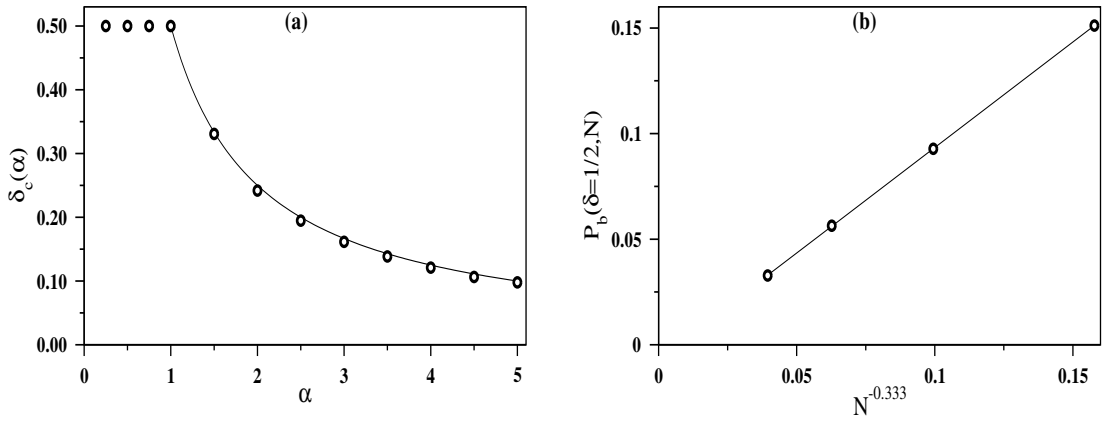

Figure 4.8: $\mathcal{G}(x) = e^{\alpha x}$: (a) Plot of the critical width $\delta_c(\alpha)$ against α using open circles. The corresponding analytical form in Eq. (4.21) has been shown in black solid line. The matching is quite good. (b) For $\alpha = \alpha_c = 1$ and for $\delta_c = 1/2$, the probability of occurrence of a brittle bundle has been plotted against $N^{-0.333}$ and a very good straight line fit has been obtained. On extrapolation, this line passes very close to the origin.

Thus $1/2 - \delta_c = x_c$ yields,

$$\delta_c(\alpha) \;=\; 1/2\alpha. \tag{4.21}$$

Numerically, to find $\delta_c(\alpha, N)$ for a particular α and N, a large sample of independent fiber bundles are considered and the value of δ is varied in small steps from 0 to $1/2$. The fraction of bundles that are brittle, is denoted by the probability for a brittle bundle $P_b(\alpha, N)$. The value of δ for which $P_b(\alpha, N) = 0$ is considered to be the value of $\delta_c(\alpha, N)$. For each value of α, this calculation is then repeated for four different values of N = 2^8, 2^{10}, 2^{12}, and 2^{14} and the $\delta_c(\alpha, N)$ values are extrapolated to obtain the asymptotic value of $\delta_c(\alpha)$.

This calculation is repeated for different values of α and $\delta_c(\alpha)$ is plotted against α in Fig. 4.8(a) along with the analytical form. The numerical result matches well with the analytical expression given by Eq. (4.21). However, this method did not work for $\alpha = 1$, where even for $\delta = 1/2$, the probabilities $P(\alpha, N)$ are found to be non-zero. We therefore calculated the probability $P(\alpha = 1, \delta = 1/2, N)$ for different values of N and extrapolated them in Fig. 4.8(b) against $N^{-0.333}$. The data fits nicely to a straight line and on extrapolation, the fitted straight line passes through the origin. From this analysis we conclude $\delta_c(\alpha = 1)$=0.5. In a similar way, for $\alpha < 1$, the probability $P(\delta, \alpha, N)$ values

for $\delta = 1/2$ are non-zero, and on extrapolation, the extrapolated value still remains larger than zero. Since, by definition δ cannot be greater than 1/2, we conclude that $\delta_c(\alpha) = 1/2$ for all values of α in the range $0 < \alpha \leq 1$.

These calculations have been repeated for the stress-strain characteristic $\mathcal{G}(x) = x^\alpha$. The corresponding value of $\delta_c(\alpha)$ in this case is given by

$$F(x, \alpha, \delta) = \frac{Nx^\alpha}{2\delta}(\delta + 1/2 - x), \tag{4.22}$$

$$x_c(\alpha, \delta) = [\alpha(2\delta + 1)]/[2(\alpha + 1), \tag{4.23}$$

$$\delta_c(\alpha) = 1/[2(2\alpha + 1)]. \tag{4.24}$$

Similarly, for $\mathcal{G}(x) = xe^{\alpha x}$,

$$F(x, \alpha, \delta) = Nxe^{\alpha x}(\delta + 1/2 - x)/2\delta, \tag{4.25}$$

$$x_c(\alpha, \delta) = (t - 2 + \sqrt{t^2 + 4})/2\alpha \tag{4.26}$$

$$\text{where } t = \alpha(1/2 + \delta), \tag{4.27}$$

$$\delta_c(\alpha) = (\alpha + 3 - \sqrt{\alpha^2 + 2\alpha + 9})/4\alpha. \tag{4.28}$$

Here, the limit of $\alpha \to 0$ implies $\mathcal{G}(x) = x$ and therefore $\lim_{\alpha \to 0} \delta_c(\alpha) = 1/6$ gives us the same result obtained in [58].

4.8 Additional examples of brittle to quasi-brittle transitions

In this section we would consider some more example cases where the brittle to quasi-brittle transitions take place. These examples have different forms of the characteristic nonlinear stress (s) - strain (x) functions, different forms of the probability distribution functions as the input. However, none of them has any discontinuity in the function $\mathcal{G}(x)$. Yet, a transition from a brittle phase to a quasi-brittle phase is observed in each case.

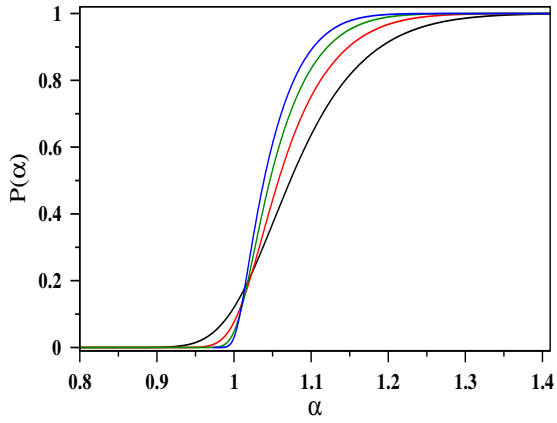

Figure 4.9: *Case I*: Probability $P(\alpha, N)$ of finding an arbitrary fiber bundle of size N in the brittle phase for a specific value of α. The bundle sizes are $N = 2^{10}$ (black), 2^{12} (red), 2^{14} (green), and 2^{16} (blue) and the distribution becomes increasingly sharper with increasing N at the critical value of $\alpha_c = 1$.

Case I: The form of the nonlinear stress (s) - strain (x) function is:

$$\mathcal{G}(x) = \begin{cases} x, & \text{for} \quad 0 \leq x < 1 \\ 1 + (x-1)^{\alpha}, & \text{for} \quad x \geq 1, \end{cases} \tag{4.29}$$

and the distribution of breaking strains is

$$P(x) = \begin{cases} 0, & \text{for} \quad 0 \leq x < 1 \\ x - 1, & \text{for} \quad 1 \leq x \leq 2. \end{cases} \tag{4.30}$$

For this case the functional form of the external load is:

$$F(x) = N \begin{cases} x, & \text{for} \quad 0 \leq x \leq 1 \\ [1 + (x-1)^{\alpha}][1 - (x-1)] & \text{for} \quad 1 \leq x \leq 2. \end{cases} \tag{4.31}$$

To study the transition in this case we plot the variation of the probability $P(\alpha, N)$ of finding an arbitrary fiber bundle of size N in the brittle phase for a specific value of α in Fig. 4.9. The distribution is seen to become sharper as the system size increases. That is, for $\alpha < \alpha_c = 1$, $P(\alpha, N) \to 0$ and for $\alpha > \alpha_c$, $P(\alpha, N)$ assumes non-zero values which approaches unity for large values of α. Next, we have plotted the variation of $\sigma_c(\alpha)$ against α in Fig. 4.10(a) which exhibits a slow decay on increasing α. Finally in Fig. 4.10(b), the fraction $f_b(\alpha, N)$ of broken fibers before the last avalanche has been

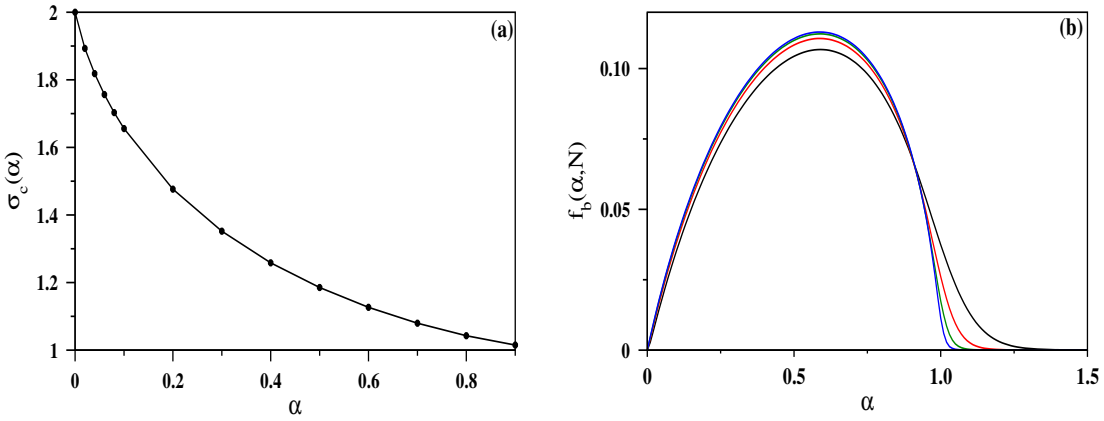

Figure 4.10: *Case I*: (a) Numerically obtained values of the asymptotic critical load $\sigma_c(\alpha)$ has been plotted against α. It gradually decreases to a value of $\sigma_c(\alpha) = 1$. (b) Fraction $f_b(\alpha, N)$ of broken fibers before the last avalanche has been plotted against α for the bundle sizes $N = 2^8$ (black), 2^{10} (red), 2^{12} (green), and 2^{14} (blue) and the curves become increasingly sharper with increasing N at the critical value of $\alpha_c = 1$.

plotted against α. When the nonlinear parameter α is very small, i.e. $\alpha \to 0$, then the fraction $f_b(\alpha, N)$ gradually tends to vanish as well. This quantity $f_b(\alpha, N)$ is also zero at the transition point given by $\alpha_c = 1$. This implies that $f_b(\alpha, N)$ has a maximum in between $0 < \alpha < 1$.

Case II: In this case the stress - strain relation is linear,

$$\mathcal{G}(x) = x, \quad \text{for} \quad 0 \leq x \tag{4.32}$$

but the distribution of breaking strains is nonlinear and is limited only between $1 \leq x < 2$ and zero otherwise, as:

$$P(x) = \begin{cases} 0, & \text{for} \quad 0 \leq x < 1 \\ (x-1)^{1/\alpha}, & \text{for} \quad 1 \leq x \leq 2. \end{cases} \tag{4.33}$$

For this case the functional form of the external load is:

$$F(x) = N \begin{cases} x, & \text{for} \quad 0 \leq x \leq 1 \\ x[1-(x-1)^{1/\alpha}] & \text{for} \quad 1 \leq x \leq 2. \end{cases} \tag{4.34}$$

Using a change of variable one can write

$$y = \begin{cases} x, & \text{for} \quad 0 \leq x < 1 \\ 1 + (x-1)^{1/\alpha}, & \text{for} \quad 1 \leq x. \end{cases} \tag{4.35}$$

which on inversion

$$x = \begin{cases} y, & \text{for } \ 0 \leq y < 1 \\ 1 + (y-1)^{\alpha}, & \text{for } \ 1 \leq y. \end{cases} \tag{4.36}$$

Therefore, the functional form of the external load becomes,

$$F(y) = F(x) = N \begin{cases} y, & \text{for } \ 0 \leq y < 1 \\ [1 + (y-1)^{\alpha}][1 - (y-1)], & \\ \text{for } \ 1 \leq y \leq 2. & \end{cases} \tag{4.37}$$

which has the same form as in Eq. (4.31) but in terms of y instead of x. However, in spite of such a change of variable, the order statistics for the breaking thresholds $s^{\lambda}_{(1)}$, $s^{\lambda}_{(2)}$, ..., $s^{\lambda}_{(N)}$ discussed in Sec. 2.2 corresponding equations for Eq. (2.3) and Eq. (2.4) remains unchanged.

Case III:

$$\mathcal{G}(x) = x, \quad \text{for } \ 0 \leq x \tag{4.38}$$

$$P(x) = \begin{cases} 0, & \text{for } \ 0 \leq x < 1 \\ 1 - 1/x^{\alpha}, & \text{for } \ 1 \leq x \leq \infty. \end{cases} \tag{4.39}$$

$$F(x) = N \begin{cases} x, & \text{for } \ 0 \leq x \leq 1 \\ x^{1-\alpha} & \text{for } \ 1 \leq x \leq \infty. \end{cases} \tag{4.40}$$

In the case of $\alpha = 1$,

$$F(x) = N \begin{cases} x, & \text{for } \ 0 \leq x \leq 1 \\ 1 & \text{for } \ 1 \leq x \leq \infty. \end{cases} \tag{4.41}$$

In both cases of II and III, our numerical simulation results confirm the brittle to quasi-brittle transition at $\alpha_c = 1$.

Case IV: The distribution of breaking strengths, i.e., either breaking stresses or breaking strains of individual fibers play an important role in determining the overall behavior of the fiber bundle. In Chapter 3 it has been shown that the power law distribution of

breaking stresses of fibers can also lead to a brittle to quasi-brittle transition where the exponent ν defined by Eq. (4.2) depends explicitly on the cut-off parameter of that distribution.

In a similar way, we define following [78] a cumulative probability distribution of breaking stresses of individual fibers in the following way:

$$P_N(s) = \begin{cases} 0, & \text{for } \ 0 \leq s < 1 \\ 1 - 1/s^{\alpha}, & \text{for } \ 1 \leq s \leq \infty. \end{cases} \tag{4.42}$$

We observe a transition here as well between the brittle and quasi-brittle phases. The transition is seen to occur at $\alpha_c = 1$. However, this transition is less sharp in this case, i.e., $P(\alpha)$ increases at a slower rate for $\alpha > \alpha_c$ in comparison to cases I and II.

4.9 Summary

To summarize, we have studied some breakdown properties of FBMs with nonlinear elastic fibers. Here, each fiber is assigned a random breaking threshold of its own. We have observed the well-known brittle to quasi-brittle phase transition at a critical value of α_c of the parameter α that defines the nonlinearity in the stress-strain characteristic function $\mathcal{G}(x)$. The relaxation time at the transition point is seen to diverge with increasing N as the critical point is approached. At the brittle phase, it diverges with a weak power law modulated logarithmic function while in the quasi-brittle phase it diverges with logarithmic functional forms. Using the analytical tools and numerical results, we have also studied the variation of $\alpha_c(\delta)$ as a function of the width δ of the distribution of the breaking strains. In addition, we have considered three more cases, where the stress-strain relations are linear, but the probability distribution of breaking thresholds is nonlinear. The brittle to quasi-brittle transition has been observed in these cases as well.

CHAPTER 5

Brittle to quasi-brittle transition in a compound fiber bundle

5.1 Introduction

It is well known when two or more different types of materials having different properties are combined together then the resulting product has properties that are distinct from its individual components. These compound materials with mixtures of different kinds of fibers are very important in industrial applications. For example, good quality fabrics are produced using mixtures of cotton and nylon fibers. This prompts us to study the properties of a compound FBM when the failure thresholds of the individual fibers assume a bimodal distribution. In this chapter, we have mainly studied the brittle to quasi-brittle transitions for the compound fiber bundles. Breaking thresholds of fibers of these materials are widely different. Keeping this in mind, one therefore likes to ask what changes in the properties of a fiber bundle take place when the bundle is made of two different types of fibers with different sets of breaking thresholds. A FBM with discontinuous distribution of breaking thresholds in a different form had been considered in the literature to study the breakdown properties [79, 80].

This chapter is arranged in the following way. In Sec. 5.2, we describe the characteristics of the bimodal distribution and determine the critical threshold of the compound

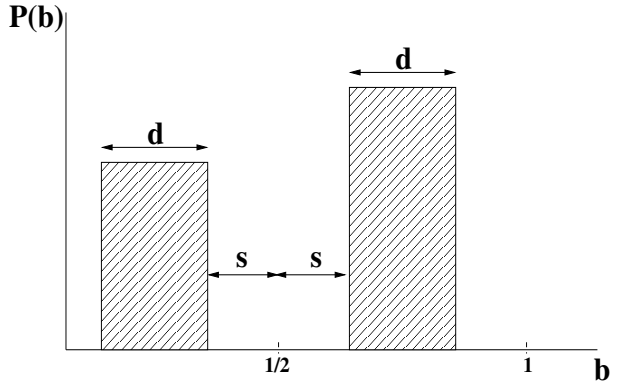

Figure 5.1: The bimodal probability density distribution $P(b)$ of the breaking thresholds b of the fibers plotted against b. The distribution consists of two rectangular blocks of width d, symmetrically placed around $b = 1/2$ keeping a gap of $2s$ between them. The total probabilities in the first and the second blocks are denoted by p and $1 - p$ respectively.

fiber bundle. In Sec. 5.3, we describe the brittle to quasi-brittle transition in this model of the fiber bundle. Finally, we summarize our work and conclude in Sec. 5.4.

5.2 Bimodal distribution and the breaking threshold

We consider a fiber bundle having N fibers whose breaking thresholds $\{b_i\}$ are drawn from a bimodal distribution. This distribution is a combination of two uniform distributions of width d, symmetrically placed about the midpoint $b = 1/2$ of the b axis, and are separated by an amount of $2s$ as shown in Fig. 5.1. The first and the second blocks are extended over the regions $1/2 - s - d \leq b \leq 1/2 - s$ and $1/2 + s \leq b \leq 1/2 + s + d$ respectively. The probability that a randomly selected fiber belongs to the first and the second block are denoted by p and $1 - p$ respectively. The cumulative probability distribution is the probability that an arbitrarily selected fiber has strength less than b is given by:

$$\begin{cases} p(b - 1/2 + s + d)/d, & \text{for block 1} \\ p + (1 - p)(b - 1/2 - s)/d, & \text{for block 2.} \end{cases} \tag{5.1}$$

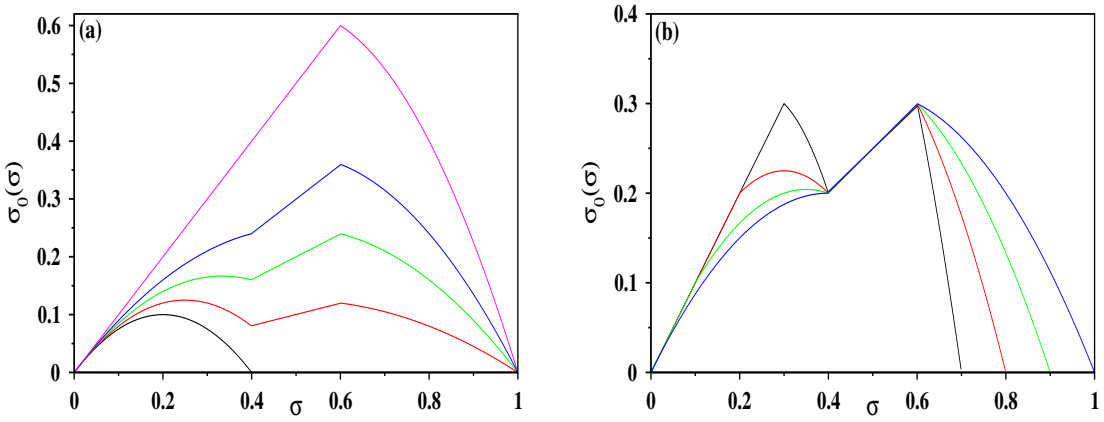

Figure 5.2: Using the Eq. (5.4), $\sigma_0(\sigma)$ has been plotted against σ for different parameter values: (a) For $s = 0.1$ and $d = 0.4$ five curves have been plotted for p = 0 (magenta), 0.4 (blue), 0.6 (green), 0.8 (red) and 1 (black) displayed from top to bottom. (b) For s = 0.1 and p = 0.5 four curves have been plotted for d = 0.1 (black), 0.2 (red), 0.3 (green) and 0.4 (blue) displayed from top to bottom in the first block and left to right in the second block.

In an arbitrary intermediate stable state the average value of the applied load $F(\sigma)$ as a function of the stress σ per intact fiber is given by [12, 19, 71]

$$F(\sigma) = N\sigma[1 - P(\sigma)]. \tag{5.2}$$

The scaled external load per fiber $\sigma_0(\sigma) = F(\sigma)/N$ is therefore,

$$\sigma_0(\sigma) = \sigma(1 - P(\sigma)). \tag{5.3}$$

For our compound fiber bundle

$$\sigma_0(\sigma) = \begin{cases} [1 - p(\sigma - 1/2 + s + d)/d]\sigma & \text{for block 1} \\ [(1-p) - (1-p)(\sigma - 1/2 - s)/d]\sigma & \text{for block 2.} \end{cases} \tag{5.4}$$

This variation of $\sigma_0(\sigma)$ against σ has been displayed in Fig. 5.2(a) for a specific set of values of the parameters s = 0.1, d = 0.4 and for five different values of the first block probability p = 0, 0.4, 0.6, 0.8, and 1. When $p = 0$, then all the fibers are in the second block which implies that all the breaking threshold values are confined between $1/2 + s$ and 1. Here, the system is always observed to be brittle and this behavior is evident from the plot in 5.2(a) which shows that $\sigma_0(\sigma)$ is always a decreasing function of σ. As the

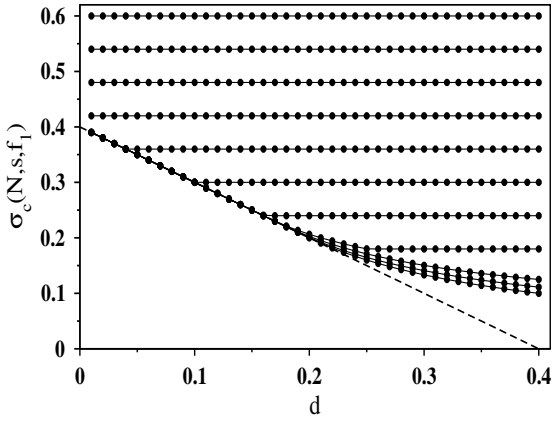

Figure 5.3: Plot of the critical load $\sigma_c(N, s, p)$ against the block width d using $N = 2^{18}$ and $s = 0.1$. The value of first block probability p has been tuned between 0 and 1 in steps of 0.1 displayed from top to bottom. The dashed line has the equation $\sigma_c(N, s, p) = 1/2 - s - d$.

value of p increases the system becomes quasi-brittle as can be seen from the variations of $\sigma_0(\sigma)$. In Fig. 5.2(b) the same variation is plotted for the specific set s = 0.1, p = 0.5 and for four different values of d = 0.1, 0.2, 0.3 and 0.4. Each plot has two regions, one for the first block and the other for the second block. In both the figures $\sigma_0(\sigma)$ varied linearly with σ between the two blocks. Here also, as the value of d is decreased the system can be seen to change from a brittle phase to a quasi-brittle phase. The critical load per fiber of the system is always the maximum value of $\sigma_0(\sigma)$ for all cases.

We first study the critical load per fiber σ_c for the global failure of the fiber bundle for different values of the parameters s, d and p. In particular, we consider the case where the value of the parameter s is fixed at 0.1 and using different values of p, we vary the value of the block width d [67, 68]. For the estimation of σ_c numerically we follow the method of [66] that has been described in details in Sec. 2.2. We first arrange the breaking thresholds of a particular bundle α in an increasing order such that $b^{\alpha}_{(1)} < b^{\alpha}_{(2)} < b^{\alpha}_{(3)} < ... < b^{\alpha}_{(N)}$. Then, the critical load per fiber $\sigma^{\alpha}_c(N)$ for a particular bundle N can be calculated from Eq. (2.4).

This critical load is then averaged over a considerably large number of configurations to get $< \sigma^{\alpha}_c(N) >= \sigma_c(N)$. We assume that it converges to $\sigma_c(\infty) \equiv \sigma_c$ in the asymptotic limit according to $\sigma_c(N) = \sigma_c + AN^{1/\nu}$ where A is a constant and $1/\nu$ is a

finite size correction exponent. For a sufficiently large N the correction term becomes negligible. In Fig. 5.3 we have plotted eleven different sets of data for different values of first block probability p tuned between 0 and 1 at equal intervals of 0.1 for $N = 2^{18}$. Since this is a considerably large number we expect that this behavior would hold for asymptotically large bundle sizes as well. For small values of p the σ_c remains constant in the entire range of variation of d. For example, $p = 0$ implies all fibers have breaking thresholds larger than $1/2 + s$ and the weakest fiber will always have the value $1/2 + s$. Since for all values of d the system is always brittle, when the external load per fiber is raised to 0.6, the weakest fiber fails and this leads to a cascade of fiber failures resulting in the break down of the entire fiber bundle. For this reason, the fiber bundle is said to be brittle for this set of parameter values, independent of the block width d. As p is increased the σ_c decreases and for $p \geq 0.3$ the values are not constant any more. This is because as the number of fibers in the first block increases it lowers the critical load of the system. The same process has also been carried out for s = 0, 0.2, 0.3 and 0.4. The dashed line has the equation $\sigma_c(N, s, p) = 1/2 - s - d$ which means that the set of (s, p, d) for which a $\sigma_c(N, s, p)$ falls on that line is a brittle system.

5.3 Brittle to quasi-brittle transition

To describe the brittle to quasi-brittle transition we analyze the following three quantities, namely: (i) the fraction $f(d, N)$ of fibers broken before the last avalanche, (ii) the average number $\langle M(d, N)\rangle$ of avalanches required for the complete failure of the bundle, and (iii) the average size $\langle \Delta(d, N)\rangle$ of the avalanches [77]. Variations of these quantities have been studied against the width parameter d over its entire range. In particular, we have estimated the critical value d_c of the width that demarcates the brittle phase of the bundle from its quasi-brittle phase.

5.3.1 Case $p = 0$

First we consider the case when only the right block exists, i.e., $p = 0$. This implies that the breaking thresholds of all the fibers in the bundle are selected from the second block. In this case, the cumulative distribution $P(b)$ reduces to

$$P(b) = (b - 1/2 - s)/d \tag{5.5}$$

and Eq. (5.4) becomes

$$\sigma_0(\sigma) = \sigma(1 - (\sigma - 1/2 - s)/d). \tag{5.6}$$

At the breaking point of the bundle, Eq. (5.6) has a maximum at $\sigma = \sigma_{0c}(d, s)$ and it is calculated to be

$$\sigma_{0c}(d, s) = d/2 + (1/2 + s)/2. \tag{5.7}$$

In this situation the value of $\sigma_{0c}(d, s)$ is equal to the minimum value of the breaking thresholds of the bundle, i.e., $1/2 + s$. Thus,

$$d_c/2 + (1/2 + s)/2 = 1/2 + s \tag{5.8}$$

which gives $d_c = 1/2 + s$, the critical point. This result implies that for a system with all the fibers in the second block, the bundle will always be brittle and no transition can be observed from a brittle to a quasi-brittle phase.

Numerically, we study the fraction $f(d, N)$ of fibers broken before the last avalanche against the block width d for four different sizes of the fiber bundle [76]. By definition, $f(d, N)$ is identically zero when the bundle is completely brittle and non-zero when it is quasi-brittle. Fig. 5.4(a) exhibits the variation of $f(d, N)$ against d. As the bundle size N increases, the larger portion of the curve coincides with the d axis. Therefore, the minimal value $d_c(N)$ of d where $f(d, N)$ is non-zero increases and approaches the value of 1/2. This implies that over the entire range of the width parameter d, the bundle is in the brittle phase.

The variation of the scaled average number $\langle M(d, N)\rangle/N$ of avalanches required for the complete failure of the bundle has been plotted against the block width d and is

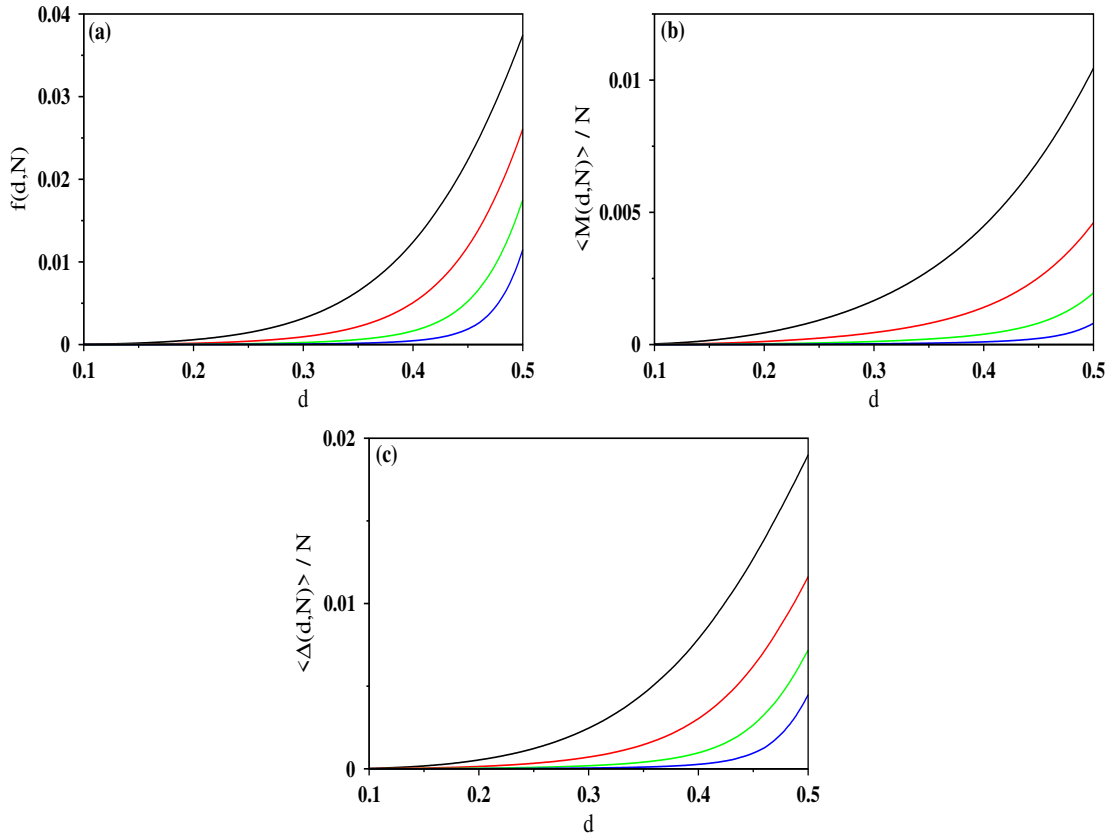

Figure 5.4: Plots are shown here for the special case when only the second block exists i.e., $p = 0$. The separation parameter $s = 0$ i.e., the left end of the block is fixed at $b = 1/2$ and its right end extends up to $1/2 + d$. Four different bundle sizes are used: $N = 2^8$ (black), 2^{10} (red), 2^{12} (green) and 2^{14} (blue) (N increasing from top to bottom). To characterize the brittle to quasi-brittle transition, three quantities have been plotted against the block width d. They are: (a) the fraction $f(d, N)$ of fibers broken before the last avalanche; (b) the fraction of the average number of avalanches $\langle M(d, N)\rangle/N$ required for complete breakdown and (c) the average avalanche size $\langle\Delta(d, N)\rangle$ scaled by the bundle size.

shown in Fig. 5.4(b). This quantity is also seen to be increasingly smaller with increasing value of the bundle size N indicating the absence of any transition in the system.

The size of an avalanche $\Delta(d, N)$ is measured by the number of fibers failed during the avalanche. Following the method of Kun et. al. [59] we define the average size of the avalanches, excluding the last avalanche. The average avalanche size $\langle\Delta(d, N)\rangle$ is defined as the ratio of second moment to the first moment of the avalanche sizes, as

$$\langle\Delta(d, N)\rangle = \Sigma_k\Delta_k^2(d, N)/\Sigma_k\Delta_k(d, N) \tag{5.9}$$

where the summation index k runs over all avalanches except the last avalanche. This

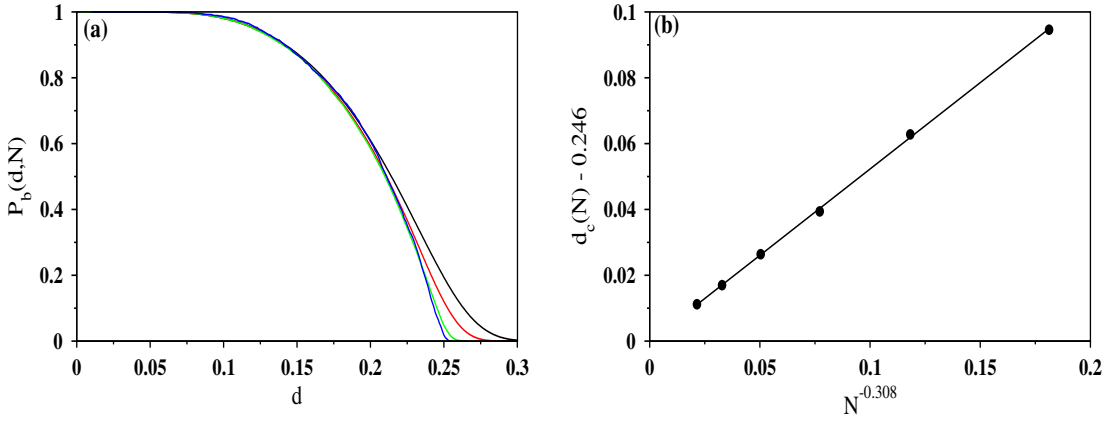

Figure 5.5: (a) The probability $P_b(d, N)$ that a randomly selected fiber bundle with $s = 0$ and $p = 1$ is brittle, has been plotted against the block width d. The bundle sizes used are: $N = 2^8$(black), 2^{10}(red), 2^{14}(green) and 2^{18}(blue) (N increasing from right to left). (b) As the bundle size N increases, the critical block width $d_c(N)$ approaches the value 0.246 as $N^{-0.308}$.

quantity $\langle \Delta(d, N) \rangle$ has been plotted in Fig. 5.4(c) that has no maximum for any value of d which proves that for this particular case there is no transition. This result is expected because the case $s = 0$ and $p = 0$ implies that all the fibers are in second block where the bundle always remains in a brittle phase.

5.3.2 Case $p = 1$

The case with $p = 1$ implies that all the fibers in the bundle have their breaking thresholds drawn from the first block. For this case

$$\sigma_{0c}(d, s) = d[1 + (1/2 - s - d)/d]/2. \tag{5.10}$$

On equating $\sigma_{0c}(d, s)$ to the value of the lowest breaking threshold for this case $1/2-s-d$ we get the transition point as

$$d_c = (1/2 - s)/2. \tag{5.11}$$

Thus, when all the fibers in the bundle are in the first block then the value of d_c decreases linearly with increase in s.

In a specific case, the result of $d_c = 1/4$ from Eq. (5.11) for $s = 0$ and $p = 1$ has been verified numerically. The probability $P_b(d, N)$ that a randomly selected sample

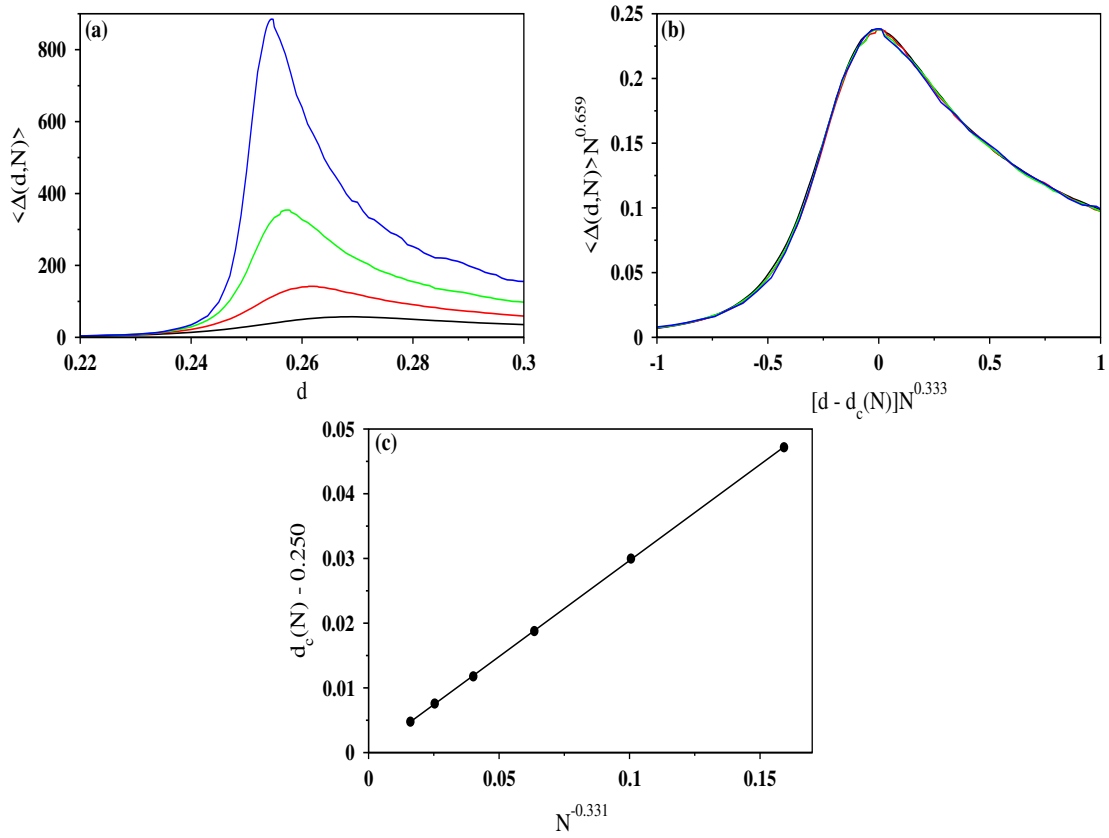

Figure 5.6: (a) Plot of the average avalanche size $\langle \Delta(d,N) \rangle$ against the block width d. (b) The finite size scaling plot of the data in (a). An excellent collapse of the data has been observed when $\langle \Delta(d,N) \rangle N^{-0.659}$ has been plotted against $[d - d_c(N)]N^{0.333}$. The bundle sizes used in both (a) and (b) are: $N = 2^{12}$(black), 2^{14}(red), 2^{16}(green) and 2^{18}(blue) (N increasing from bottom to top in (a)). (c) The critical width $d_c(N)$ of the first block obtained from the widths corresponding to the maximum values of the average avalanche size $\langle \Delta(d,N) \rangle$ shown in (a). The difference $d_c(N) - 0.250$ vanishes when plotted against $N^{-0.331}$. Therefore, $d_c(\infty) = 0.250$ is very much consistent with the analytical value of $d_c = 1/4$ as given in Eq. (5.11).

of the fiber bundle is brittle has been plotted against d in Fig. 5.5(a) for four different bundle sizes. The critical width $d_c(N)$ for a specific bundle size N is defined as the minimum value of d for which $P_b(d,N)$ vanishes. The estimated values of $d_c(N)$ are assumed to converge to their asymptotic value d_c as:

$$d_c(N) - d_c = BN^{-1/\nu}. \tag{5.12}$$

To estimate the asymptotic value d_c and the exponent ν we have plotted the $d_c(N)$ against $N^{-1/\nu}$ in Fig. 5.5(b). The precise value of the exponent is tuned so that we get the best straight line with minimal fitting error. Our best estimate from this plot are $d_c = 0.246$

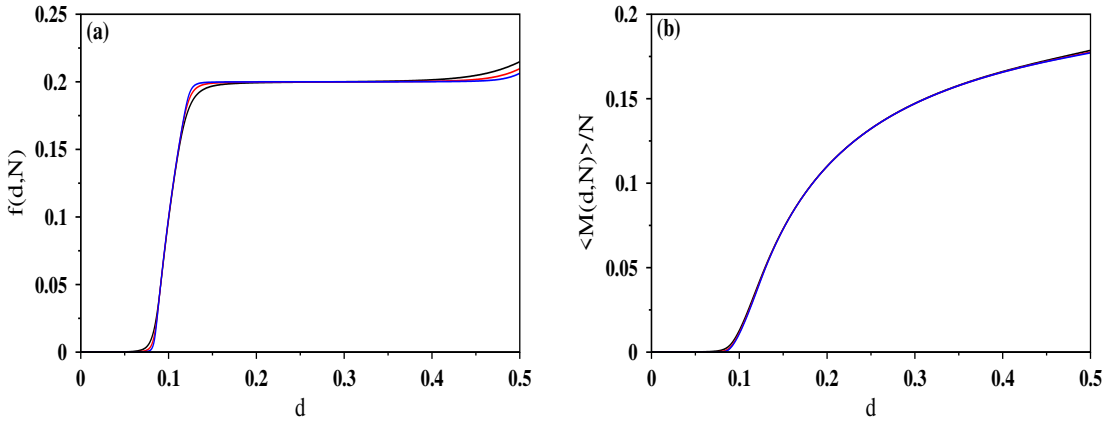

Figure 5.7: Variation of the same quantities plotted in Fig. 5.4(a) and Fig. 5.4(b), i.e., $f(d, N)$ and $\langle M(d, N)\rangle/N$ against the block width d have been displayed for $s = 0$ and $p = 0.2$. The bundle sizes are $N = 2^{12}$ (black), 2^{14} (red) and 2^{16} (blue). These plots are characteristically different from those in Fig. 5.4. Each indicates the existence of a transition from the brittle phase to the quasi-brittle phase.

and $1/\nu = 0.308$.

The critical width $d_c(N)$ has also been estimated from the statistics of avalanche sizes. The average size of the avalanches $\langle\Delta(d, N)\rangle$ given by Eq. (5.9) has been studied and plotted against d in Fig. 5.6(a) for four different values of the bundle sizes. It is seen that for every bundle size the curve has a maximum at a certain value of d which we assume as the second definition of $d_c(N)$. A finite size scaling of the data turned out to be very nice when we plotted $\langle\Delta(d, N)\rangle N^{0.659}$ against $[d - d_c(N)]N^{0.333}$. We use the $d_c(N)$ values estimated from the peak positions and in Fig. 5.6(b) all four curves fall very closely on one another. In Fig. 5.6(c) we again plot $d_c(N) - d_c$ against $N^{-1/\nu}$ and tune ν to get the best fitted straight line. Our results are $d_c = 0.250$ and $1/\nu = 0.331$.

5.3.3 Case $0 < p < 1$

We have further observed that for other intermediate values of the first block probability parameter p, again with the separation parameter $s = 0$, there exists non-trivial phase transitions from the brittle to the quasi-brittle phases. For example, in a particular case of $p = 0.2$, we have again studied the same quantities, namely the fraction $f(d, N)$ of fibers broken before the last avalanche, the average number $\langle M(d, N)\rangle$ of avalanches

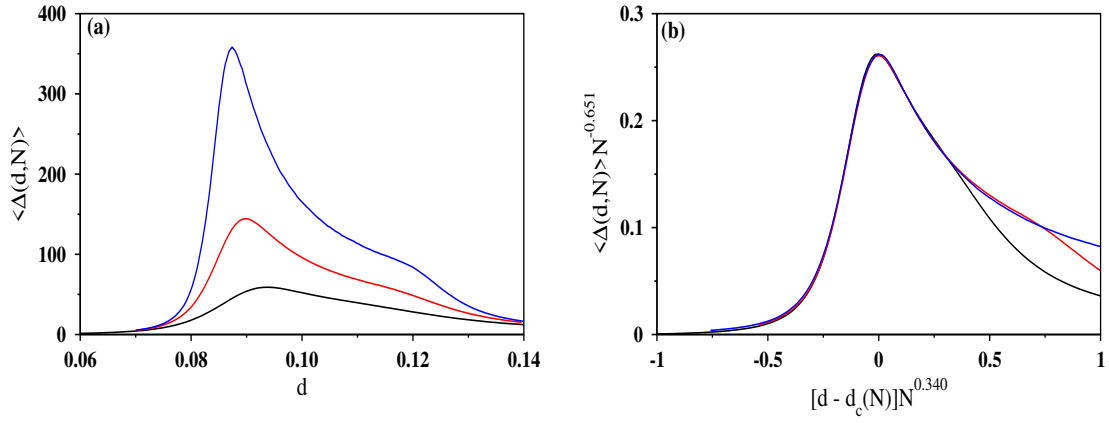

Figure 5.8: (a) Plot of the variation of the quantity plotted in Fig. 5.4(c), i.e., $\langle\Delta(d,N)\rangle/N$ against the block width d have been displayed for $s = 0$ and $p = 0.2$ for $N = 2^{12}$(black), 2^{14}(red), and 2^{16}(blue) (N increasing from bottom to top)). The quantity shows a maximum at a certain value of d_c which indicates a transition from a brittle to a quasi-brittle state. (b) Finite size scaling of the average avalanche size $\langle\Delta(d,N)\rangle N^{-0.651}$ against $[d - d_c(N)]N^{0.340}$ using the data in (a) exhibits an excellent data collapse.

required for the complete failure of the bundle and the average size $\langle\Delta(d,N)\rangle$ of the avalanches. These quantities have been plotted against the block width d in Figs. 5.7(a), 5.7(b) and 5.8(a) where d has been tuned from 0 to $1/2$ at the interval of 0.0001. It is again observed that $\langle\Delta(d,N)\rangle$ exhibits a maximum at $d_c(N)$ and grows with the bundle size indicating a phase transition. Finally, in Fig. 5.8(b) we have plotted the scaled variable $\langle\Delta(d,N)\rangle N^{0.651}$ against $[d - d_c(N)]N^{0.340}$ which exhibits a good collapse of data. The value of d_c for large N have been estimated by extrapolating the bundle sizes against $N^{-0.325}$ over $N = 2^{14}, 2^{16}$ and 2^{18}.

Similarly, the calculation for $d_c(s,p)$ for $s = 0$ has been repeated for the other values of p in the range $0 < p \leq 1$ at the interval of 0.1 and plotted in Fig. 5.9. It may be noted that the bundle is always brittle for $p = 0$. On the other hand, for $p > 0$ the bundle has the non-vanishing critical width i.e., $d_c > 0$. Moreover, four other sets of data of $d_c(s,p)$ against p for s = 0.1, 0.2, 0.3 and 0.4 have been plotted in the same Fig. 5.9.

From Eq. (5.4), one obtains the maximum value of $\sigma_{0c}(d,s,p)$ for a quasi-brittle state for the first block as

$$\sigma_{0c}(d,s,p) = d[1 + p(1/2 - s - d)/d]/(2p). \tag{5.13}$$

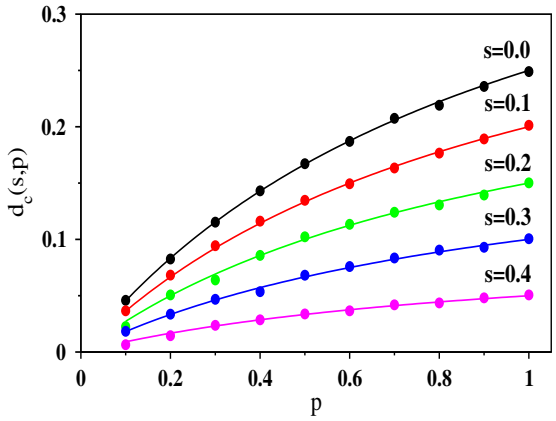

Figure 5.9: The extrapolated values of the critical block width $d_c(s,p)$ in the asymptotic limit of large bundle sizes have been plotted using filled circles against the first block probability p for different values of the separation parameter $s = 0$ (black), 0.1 (red), 0.2 (green), 0.3 (blue) and 0.4 (magenta) with s increasing from top to bottom. The continuous curves are the plots of the Eq. (5.14) which match very well with the numerical data.

When a bundle is in a brittle state, the critical load per fiber $\sigma_{0c}(d,s,p)$ at the breaking point of the bundle should be equal to the value of the weakest fiber in it i.e. $(1/2-s-d)$. Therefore, on solving for d we get

$$d_c(s,p) = p(1/2-s)/(1+p). \tag{5.14}$$

Substituting the values of $s = 0$ and $p = 1/2$ one gets back the well established result of the critical width $d_c = 1/6$ [58]. The cases $p = 0$ and $p = 1$ gives back the results of the limiting cases discussed in previous sections. The Eq. (5.14) has been plotted in Fig. 5.9 for $s = 0, 0.1, 0.2, 0.3$ and 0.4 along with the numerical results.

Next, we studied the average avalanche size $\langle\Delta(d,N)\rangle$ against d. The average avalanche size for cases when $s \neq 0.0$ behaves differently depending on the fraction of fibers p in the first block. This quantity is plotted in Fig. 5.10(a) for s = 0.1 and four different values of p = 0.4,0.5 and 0.6. For small values of d for $s = 0.1$ and $p = 0.4$ the value of $\langle\Delta(d,N)\rangle$ is vanishingly small followed by a discontinuous jump leading to a plateau. Then it's value sharply decreases as d is increased further. Similar curves are observed for p = 0.5 as well. However, no plateau is observed for p = 0.6. On the other hand for a much smaller value of $\langle\Delta(d,N)\rangle$, a small peak is observed for the same

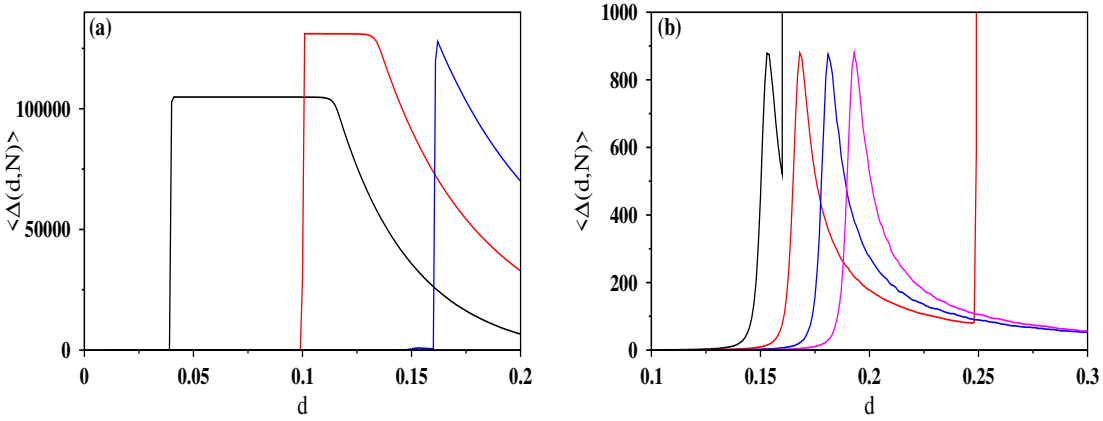

Figure 5.10: Plot of the average avalanche size $\langle \Delta(d, N) \rangle$ against the block width d for different values of (a) p = 0.4, 0.5, 0.6 and (b) p = 0.6, 0.7, 0.8, 0.9 for a bundle of size $N = 2^{18}$ with $s = 0.1$. Here, p increases from left to right in both the figures.

plot as shown in Fig. 5.10(b). Such behavior is observed till p = 0.7 after which only the small peaks remain and the large peaks vanish.

The formation of the plateau region occurs because when d is small, the bundle is in the brittle regime and all the fibers from the first block break in either one or a very small number of avalanches. Thus the average avalanche size $\langle \Delta(d, N) \rangle$ excluding the last avalanche remains constant as the total load released by these broken fibers is not enough to break even the weakest fiber in the second block. At the edge of the plateau the number of avalanches increase significantly and thus the value of $\langle \Delta(d, N) \rangle$ is seen to fall sharply. In this case, we define the critical width d_c to be located at the end of the plateau instead of the beginning. This is because even though more than one avalanche is required to break all the fibers in the first block, the breakdown is rapid and the number of such avalanches is very small. Since the number of avalanches is very small in the plateau region, it is not possible to observe a wide distribution for the avalanche sizes. Moreover, as discussed in Sec. 3.3, the brittle to quasi-brittle transition is characterized by a crossover in the exponent value of the power law followed by the avalanche size distribution. In this case, this crossover has been observed at the end of the plateau region.

Therefore, the value of the width d at the right edge of the plateau where $\langle \Delta(d, N) \rangle$ sharply decreases is considered to be the critical width $d_c(N)$ for the system size N. The

numerical values obtained have been plotted in Fig. 5.9. For s = 0.1 and p = 0.6 and 0.7, two significant peaks have been observed. The value of d at which the smaller peak occurs as shown in Fig. 5.10(b) has been defined as the $d_c(N)$ for these cases. This is because the small peak indicates that a considerable number of avalanches occur of small sizes as p is large enough and d is not too small. All the values of $d_c(N)$ obtained through the above mentioned method have been observed to match very closely with the analytical result obtained in Eq. (5.14).

5.4 Summary

To summarize, we have studied the brittle to quasi-brittle transition in a compound FBM characterized by bimodal distribution of fiber breaking thresholds. We have observed that the critical load per fiber for the failure of the bundle strongly depends on all the three parameters, namely, the width d of the blocks, the separation s between the blocks and the probability p of the first block. We have parameterized such a transition using three different quantities, namely: (i) the average fraction of fibers broken before the last avalanche, (ii) the average number of avalanches required for the complete breakdown of a fiber bundle and (iii) the average avalanche size excluding the last avalanche. In addition, we could formulate a general expression for the critical width $d_c(s, p)$ of the phase transition analytically and have verified it by the numerical analysis.

Bibliography

[1] *http://pirun.ku.ac.th/ fengppt/213211/Slides/10-Failure-Slides.pdf.*

[2] M. L. Williams and G. A. Ellinger. Invastigation of stractural failures of welded ships. *Welding Journal*, 32:498–528, 1953.

[3] T. L. Anderson. Fracture mechanics: Fundamentals and applications. 2005.

[4] O. Ramos, P.-P. Cortet, S. Ciliberto, and L. Vanel. *Phys. Rev. Lett.*, **110**:165506, 2013.

[5] H. Kawamura, T. Hatano, N. Kato, S. Biswas, and B. K. Chakrabarti. *Rev. Mod. Phys.*, 84(2):839, 2012.

[6] P. Bhattacharya and B. K. Chakrabarti. Modeling critical and catastrophic phenomena in geoscience. 2006.

[7] Jay R. Lund and Joseph P. Byrne. *Civil Eng. and Env. Syst.*, 00:1–8, 2000.

[8] L. Da Vinci. I libri di meccanica, reconstructed from the original notes by arturo uccelli. 1972.

[9] A. A. Griffith. *Philosophical Transactions, Series A*, 221:163–198, 1920.

[10] B. Lawn. Fracture of brittle solids - second edition. 1993.

[11] S. Tandon and K. T. Faber. Fracture of brittle and quasi-brittle engineering materials. *Cements Research Progress. American Ceramic Society , Columbus, OH*, pages 209–239, 1993.

[12] S. Pradhan and P. C. Hemmer. *Phys. Rev. E*, 75:056112, 2007.

[13] L. de Arcangelis, S. Redner, and H. J. Herrmann. *J. Phys. Lett.*, 46:L585, 1985.

[14] B. Kahng, G. G. Batrouni, S. Redner, L. de Arcangelis, and H. J. Herrmann. *Phys. Rev. B*, **37**:7625, 1985.

[15] A. A. Moreira, C. L. N. Oliveira, A. Hansen, N. A. M. Araujo, H. J. Hermann, and Jr. J. S. Andrade. *Phys. Rev. Lett.*, 109:255701, 2012.

[16] P. M. Duxbury, P.D. Beale, and P. L. Leath. *Phys. Rev. Lett*, 57:1052, 1986.

[17] S. S. Manna and B. K. Chakrabarti. *Phys. Rev. B*, 36:4078, 1987.

[18] A. Hansen, P. C. Hemmer, and S. Pradhan. The fiber bundle model: Modeling failure in materials. 2015.

[19] S. Pradhan, A. Hansen, and B. K. Chakrabarti. *Rev. Mod. Phys.*, 82(1):499, 2010.

[20] S. Biswas, P. Ray, and B. K. Chakrabarti. Statistical physics of fracture, breakdown and earthquake: Effects of disorder and heterogeneity. 2015.

[21] F. T. Pierce. *J. Text. Inst.*, 17:T355, 1926.

[22] H. E. Daniels. *Proc. R. Soc. London A*, 183:405, 1945.

[23] Xiong Zhu and Yang Qingsheng. *ICCM13 Proceedings*, pages ID–1543.

[24] F. Kun and H. J. Herrmann. *Journal of Materials Science*, 35:4685, 2000.

[25] S. L. Phoenix, M. Ibnabdeljalil, and C. Y. Hui. *Int. J. Solids Structures*, 34(5):545–568, 1997.

[26] S. L. Phoenix and R. Raj. *Acta metall, mater*, 40(11):2813–2828, 1992.

[27] W. A. Curtin. *J. Mech. Phys. Solids.*, 41(2):217–245, 1993.

[28] W. A. Curtin. *J. Am. Ceram. Soc.*, 74(11):2837, 1991.

[29] M. Monterrubio-Velasco, F. R. Zúñiga, V. H. Márquez-Ramírez, and A. Figueroa-Soto. Simulation of spatial and temporal properties of aftershocks by means of the fiber bundle model. *J Seismol*, 2017.

[30] M. Monterrubio-Velasco, J. C. Carrasco-Jiménez, A. Aguilar-Meléndez, O. Castillo, and J. De la Puente. Earthquake simulation by fiber bundle model and machine learning techniques. *5th BSC Severo Ochoa Doctoral Symposium*, 2018.

[31] S. Roy and T. Hatano. *Arxive*, 2017.

[32] B. K. Chakrabarti. *Physica A*, 372:162, 2006.

[33] J. F. Zheng, Z. Y. Gao, and X. M. Zhao. *International Journal of Modern Physics C*, 19(11):1727–1735, 2008.

[34] Z. Domański, T. Derda, and N. Sczygiol. Proceedings of the international multi-conference of engineers and computer scientists. *IMECS 2013, Vol. II*, 2013.

[35] E. Fjær and O.M. Nes. *Rock Mechanics and Rock Engineering*, 10.1007/s00603–014–0598–5, 2014.

[36] D. Sornette. Critical phenomena in natural sciences. 2006.

[37] R. da Silveira. *Am. J. Phys.*, 67:1177, 1999.

[38] S. Pradhan and B. K. Chakrabarti. *Phys. Rev. E*, 65:016113, 2001.

[39] S. Pradhan, P. Bhattacharyya, and B. K. Chakrabarti. *Phys. Rev. E*, 66:016116, 2002.

[40] D. G. Harlow and S. L. Phoenix. *J. Mech. Phys. Solids*, 39:173, 1991.

[41] M. Kloster, A. Hansen, and P. C. Hemmer. *Phys. Rev. E*, 56:2615, 1997.

[42] A. Hansen and P. C. Hemmer. *Phys. Lett. A*, 184:394, 1994b.

[43] D. G. Harlow. *Proc. R. Soc. London, Ser. A*, 397:211, 1985.

[44] J. B. Gomez, D. Iniguesz, and A. F. Pacheco. *Phys. Rev. Lett.*, 71:380, 1993.

[45] P. M. Duxbury and P. M. Leath. *Phys. Rev. B*, 49:12676, 1994.

[46] S. D. Zhang and E. J. Ding. *Phys. Lett. A*, 193:425, 1994.

[47] S. Sinha, J. T. Kjellstadli, and A. Hansen. *Phys. Rev. E*, 92:020401(R), 2015.

[48] A. Stormo, O. Lengliné, J. Schmittbuhl, and A. Hansen. *Front. Phys.*, 4:18, 2016.

[49] R. C. Hidalgo, Y. Moreno, F. Kun, and H. J. Hermann. *Phys. Rev. E*, 65:046148, 2002.

[50] O. E. Yewande, Y. Moreno, F. Kun, R. C. Hidalgo, and H. J. Herrmann. *Phys. Rev. E*, 68:026116, 2003.

[51] S. Biswas and P. Sen. *Physica A*, 509:1087–1094, 2018.

[52] S. Biswas and L. Goehring. *New J. Phys.*, 18:103048, 2016.

[53] P. C. Hemmer and A. Hansen. *J. Appl. Mech.*, 59:909, 1992.

[54] S. Pradhan, A. Hansen, and P. C. Hemmer. *Phys. Rev. Lett.*, 95:125501, 2005.

[55] H. J. Herrmann and S. Roux. Statistical models for the fracture of disordered media. 1990.

[56] B. K. Chakrabarti and L. G. Benguigui. Statistical physics of fracture and breakdown in disordered systems. 1997.

[57] M. Sahimi. Heterogenous materials ii: Nonlinear and breakdown properties. 2003.

[58] S. Roy and P. Ray. *Euro. Phys. Lett.*, 112:26004, 2015.

[59] E. Karpas and F. Kun. *Euro. Phys. Lett.*, 95:16004, 2011.

[60] I. Ojala, B. T. Ngwenya, I. G. Main, and S. C. Elphick. *J. Geophys. Res.*, 108:2268, 2003.

[61] S. Lennartz-Sassinek, Z. Danku, F. Kun, I. G. Main, and M. Zaiser. *Journal of Physics: Conference Series*, 410:012064, 2013.

[62] F. Kun, Z. Halász, J. S. Andrade Jr., and H. J. Herrmann. *J. Stat. Mech.*, page P01021, 2009.

[63] Z. Halász, Z. Danku, and F. Kun. *Phys. Rev. E*, 85:016116, 2012.

[64] S. L. Phoenix. *SIAM, J. Appl. Math.*, 34:227, 1978.

[65] S. L. Phoenix. *Adv. Appl. Prob.*, 11:153, 1979.

[66] R. L. Smith and S. L. Phoenix. *ASME J. Appl. Mech.*, 48:75, 1981.

[67] R. L. Smith. *Ann. Prob.*, 10:137, 1982.

[68] L. N. McCartney and R. L. Smith. *ASME J. Appl. Mech.*, 50:601, 1983.

[69] *https://en.wikipedia.org/wiki/Quicksort*.

[70] H. E. Daniels and T. H. R. Skyrme. *Adv. Appl. Probab.*, 17:85, 1985.

[71] C. Roy, S. Kundu, and S. S. Manna. *Phys. Rev. E*, 67:062137, 2013.

[72] S. Roy. *Phys. Rev. E.*, 96:042142, 2017.

[73] S. Roy, S. Biswas, and P. Ray. *Phys. Rev. E.*, 96:063003, 2017.

[74] H. E. Daniels and T. H. R. Skyrme. *Adv. Appl. Probab.*, 21:315, 1989.

[75] S. Pradhan, A. Hansen, and P. C. Hemmer. *Phys. Rev. E*, 74:016122, 2006.

[76] C. Roy, S. Kundu, and S. S. Manna. *Phys. Rev. E*, 91:032103, 2015.

[77] C. Roy and S. S. Manna. *Phys. Rev. E*, 94:032126, 2016.

[78] S. L. Phoenix. *Fiber Sci. Tech.*, 7:15, 1974.

[79] U. Divakaran and A. Dutta. *Phys. Rev. E*, 75:011117, 2007.

[80] U. Divakaran and A. Dutta. *Phys. Rev. E*, 78:021118, 2008.